

2008

## Modal Characterization of Micron-Scale Structures

Pakeeza Hafeez

Follow this and additional works at: <https://ir.lib.uwo.ca/digitizedtheses>

---

### Recommended Citation

Hafeez, Pakeeza, "Modal Characterization of Micron-Scale Structures" (2008). *Digitized Theses*. 4332.  
<https://ir.lib.uwo.ca/digitizedtheses/4332>

This Thesis is brought to you for free and open access by the Digitized Special Collections at Scholarship@Western. It has been accepted for inclusion in Digitized Theses by an authorized administrator of Scholarship@Western. For more information, please contact [wlsadmin@uwo.ca](mailto:wlsadmin@uwo.ca).

# Modal Characterization of Micron-Scale Structures

(Thesis format: Monograph)

by

Pakeeza Hafeez

Graduate Program in Engineering Science  
Department of Mechanical and Materials Engineering

↓

Submitted in partial fulfillment  
of the requirements for the degree of  
Master of Engineering Science

School of Graduate and Postdoctoral Studies

The University of Western Ontario

London, Ontario

December, 2008

© Pakeeza Hafeez 2008

# Abstract

This thesis is mainly concerned with the application of Stochastic Subspace Identification algorithms to extract dynamic characteristics of smaller-scale structural elements. It also emphasizes the development of a suitable identification procedure for extracting modal characteristics of insect's sensory systems, which are typically of the order of microns in length. The traditional way of extracting modal parameters by forming a transfer function is not practical for micron-scale structures owing to the practical limitations in applying a quantifiable input to excite such structures. Output-only identification and Stochastic Subspace Identification (SSI) methods attempt to extract modal parameters from the output response data and hence eliminate the need for quantifying the input. The input in this case is assumed as a broad band white noise and is assumed to arise from ambient sources. A program, Modal Analysis on Civil Engineering Structures (MACEC), is used as a modal analysis tool for extracting the modal parameters of macro as well as micron-size structures. It provides a Graphical User Interface (GUI) for performing output-only system identification within the MATLAB programming environment. MACEC offers system identification via two different methods: SSI and Peak Picking Method (PPM) and provides animated visualization of mode shapes. As part of this thesis, a detailed verification for using this program for analysing micron-size structures is performed. An experiment is carried out on a meter long beam where data is collected using Laser Doppler Vibrometry (LDV) and mode shapes and modal frequencies are identified via MACEC. These results are also verified from the data collected using conventional system identification methods. The same methodology is then employed on further experiments which are carried out on submillimeter size beams. The data in this case is collected using Microscope Scanning Vibrometer (MSV). Frequencies are identified using SSI via MACEC. Based on the procedure used for submillimeter size beams, a preliminary experiment is carried out on micron-size mechanoreceptor hair on the cercus of a cricket and modal frequencies are identified using SSI via MACEC. The test procedures and methodology developed in this case is envisaged further work to be performed in the area of dynamic characterization of insect's sensory systems.

**Keywords:** System Identification (SI), Modal Analysis, Stochastic State-space model, Output-only system, White noise.



# Acknowledgement

I deeply thank my advisor, Dr S.F. Asokanthan, whose help, advice and supervision was invaluable thought the period I stayed with him.

I gratefully acknowledge NSERC, for funding for student support and experimentation for this thesis.

I am also thankful to Joel Martin Book, with whom I discussed every part of my thesis and whose comments substantially improved the material and presentation of this thesis. I thank my colleagues Tianfu, Ken and Yukaung for their help in setting up the experiments. Finally, I thank to my parents, my brother and my sisters for their love, understanding and moral support.

I am very thankful to God for His blessings on me.

# Contents

<b>Certificate of Examination</b>	<b>ii</b>
<b>Abstract</b>	<b>iii</b>
<b>Acknowledgment</b>	<b>v</b>
<b>Table of Contents</b>	<b>vi</b>
<b>List of Tables</b>	<b>viii</b>
<b>List of Figures</b>	<b>ix</b>
<b>Abbreviations and Symbols</b>	<b>xii</b>
1 Introduction and Literature Review .....	1
1.1 Introduction .....	1
1.2 Motivation and Significance .....	3
1.3 Literature Review.....	6
1.3.1 A Brief Survey on System Identification .....	6
1.3.2 Research done in Biomimetic and Engineering Paradigm.....	7
1.4 Focus of the Thesis.....	8
1.5 Organization of the Text .....	9
1.6 Chapter Summary.....	10
2 Stochastic Subspace Identification .....	11
2.1 Introduction .....	11
2.2 State Space modelling of Vibrating Structures .....	13
2.2.1 A Physical Model .....	13
2.2.2 Need for a State Space Model .....	13
2.2.3 A State Space Model .....	14
2.3 Output-only Identification via Peak Picking Method .....	18
2.4 Chapter Summary.....	20
3 Interactive System Identification .....	21
3.1 Introduction .....	21
3.1.1 Graphical User Interface (GUI).....	21
3.2 Interaction between System Identification and GUI.....	22
3.2.1 Implementation of MACEC .....	23
3.3 Functions of MACEC.....	25
3.3.1 Section 1:Pre-processing .....	26
3.3.2 Section 2: Processing .....	35
3.3.3 section 3: Post processing .....	42
3.4 Chapter Summary.....	44
4 Modal Characterization of a Cantilever Beam using MACEC.....	45
4.1 Introduction .....	45
4.2 Cantilever Beam Model .....	46
4.2.1 Description of the Beam Model .....	47
4.2.2 Analytical Results .....	48
4.3 Simulation of Cantilever Beam .....	49

4.4	Physical Experiments on Beam.....	49
4.5	Experiment 1 .....	50
4.6	Experiment 2 .....	53
4.7	Experiment 3 .....	56
4.7.1	Modal characterization in MACEC.....	58
4.8	Experiment 4 .....	63
4.9	Comparison and Discussion of Results.....	65
4.10	Chapter Summary .....	67
5	Modal Characterization of Smaller Structures.....	68
5.1	Introduction .....	68
5.2	Micron-size Cantilever Beam Model .....	69
5.3	Physical Experiment on Micro Cantilever Beam.....	69
5.3.1	Preparation and Positioning of the Specimen .....	71
5.4	Transverse Vibration Measurements on Beam Type Structures.....	74
5.4.1	Time Measurements .....	74
5.4.2	Results for Time Measurement .....	78
5.4.3	Frequency Measurements on Beam .....	79
5.4.4	Results for Frequency Measurements .....	80
5.5	Background for Insects.....	81
5.6	Experiment on Insect's Sensory System .....	82
5.6.1	Materials and Method: .....	82
5.7	Transverse Vibration Measurements on Hair of the Insect.....	84
5.7.1	Time Measurements .....	84
5.7.2	Results .....	87
5.8	Frequency Measurements on Hair of the Insect.....	88
5.8.1	Results .....	88
5.9	Discussion of the Results .....	89
5.10	Experimental Approach Extended towards two-dimensional Micro-structures	93
5.11	Chapter Summary .....	94
6	Conclusions and Recommendations .....	96
6.1	Summary .....	96
6.2	Thesis Contribution.....	98
6.3	Recommendations for Future Work.....	99
7	References.....	101
8	Appendix	
9	A Mode shape Figures	104
	B stabilization diagrams and ANSPD	106
	C FRF plots from Polytec	109
	Vitae	110

# List of Tables

Table 3.1	Structure of a slave file	42
Table 4.1	Results obtained from MACEC (SSI and PPM)	62
Table 4.2	Comparison of the results obtained from different experiments	65
Table 4.3	Results for mode 1 obtained from different experiments	66
Table 4.4	Results for mode 2 from SSI and FRF from Polytec	66
Table 4.5	Results for mode 3 obtained from different experiments	67
Table 5.1	Analytical results for micron- size cantilever beam	69
Table 5.2	Modal frequencies for 9mm long beam	79
Table 5.3	Modal frequencies for 7.5mm long beam	79
Table 5.4	Modal frequencies for 6.4mm long beam	79
Table 5.5	FFT results obtained from Polytec for three different lengths of beam.	80
Table 5.6	SSI and PPM results of time measurements from MACEC	88
Table 5.7	Percent difference between calculated and identified frequencies	89
Table 5.8	Comparison of FFT results from Polytec and identified frequencies ( SSI) from MACEC	90

# List of Figures

Figure 3.1	MACEC main window	26
Figure 3.2	Preference window in MACEC	27
Figure 3.3	MACEC sensitivity window	27
Figure 3.4	SIT specification window	27
Figure 3.5	Frequency and time domain data	28
Figure 3.6	Default window length	31
Figure 3.7	Customized window length (1024)	31
Figure 3.8	Amplitude spectrum of FFT with frequency on x-axis and amplitude on y-axis	32
Figure 3.9	y-axis of figure 9 is zoomed in to $4 \times 10^{-3}$ to show spectral leakage	32
Figure 3.10	Boxcar Window (MATLAB help file)	33
Figure 3.11	Hanning window (MATLAB help file)	34
Figure 3.12	PSD calculated using Hanning window function	35
Figure 3.13	PSD calculated using Boxcar Window function	35
Figure 3.14	SSI window (calculation tab)	36
Figure 3.15	SSI window (Option tab)	36
Figure 3.16	Principal angles illustration from MACEC	38
Figure 3.17	Stabilization diagram from MACEC	39
Figure 3.18	MOD file	40
Figure 3.19	Moving Mode	40
Figure 3.20	Peak picking method window	41
Figure 3.21	Average normalized psd window	42
Figure 3.22	Beam Generators	43
Figure 3.23(a)	Mode 1 via SSI MACEC case study “Frame Structure” MACEC manual 2.0	44
Figure 3.23(b)	Mode 2 via SSI MACEC case study “Frame Structure” MACEC manual 2.0	44
Figure 4.1	Cantilever beam used in experiments	47
Figure 4.2	Setup for a typical experiment	48

Figure 4.3	Schematic diagrams of the experimental setup for experiment 1	50
Figure 4.4	FRF from experiment 1, velocity vs Force	52
Figure 4.5	FRF from experiment 1, Acceleration vs Force	52
Figure 4.6	Schematic diagram of the experimental setup for experiment 2	53
Figure 4.7	Signals generated in MATLAB using random numbers	55
Figure 4.8	FRF obtained in experiment 2-Aceleration vs Force	55
Figure 4.9	Experimental layout for experiment 3	56
Figure 4.10	principal angle diagrams from MACEC	60
Figure 4.11	Stabilization diagram for beam from SSI (MACEC)	61
Figure 4.12	ANPSD from PPM (MACEC)	61
Figure 4.13(a)	Mode number 1, via SSI MACEC	62
Figure 4.13(b)	Mode number 2 via SSI MACEC	62
Figure 4.13(c)	Mode number3 via SSI MACEC	62
Figure 4.14(a)	Mode number 1 via PPM MACEC	63
Figure 4.14(b)	Mode number 2 via PPM MACEC	63
Figure 4.14(c)	Mode number 3 via PPM MACEC	63
Figure 4.15	FRF obtained from Polytec software Velocity vs Force	64
Figure 5.1	Different lengths of submillimeter size cantilever beam	69
Figure 5.2	Experimental setup for measuring velocity on micron- size beam and hair on insect's cercus	70
Figure 5.3(a)	Schematic diagram of stand carrying wire specimen	72
Figure 5.3(b)	Real photo of the stand carrying specimen of wire beam	72
Figure 5.3(c)	Zoom in photo of wire beam glued on piano wire	72
Figure 5.4	Principal angle diagram from MACEC for 9mm long beam	77
Figure 5.5	Stabilization diagram for 9 mm long beam.	77
Figure 5.6	ANPSD for 9mm long beam	78
Figure 5.7	Average spectrum of frequency measurements form MSV for 9mm long beam	80
Figure 5.8	Female crickets under the dissection microscope at DASSL	82
Figure 5.9	Mechanoreceptor hairs on cercus of an insect	83

Figure 5.10	Principal angle diagram that shows a gap between 4th and 5th order of the system.	85
Figure 5.11	Stabilization diagram showing stabilized poles around 48.09Hz	86
Figure 5.12	ANPSD from PPM	87
Figure 5.13	FFT results for hair from PSV Polytec (linear scale)	88
Figure 5.14	First ODS of sensory hair from Polytec software (point 1 to point 7 starting from right to left)	91
Figure 5.15	Second ODS of sensory hair from Polytec software (point 1 to point 7 starting from right to left)	92
Figure 5.16	Diaphragm of microphone with two metal bits on top surface of it	93

# Abbreviations and Symbols

ANPSD	Average normalized power spectral density
ARMA	Auto-Regressive Moving Average
CMIF	Complex Mode Indication Function
DFT	Discrete Fourier Transform
DOF	Degrees of Freedom
FEM	Finite Element Modelling
FFT	Fast Fourier Transform
FRF	Frequency Response Function
GUI	Graphical User Interface
IV	Instrumental Variable
LDV	Laser Doppler Vibrometer
MAC	Modal Assurance Criterion
MACEC	Modal Analysis on Civil Engineering Constructions
MEMS	Micro Electro Mechanical Systems
MSV	Micro Structure Vibrometer
PPM	Peak Picking Method
SSI	Stochastic Subspace Identification
SVD	Singular Value Decomposition
ZOH	Zero Order Hold
$A, B, C, D$	Discrete -time state-space model
$A_c, B_c, C_c, D_c$	Continuous-time state space model
$B_2$	Input Location matrix (FE Model)
$C_2$	Damping matrix (FE Model)
$C_a, C_v, C_d$	Output location matrix for acceleration, velocity and displacement (FE Model)
$E$	Expected value operator (used in chapter 2 of the present thesis))
$E$	Young's Modulus
$f(t)$	Excitation force vector (FE model)
$I$	Moment of inertia
$l$	Length of the beam
$K$	Stiffness matrix (FE model)



$M$	Mass (FE model)
$t$	Thickness of the beam
$w$	Width of the beam
$v_k$	Measurement noise at time instant $k$
$w_k$	Process noise vector at time instant $k$
$x_k$	State at time instant $k$
$x(t)$	State at time $t$
$y_k$	Output at time instant $k$
$y(t)$	Output at time $t$
$\rho$	Density of the beam
$\beta_n l$	Weighted natural frequencies

# Chapter 1

## Introduction and Literature Review

### 1.1 Introduction

Humans, from the stone age have interacted with the environment and learned to control their actions by predicting the environmental effects. These efforts are concentrated on one part of reality at a time, called the system, ignoring the environment around it. The system could be stationary or set in motion under the effects of external forces. From the basic laws of physics, it is determined that the motion of a mass with changing velocity is determined by the net force acting on the mass. Determination of the response of a system under the effect of forces unlocks the doors for finding dynamic characteristics of a system. Systems, where system values are changing with time are called dynamic systems.

Modelling is a process of writing down an equation or system of equations to describe the behaviour in general of a physical device. The term “model” in the context of dynamic systems typically, means a set of differential equations that describe the dynamic behaviour of a process. A model can be obtained using principles of underlying physics or can be obtained by testing a prototype of a device measuring its response to prescribed input and using the data to construct an analytical model. A mathematical model is an essential step to carry out scientific research. They are useful in situations where performing experiments on the real system is expensive, dangerous and difficult. They are applicable in every field of science for such purposes as simulation, operator training, analysis, monitoring, prediction, control system design and quality control.

Many systems are not deterministic. They show stochastic behaviour that makes it impossible to predict their output exactly. Noise in a radio receiver, Brownian motion of small particles, and variation of wind speed in a thunder storm are some examples of this type of processes. Usually, a model is composed of two parts, a deterministic part and a stochastic part. The deterministic aspects can be stored by a mathematical system model. While stochastic behaviour is modelled as a noise distortion. The aim of a system identification methodology is to provide a systematic approach to fit a mathematical model to the deterministic part and to eliminate the noise distortions as much as possible.

The process of finding a model from experimental data is called system identification (SI). System identification problems are fundamental problems of science, medicine and engineering. They deal with the problem of building mathematical models of dynamic systems based on observed data from a system. Basic steps in system identification are to collect information about the system which could be performed either by watching the natural fluctuations (e.g., vibration analysis of a bridge that is excited by normal traffic) or by setting experiments that actively excite the system, selecting a model structure to represent the system, choosing the model parameters to fit the model and measurements, and finally validating the selected model to ensure that the selected model adequately describes the available data (Ljung, 1999).

Application of system identification to vibrating structures has resulted in a new research domain in mechanical engineering known as experimental modal analysis. The identified model in this case is a modal model consisting of eigenfrequencies, damping ratios, mode shapes and modal participation factors.

In the last few decades tremendous development has been made in system identification and experimental modal analysis in the field of civil, electrical and mechanical engineering. For a small and medium size structure there are certain ways to induce excitation, such as use of impulse hammer and hydraulic shakers etc. With the known input force, there is a wide variety of input-output modal identification methods to find out dynamic characteristics of the system under consideration. But in the case of larger

structures (i.e. large buildings, dams and bridges) it is very difficult to excite them with sufficient amounts of energy. Similar difficulties are also encountered when exciting micron-size structures with load conditions owing to their smaller size. Therefore output-only modal identification has become an important alternative for the civil engineering structures, where the traffic, winds and ambient conditions act as agents for natural excitation. This alternative received an extraordinary emphasis with the emergence of structural health monitoring (SHM) which obtained its roots deeply in vibroacoustic and non-destructive testing and evaluation.

The modeling of output-only data obtained from naturally excited structure is particularly interesting because test structure remains in its normal in-operation condition during the test. In the past, different methods were developed to process output-only data. These methods can be used for situations where it is difficult to perform an artificial forced excitation. The main idea of output-only modal analysis is to use the unknown natural forces as excitation (e.g. traffic/wind excitation for civil structures, atmospheric turbulence for airplanes etc). A bridge excited with a shaker but at the same time by the traffic, or flight flutter tests where the airplane is excited by its flaps but at the same time by atmospheric turbulence, are practical examples in which the structure is excited with a known force but at the same time with unknown forces. Since it is impossible to measure the ambient excitation sources, deterministic knowledge of the input is replaced by the assumption that the input is a realization of a stochastic process (white noise).

The present thesis focuses on exploring the application of the above output-only identification techniques for identifying micron-scale structural elements. It is envisaged that the procedure developed and validated on the present study will pave the way for more detailed prediction of insect's sensory organ which are typically of micron-scale size.

## **1.2 Motivation and Significance**

Experimental modal analysis has greatly focused on the industrial applications and is currently one of the key technologies to solve the specific problems related to testing and

modelling the large industrial structures. It has become an essential part in aerospace, construction and in transportation industries in modern era. Aircrafts play an important role in the economy of a country. In-flight tests are conducted to validate analytical models, during the modelling and testing stage of the aircraft development cycle. For safety purposes and to avoid flutter, it is necessary to get good knowledge about flutter margin on an in flight test, therefore the need arises to perform system identification during the flight using atmospheric turbulence (Mevel *et al*, 2006) as an additional excitation source to investigate the dynamic characteristics of the system.

Similarly the large and complex civil engineering structures (dams, high rise buildings and bridges) also require identification of structural dynamic properties to prevent structural deterioration. However, it is difficult to excite the large structures and to measure input dynamic forces acting on them therefore, output-only identification can be considered as an alternative.

There are many modal analysis software packages which are developed in mechanical engineering for identification based on input/output data. Today, some of these packages also have some modules for output-only modal analysis but most of the commercial software packages do not provide the user with the information about the implementation of algorithm and are difficult to add one's own developments to. Therefore the department of civil engineering at Katholieke University Leuven, decided to develop their own program for output-only modal analysis, and finally MACEC came into existence. MACEC is the acronym of Modal Analysis on Civil Engineering Constructions. In the past MACEC has been used for large-scale civil structures, so the need arises to validate this useful program for small-scale structures.

Humans have always been inspired by the nature. Nature is rich in micron-scale structures and a natural curiosity arises to know about such structures. The abstraction of good designs from nature is called biomimetics. It is seen that the application of biomimetics to engineering has produced the innovations far better than what human brain could have produced alone. A very well known example is that the Wright brothers modelled their

plane on the structure of a bird's wing. Creatures that can fly, creep and crawl can penetrate into military defence more secretively and skilfully than trained human spy. Since it is very difficult to train these species, Defence Advanced Research Project Agency is concentrating to mimic them (Chalmers, 2000). The implementation of biomimetics is gathering momentum these days. It is very useful in robotics and pharmaceutical industries. Engineers are thinking how an insect in the low reynolds number regime gets off the ground, how the aerodynamics in small insects works, and how they create cosmetics that mimic the mysterious glitter found on butterfly's wing. Therefore insects are the main fodder for emulation of nature.

Based on the research in the wake of engineering and biomimetics paradigm, several attempts are made to build micromechanical insects. Sensing necessarily occurs at molecular level. Sensitivity is much higher in the campaniform sensillum of insects, for instance nanometer displacements can be registered. By mimicking the beetle's sensory capability which can sense smoke and infrared emissions from about, 70 Kilo meters away, its robotic counterpart may be able to detect chemical and infrared emissions with greater sensitivity (Chalmers, 2000). NASA is investigating the locomotive strategies and navigational systems of insects to design autonomous robots and vehicles. The rough skin of shark is used as inspiration in developing striated foil wings of aircraft which has resulted in six percent less friction and improved fuel consumption. Similarly, researchers are also working on "Gecko Tape" by inspiration of lizard's ability to climb up walls and walk along ceilings (Butler, 2005).

The thesis aims to provide a significant step towards these attempts by extracting the dynamic characteristics of such sensory systems available in nature. The results and experiments from the present thesis will also form the basis of stochastic subspace identification (SSI) application on micron-scale structures. The study of dynamic behaviour of insect's sensory organ would be of great help to agriculturist keen to know about insect's behaviour, and researchers working on biomimetics, and robotics. The application of modal analysis program, MACEC for modal identification of macro and

micron-size structures, is expected to make the identification process more user-friendly and to make this class of techniques applicable for more wide-spread use.

## 1.3 Literature Review

The literature survey for this thesis is divided into two sections. The first section describes the contribution of different researchers in the field of system identification and the second section gives a brief literature review of study of the vibration of sensory organs of insects, and its applications in biomimetics.

### 1.3.1 A Brief Survey on System Identification

System identification has been at the center of attention for the last few decades. The theory gathered momentum with the development of subspace identification methods, which have their origin in state space realization theory developed in 1960s. It is creditable to mention the contribution by Ho and Kalman (1966), who developed the scheme for recovering the system matrices from impulse response measurements which was later improved by Zeiger and McEwen (1974), King *et al* (1988), and Bayard (1992). But obtaining reliable non-parametric estimates of impulse response using this approach was found to be difficult. In order to overcome this difficulty, an early attempt was made by Gopinath (1969), and recently, Overchee and Moor (1993). Traditional system identification algorithms such as prediction error Method (PEM) by using auto-regressive moving average (ARMA) are well defined in the book by Ljung (1995). The primary focus in this book, are systems with known inputs and outputs.

A broad explanation of subspace identification and implementation is provided by Overchee and Moor (1996). Subspace identification algorithms from stochastic and combine stochastic and deterministic points of view are discussed in their study. They showed that with certain assumptions, identification for deterministic systems can be extended to stochastic systems. Tasker *et al.* (1998), describe real-time modal parameter estimation algorithm via subspace identification methods. Cock *et al* (2002), discuss covariance based subspace identification algorithm theory and applications. Peeter and Roeck (1999), proposed a data reduction method in SSI algorithm. In this case, some

selected outputs were taken as reference and data from those sensors are considered as past outputs. They applied their theory on a steel mast and compared the results with direct SSI algorithms. A review paper outlining the output-only algorithms is given by Peeter and Roeck (2001). The basic steps for SSI, Peak picking (PP), complex mode identification method (CMIF), and instrumental variable (IV) are described there. Accuracy of different algorithms in terms of identified modal parameters of a mast is compared by means of Monte-Carlo analysis of 100 simulations runs. Another comparative study of the available algorithms applied to modal parameters estimation of a bridge from output data is performed by Peters and Ventura (2003). Ali (2006), has demonstrated the applicability of SSI algorithm on large and moderate size structures such as a beam and bridge. He identified the modal parameters by developing special subroutines in MATLAB while MACEC was used for visualization of mode shapes of vibrating bridge.

### **1.3.2 Research done in Biomimetic and Engineering Paradigm**

As discussed in section 1.2, application of engineering in the field of biomimetics has been the object of intensive study on several fronts and several attempts are made to mimic the sensors from insect behaviour. The ability of an insect to produce the appropriate behavioural response is determined by the characteristics and capabilities of its sensory organs. Stimuli caused by locomotion, posture and external events induce mechanical strains in the cuticle which have a rich variety of sensory information. This information is picked up by sensilla formed in the cuticle. Examples are the campaniform sensilla of insects and the slit sense organs of arachnids (Skordosay and Vincent, 2002).

Many insects can detect movement of ambient air by means of hair sensilla which can respond to both wind and sound. The abdominal cerci of crickets, cockroaches and grasshoppers bear several thousands filiform sensory hairs. The study of behaviour of these mechanoreceptor hairs got greater concern since early 80s. Prior to this, Dumpert and Gnatzy (1977), showed the combined mechanoreceptor and kicking response of cricket. They concluded that campaniform sensilla on the cercus of cricket species (*Gryllus*) trigger the kicking response excited by air currents. Tautz (1977), and Fletcher



(1979), have developed mechanical model for the behaviour of hair-like acoustical sensory receptors in insects. Gnatzy and Tautz (1980), showed that filiform hair when stimulated by vibration of medium produce regular or irregular oscillation depending upon stimulus intensity. Kämper and Kleindienst (1990), defined the oscillatory characteristics (frequency, maximum displacement) of cricket sensory hairs in a low-frequency sound field (10-200 Hz). Schimozawa and Kanou (1984) showed that the long filiform hairs are spontaneously active and sensitive to a low frequency stimulus and are called velocity sensitive hairs compared to the short hairs.

Various receptors located in and on the insect leg detect substrate-borne sound. Shaw (1994), found that posterior legs of cockroach *Periplaneta americana* have a sense organ which is extremely responsive to vibration but also detects the sound (best response near 1.8 kHz) with sensitivity similar to some insect's auditory organ of insect. Recently, Cocroft and Tieu (2000), used laser doppler vibrometry to make non-invasive measurements of insects and substrate, to show the mechanical response of an intact, unrestrained insect (membraicd treehopper) on an appropriate substrate. They characterized the mechanical response of free standing stationary insects while varying the direction of travel of a random noise vibration. Stolting and Stumpner (2007), made use of laser vibrometer and to measure the mechanical vibration of pCO of fly (*Sarcophaga bullata*) with in the frequency range of 100 Hz to 10 kHz. He showed that substrate vibrations are transmitted to the sensory organ and pCO responds to vibration in the frequency ranges up to at least 10 kHz.

## 1.4 Focus of the Thesis

Main objectives of the thesis, based on the motivation discussed in section 1.2 can be listed as follows:

- Validate MACEC as a modal parameter extraction program for macro and micro-scale structures.
- Perform comprehensive study of the SSI algorithm and provide a summary for the purpose of using MACEC for output-only identification in practice.

- Apply SSI algorithm on a macro-scale structure such as a cantilever beam by performing a laboratory experiment. Extract its modal parameters using MACEC.
- Show practical applications of SSI algorithm via MACEC on smaller structures by performing experiments on (a) a one-dimensional structure such as a micron-size cantilever beam (b) a two-dimensional structure such as a microphone and, (c ) a typical sensory organ of an insect.

## 1.5 Organization of the Text

The present thesis is organised as follows:

Chapter 1 introduces the thesis with broader area of applications and significance.

Chapter 2 describes theoretical overview of identification techniques and algorithms available for implementation. A brief overview of SSI algorithm is given in comparison with other SI methods.

Chapter 3 discusses the implementation of MACEC to extract modal parameters using SSI and Peak picking methods. Use of stabilization diagram, creation of surface structures and visualization of different modes are defined briefly.

Chapter 4 describes the implementation of SSI algorithms, to a macro-scale structure by performing a laboratory experiment on a meter long cantilever beam and validation of MACEC for structural identification. In this chapter of the thesis, a methodology is developed for further use on smaller-scale structures.

Chapter 5 provides details on the experiments carried out on small-scale structures microphones, and insects. The data obtained from experiments are analysed via MACEC for extraction of modal parameters.

Chapter 6 summarizes the results and recommendations from the thesis and outlines the possible future research in this area.

## **1.6 Chapter Summary**

In this chapter, system identification concepts are introduced along with their applications. MACEC as a modal identification tool is also introduced. Motivation for the thesis and its significance are described. A brief literature review is given outlining the research performed previously by researchers in the field of system identification and biomimetics. Finally, focus of the thesis is given briefly together with the organization of the chapters that form this thesis.

# Chapter 2

## Stochastic Subspace Identification

### 2.1 Introduction

Investigation into the dynamic behaviour of both large and small structures has been the subject of investigation for some time. Mathematical modelling, given input and output data from a dynamic system is called System Identification. It is a practical tool to extract the modal parameters (frequencies, damping ratios and mode shapes) from dynamic measurements. As discussed in Ljung (1995), the first step in system identification is to adopt a certain model structure then measured data is used to estimate parameters for the chosen model, and finally the model is validated.

Conventionally, modal parameters are extracted using different parameter estimation techniques, once output is obtained by artificially exciting the structure with a measurable input. However it is known that in the case of large-scale civil engineering structures, it is not easy to quantify the input or excitation level of a structure during its operational condition. The only available option, for such cases, is to rely upon available ambient excitation sources. The output-only data dynamic testing has an advantage of being inexpensive since no equipment is used to excite the structure. Practically, it is impossible to measure the ambient excitation sources and output is the only information that can be passed on to a system identification algorithm. This feature has led to the development of output-only system identification, where the deterministic knowledge of input is replaced

with the assumption that input takes the form of a stochastic process (white noise), hence the technique is known as stochastic system identification.

System identification techniques often originate in electrical engineering and are thereafter adapted to civil engineering, but the need to perform output-only modal analysis probably first emerged in civil engineering where it is very troublesome and expensive to excite large -scale structures. This technique is also very useful in the field of mechanical engineering, where it is used to obtain modal parameter during road testing of cars and flight testing of aeroplanes.

There have been several techniques available for output-only modal identification of data developed by different researchers, such as the peak picking method (Bendat and Piersol, 1993), auto-regressive moving average (ARMA) models based on discrete time data (Andersen *et al*, 1996), the natural excitation technique (NExT) (James *et al*, 1995) and stochastic subspace identification (Overchee and Moor, 1996), (Peters and Roeck, 2000).

The mathematical basis of different output-only modal identification techniques is similar but differences arise in implementation, such as data reduction, the type of equation solver, and the sequence of matrix operations ( Peeters and Roeck, 2001).

Recently, subspace based methods for system identification have gathered momentum in the field of electrical engineering. This interest is due to the ability of providing accurate state space models for multivariate linear systems directly from measured data. The main theorem of subspace theory demonstrate how the Kalman filter states can be obtained from input-output data using linear algebra tools such as: singular value decomposition (SVD) and QR factorization. Once these states are known, the identification problem becomes a linear least square problem in the unknown system matrices (Kirkegaard and Andersen, 1999).Further, different model structures, such as Finite element model (FEM), State Space Models, and Auto Regressive Moving Average (ARMA) have found their use in the system modelling process. Among these, state space models are very relevant in the

context of system identification. Several identification algorithms, including SSI, are based on state space models. Therefore it is worthwhile to discuss them in this context.

## 2.2 State Space modelling of Vibrating Structures

### 2.2.1 A Physical Model

Let us consider a physical model, described by Equation (2.1), which represents the dynamic behaviour of a discrete mechanical system consisting of  $n_2$  masses connected through springs and dampers:

$$M \ddot{q}(t) + C_2 \dot{q}(t) + Kq(t) = f(t) = B_2 u(t), \quad (2.1)$$

where  $M, C_2, K \in R^{n_2 \times n_2}$  are the mass, damping and stiffness matrices, and  $q(t) \in R^{n_2}$  is the displacement vector at continuous-time  $t$ . The vector  $f(t) \in R^{n_2}$  is the excitation force, and  $B_2 \in R^{n_2 \times m}$  describes the location of input and a vector  $u(t) \in R^m$  describes  $m$  inputs in time. For a system with distributed parameters, Equation (2.1) is known as a FE (finite element) approximation of the system with  $n_2$  degrees of freedom (DOF).

### 2.2.2 Need for a State Space Model

Although Equation (2.1) represents the true behaviour of a vibrating structure, it cannot be used directly in the system identification methods used in this thesis, for the following reasons:

1. This equation is in continuous-time while the measurements are sampled at discrete-time instants.
2. It is not possible to measure all of the degrees of freedom.
3. Noise modelling is needed to fit experimental data into model.

### 2.2.3 A State Space Model

State space models originate from control theory but became popular in mechanical and civil engineering as well. State space idea comes from vector algebra concept. A state space model can be stated in continuous and discrete-time form, and a direct implementation of experimental data is possible in discrete form. A state space model is described by two equations i.e. state equation and observation equation.

#### The State Equation:

Equation (2.1) is a second order equation which can be used to derive a set of first order by defining the following parameters:

$$x(t) = \begin{pmatrix} q(t) \\ \dot{q}(t) \end{pmatrix}, \quad P = \begin{pmatrix} C_2 & M \\ M & 0 \end{pmatrix}, \quad Q = \begin{pmatrix} K & 0 \\ 0 & -M \end{pmatrix}, \quad (2.2)$$

$$P \dot{x}(t) + Qx(t) = \begin{pmatrix} B_2 \\ 0 \end{pmatrix} u(t), \quad (2.3)$$

where  $x(t) \in R^n$  is called the state vector. The following is the state equation which is obtained by pre-multiplying Equation (2.3) by  $P^{-1}$ :

$$\dot{x}(t) = A_c x(t) + B_c u(t), \quad (2.4)$$

where  $A_c \in R^{n \times n}$  and  $B_c \in R^{n \times m}$  are defined as

$$A_c = -P^{-1}Q = \begin{pmatrix} 0 & I \\ -M^{-1}K & -M^{-1}C_2 \end{pmatrix},$$

$$B_c = -P^{-1} \begin{pmatrix} B_2 \\ 0 \end{pmatrix} = \begin{pmatrix} 0 \\ M^{-1} B_2 \end{pmatrix}.$$

In Equation (2.4),  $A$  and  $B$ , respectively are called the dynamic state matrix and input matrix while subindex 'c' represents continuous-time.

The observation equation:

In a practical vibration experiment, not all  $n_2$  DOFs of the structure are measured, but only a subset. If it is assumed that measurements are taken at  $l$  locations and that the sensors are chosen to be either accelerometer, velocity or displacement transducers, the observation equation becomes:

$$y(t) = C_a \ddot{q}(t) + C_v \dot{q}(t) + C_d q(t), \quad (2.5)$$

where,  $y(t) \in R^l$  is the output and,  $C_a, C_v, C_d \in R^{l \times n_2}$  are, respectively, the output location matrices for acceleration, velocity and displacement. Practically it is possible to measure velocity and acceleration simultaneously using Equation (2.1) to eliminate  $\ddot{q}(t)$ , and using state vector definition (Equation 2.2), Equation (2.5) can be transformed into following equation :

$$y(t) = C_x x(t) + D_c u(t), \quad (2.6)$$

where  $C_x \in R^{l \times n}$  is the output matrix and  $D_c \in R^{l \times m}$  is the direct transmission matrix.

Deterministic Model:

The classical continuous-time state space model is obtained by combining Equations (2.4) and (2.6):



$$\begin{aligned}\dot{x}(t) &= A_c x(t) + B_c u(t), \\ y(t) &= C_c x(t) + D_c u(t).\end{aligned}\tag{2.7}$$

The model represented by Equation (2.4) and (2.6) is also called a deterministic model as its input can be determined exactly. Since matrices  $A$ ,  $B$ ,  $C$  and  $D$  hold information about the state vector and input vector, it is called a state space model.

In this model,  $A_c \in R^{n \times n}$ ,  $B_c \in R^{n \times l}$ ,  $C_c \in R^{m \times n}$  and  $D_c \in R^{m \times l}$  are the continuous state space system matrices. The subindex 'c' indicates the continuous state while 'n' represents the order of the state space model and is defined as the dimension of the state vector, and 'm' and 'l' are the numbers of inputs and outputs, respectively. The state vector  $x(t)$ , contains the displacements and velocities of all degrees of freedom (DOFs), and  $y(t)$  is the response of the structure to a given input  $u(t)$ .

In real life, measurements are taken at discrete-time instants, and for system identification these measurements need to be fitted in a discrete time model. The equivalent discrete-time state space model is obtained by discretizing the set of equations for continuous-time state space model, represented by Equation (2.7) by making a Zero Order Hold (ZOH) assumption, which says that the input is piecewise constant over the sampling period:

$$\begin{aligned}x_{k+1} &= A x_k + B u_k, \\ y_k &= C x_k + D u_k,\end{aligned}\tag{2.8}$$

where  $x_k = x(k\Delta t)$  is the discrete-time state vector which contains the sample displacements and velocities while  $u_k, y_k$  are the sampled input and output,  $A$  is the discrete state matrix,  $B$  is the discrete input matrix  $C$ , is the discrete output matrix and  $D$  is the direct transmission matrix (Overchee and Moore 1996).

Combined Deterministic and Stochastic Model:

Measurements on the structures are often contaminated by large amounts of measurement noise, and hence the deterministic models are not able to describe real measurement data and stochastic components must be considered for this purpose. The discrete-time combined deterministic and stochastic state space model is obtained as:

$$\begin{aligned}x_{k+1} &= A x_k + B u_k + w_k, \\y_k &= C x_k + D u_k + v_k,\end{aligned}\tag{2.10}$$

with,

$$E \left[ \begin{pmatrix} w_p \\ v_p \end{pmatrix} \begin{pmatrix} w_q^T & v_q^T \end{pmatrix} \right] = \begin{pmatrix} Q & S \\ S^T & R \end{pmatrix} \delta_{pq} \geq 0,$$

where  $w_k \in R^n$  process is the noise due to disturbances and modelling inaccuracies, and  $v_k \in R^l$  is the measurement noise due to sensor inaccuracy. It is assumed that these noise terms are zero mean white noise vector sequences and  $w_k$  as an input will have dynamic effects on the state  $x_k$  and output  $y_k$ , while  $v_k$  only effects the output  $y_k$ . The symbol  $E$  denotes the expected value operator, and  $\delta_{pq}$  represents the Kronecker delta ( $\delta_{pq} = 0$  if  $p \neq q$ , and  $\delta_{pq} = 1$  if  $p = q$ ).

Stochastic Subspace Model:

Since the lack of input knowledge makes it impossible to distinguish the input term  $u_k$  from noise terms  $w_k$  and  $v_k$ , modelling the input term by the noise term in Equations (2.10), gives the discrete-time stochastic state space model as follows:

$$\begin{aligned}x_{k+1} &= A x_k + w_k, \\y_k &= C x_k + v_k,\end{aligned}\tag{2.11}$$

However, the white noise assumption of these noise terms cannot be omitted. If the assumption is violated, then the input, in addition to white noise, also contains some dominant frequency components, which cannot be separated from the eigenfrequencies of the system and will appear as spurious poles of the system matrix  $A$ .

There are many techniques to implement a system identification algorithm through the Equations (2.11). The stochastic subspace identification algorithm is probably the most advanced method for ambient vibration system identification. The subspace method identifies the state space matrices based on the measurements and by using robust numerical techniques such as QR factorization, singular value decomposition (SVD) and least squares. It may be noted that the QR factorization results in significant data reduction, while the SVD is used to reject the noise (assumed to be represented by higher singular values). Once the mathematical description of the structure (the state space model) is extracted in the state space form, it is straightforward to determine the modal parameter (by eigenvalue decomposition): natural frequencies, damping ratios and mode shapes (Hung and Ko, 2001).

### 2.3 Output-only Identification via Peak Picking Method

This method can be characterized as a spectrum driven identification method that estimates the parameters of a spectrum model from “measured” samples of spectrum matrix. The method is named after the key step of the method: the identification of eigenfrequencies as the peaks of power spectrum.

The method assumes the condition of low damping and well-separated eigenfrequencies to define the spectrum around eigenfrequencies  $\omega_i$  as follow:

$$S_y(j\omega_i) \approx \alpha_i \{V_i\}\{V_i^H\}, \quad (2.12)$$

where  $\alpha_i$  is the scale factor which depends upon four factors: damping ratio, eigenfrequencies, the modal participation factor and the input covariance matrix. Vector

$\{V_i\}$  is the  $i^{\text{th}}$  mode shape. It is obvious from Equation (2.12) that each column or row of the spectrum matrix at an eigenfrequency can be considered as an estimate of the mode shape at that frequency. Therefore it is sufficient to find only one column or row of the spectrum matrix. The half-power bandwidth method is recommended for obtaining damping ratios, as it is able to quantify the sharpness of a resonance peak. It is widely accepted that this method is not a very accurate one. If the basic assumptions (low damping and well separated peaks) are not followed properly, there are high possibilities of getting incorrect results and the method identifies operational deflection shapes instead of mode shapes and for closely spaced modes such an operational deflection shape will be superposition of multiple modes. Further, the selection of the eigenfrequencies can become a subjective task if the spectrum peaks are not very clear, and the eigenfrequencies have to be a subset of the discrete frequency values of the Discrete Fourier Transform (Peters and Roeck, 2001). This method is popular despite the drawbacks because of its simplicity and speed. The only algorithm that is needed is the Fast Fourier Transform to convert time data to spectra.

There are some other algorithms available for output-only identification other than SSI such as Complex Mode Indication Function (CMIF), Instrumental Variable Method (IVM) and Auto Regressive Moving Average (ARMA) which is a classical system identification method. CMIF is the more advanced method which calculates the SVD of spectrum matrix. Initially, the method was used to find modes of a vibrating system under the effect of natural excitations but later it was applied to Frequency Response Function (FRF) and was called complex mode indication function. It is seen that an ARMA model of suitable order can give good representation of a vibrating structure. It composed of two parts: Auto Regressive (AR) part and Moving Average (MA) part. It is deduced from state space model by eliminating the state vector. An IV method is well known because it identifies only AR parameters in a linear way leaving the original model as an ARMA model.

## 2.4 Chapter Summary

An overview of system identification is given in this chapter. Various model structures that are often considered in the system identification context are also discussed. The state space modelling of vibrating structures is also discussed together with the stochastic representations that take the process and measurement noise into account. Algorithms available for identification from output-only data are also discussed briefly. An algorithm available other than SSI, for system identifications such as PPM is discussed briefly.

# Chapter 3

## Interactive System Identification

### 3.1 Introduction

In this chapter, first the current trend of software towards graphical user interface (GUI) is defined. MACEC (Modal Analysis on Civil Engineering Constructions) is explained which was developed by Katholieke University Leuven to perform interactive system identification in a user friendly environment. This program extracts modal parameters from the data obtained from output-only identification technique. Its implementation is discussed briefly in an effort to understand all of the functions of MACEC involved in modal identification of a structure. In the present thesis, modal identification is carried out using both SSI and a traditional PPM via MACEC.

#### 3.1.1 Graphical User Interface (GUI)

Three types of user interfaces are typically used in programming as found by the history of user interface for system identification and control process. Program user interface, command line user interface and graphical user interface. Program user interface involves writing a library of applicable functions for solving a problem, which are then combined to a program. This evolved in the era of low level programming languages. The command line interface allows user to enter commands at the command line. It made writing programs and experimenting with different methods less time consuming. However it was still not easy for a beginner to use toolboxes, which required extensive trainings. Though command line interface was significantly easier and flexible than program user interface, it

had some drawbacks due to the extended syntax, complicated interconnections of commands and the lack of user guidance.

GUI, the most recent interface is made up of graphical objects such as menus, buttons and plots. These are very straightforward to use, by manipulating the three mouse buttons and rare cases involve typing the name of object or data file. The first advantage of this interface is that it obsoletes the dependence upon thick manuals. Functions can be found by browsing through the menus of interface. Secondly, it presents the results graphically and becomes a successful tool for performing varying parameter experiments. It has become popular in the context of system identification, as the user is guided through the interconnections of complicated functions.

### **3.2 Interaction between System Identification and GUI**

Many modal analysis software packages have been developed in the recent past for identification of mechanical systems based on input-output data. Today, some of these packages also have modules for output-only modal analysis (e.g. recent version of LMS CADA-X). Most of the commercial software packages, however, do not provide the user with information about the implementation of the algorithm and are difficult to add one's own developments to (Peeters *et al*, 1999).

MATLAB is a high-level technical computing language. It provides an interactive environment for algorithm development, data visualization, data analysis, and numeric computation. The system identification toolbox, and the frequency domain system identification toolbox offered in MATLAB can be considered as useful tools for data processing, system identification and model validation. It also lets one construct mathematical models of dynamic systems from measured input-output data. It facilitates in analysing and processing the data, determining the most suitable model structure and order, estimating model parameters and validating model accuracy, and viewing the model responses and their uncertainties. All of these tasks can be performed either by using command-line functions or through a graphical user interface (GUI).

The Frequency Domain System Identification Toolbox (FDIDENT) provides specialized tools for identifying linear dynamic single-input/single-output (SISO) systems from time responses or measurements of the system's frequency response. Frequency domain methods support continuous time modeling, which can be a powerful and highly accurate complement to the more commonly used discrete time methods. The methods in the toolbox can be applied to problems such as the modeling of electronic, mechanical, and acoustical systems (Ljung, 2005).

These toolboxes have been used previously in civil engineering to find the dynamic response of a bridge assuming it to be a linear dynamic system. Since these tool boxes offer a mathematical model that best fits the data, but do not provide sufficient information for extraction of model parameters along with increase in model order. There are some MATLAB related third party products, such as the structural dynamics tool box which are capable of mode shape visualization, but since the identification is based on FRFs, they are not suitable for output-only modal analysis. Therefore, the department of civil engineering at Katholieke University Leuven decided to develop their own program for output-only modal analysis, and finally MACEC was developed. MACEC is an acronym of Modal Analysis on Civil Engineering Constructions. MACEC provides a GUI for output-only modal analysis.

### **3.2.1 Implementation of MACEC**

In the past, MACEC has been employed to apply SSI methods to estimate the modal parameters of large-scale structures, such as bridges, excited by an unknown force. Present chapter of the thesis describes the importance of MACEC for determining the dynamic response of micron-scale structural elements, in an effort to extract dynamic characteristic of sensory organs of insects.

MACEC is not a stand alone program and is designed to work within a recent version of MATLAB (5.1 or higher). The advantage of the MATLAB environment is that the program does not need to be compiled and the user is always able to add new features or change the existing code. For installation of MACEC, it is recommended that the whole



directory named MACEC on the CD ROM be copied to the directory where the MATLAB toolboxes are installed. Then MATLAB can be started and the directory must be added to the default path. Now MACEC can be started in the MATLAB command window by invoking “MACEC” to get the main window of MACEC.

#### Data format required in MACEC:

The standard internal file format used in MACEC is called SIT (system identification tool box). The time data for the analysis can be imported into the program in ASCII, DDF or F32 format. DDF files are generated by the data acquisition program DasyLab and F32 is an internal format used in the department of Civil Engineering at K.U. Leuven University. In the present thesis, ASCII format is used.

There are certain specifications required for an ASCII file before it is imported to MACEC. These specifications are well defined in the manual of MACEC version 2.0. A brief explanation of these specifications is given below:

- Each column represents the time data (time series) of one channel. A channel is the data point in scanned object. All channels should have same number of data points; i.e. the time series for each channel has same length. There are different channels for output and input data. In the example below,  $A_1, A_2, \dots, A_N$ , represent time series for channel 1 and so on.

$$\begin{bmatrix} ch1 & ch2 & ch3 & \dots \\ A_1 & B_1 & C_1 & \dots \\ A_2 & B_2 & C_2 & \dots \\ A_N & B_N & C_N & \dots \end{bmatrix}$$

- ASCII files only represent the time data irrespective of other information such as information about channels, sampling frequency, power spectrum density (PSD) specifications, and input/output channels. However, this

information can be applied once an ASCII file is converted to a SIT file, which is the internal format used in MACEC. There are different GUI windows in the program for applying each of these properties.

- The units used in MACEC are different for input and output data. For instance the force applied on a structure is input to a physical system and it is expressed in Newton ( $N$ ). By applying the force acceleration is measured in  $m/s^2$ , which is the output of that system. If data is imported to MACEC in  $m/s^2$  then there is no need to consider sensitivity. However, if the data is imported from analog sensors in “volts” then, MACEC needs to divide the volts by sensitivity. Sensitivity is expressed as  $mv/EU$ , where  $EU$  stands for engineering unit which could be,  $m/s^2$  or Newton ( $N$ ). In short sensitivities are applied to the channels to get correct units, or for scaling, as per requirement.
  
- It is recommended to use “asc” as an ASCII file extension.

### 3.3 Functions of MACEC

MACEC performs three main functions: preprocessing: system identification and visualization. The main window of MACEC is accordingly divided into three sections. “Pre processing”, “Processing” and “Postprocessing”, and each of the functions is carried out in the MACEC main window shown in Figure 3.1. These sections are explained here briefly.

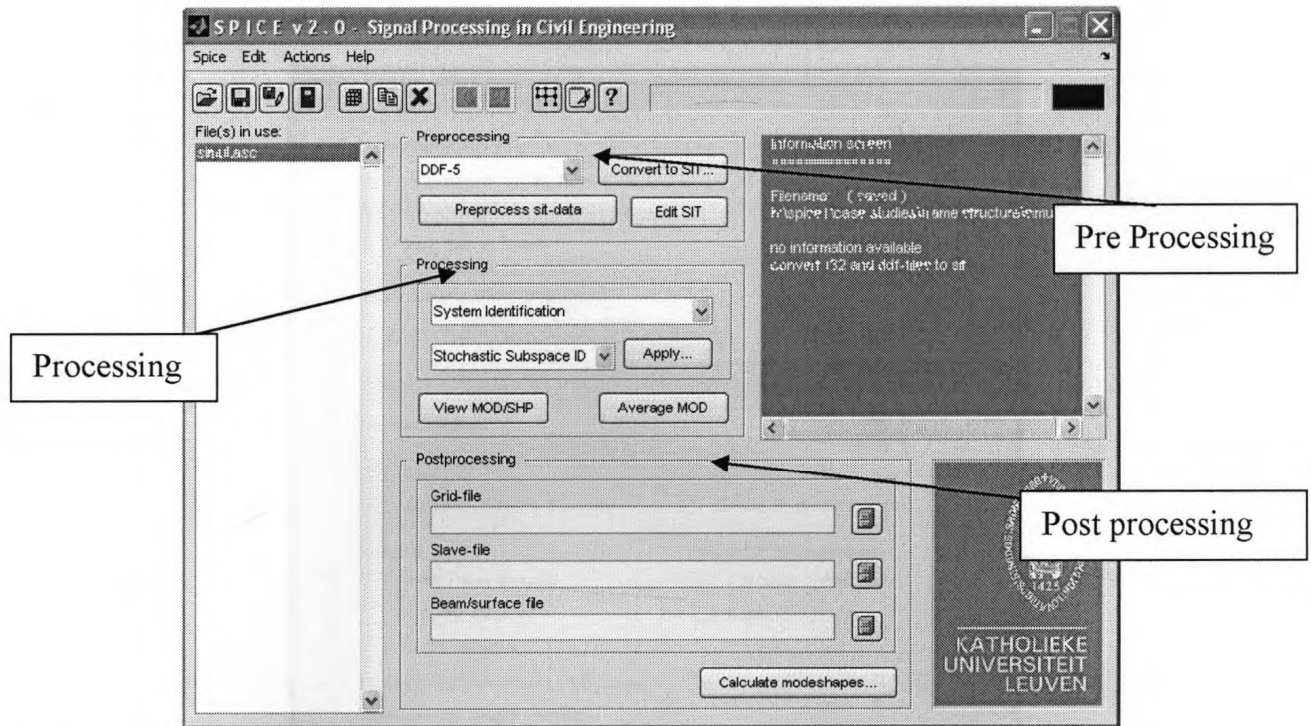


Figure 3.1 MACEC main window shows three different sections i.e pre processing, processing and post processing.

### 3.3.1 Section 1:Pre-processing

Before, the actual pre-processing starts, the data needs to be converted into SIT format, which is the internal format of MACEC. This format contains the time data of different channels along with various specifications, such as sampling frequency, number of channels, PSD length, PSD window, DOF (degree of freedom), etc. Details of this format can be found in MACEC manual version 2.0. A SIT file can be saved as a 32 bit binary file or as an ASCII file. This selection can be made in preferences window of the program as shown in Figure 3.2. Since ASCII files are approximately four times larger than the 32 bit binary SIT file, and only capable of storing data without specification for each channel, the data for the experiments described in this thesis are stored in 32 bit binary SIT format.

An important factor to be considered in SIT conversion is unit correction, as discussed in section 3.2.1. The scaling of data or unit correction is performed by applying sensitivities to each channel to convert data to required units. The button “convert to SIT” as shown in Figure 3.1, leads to a sensitivity window where the unit correction is carried out by “loading” sensitivities and enabling the check box “use sensitivities”.



Figure 3.2 Preference window in MACEC

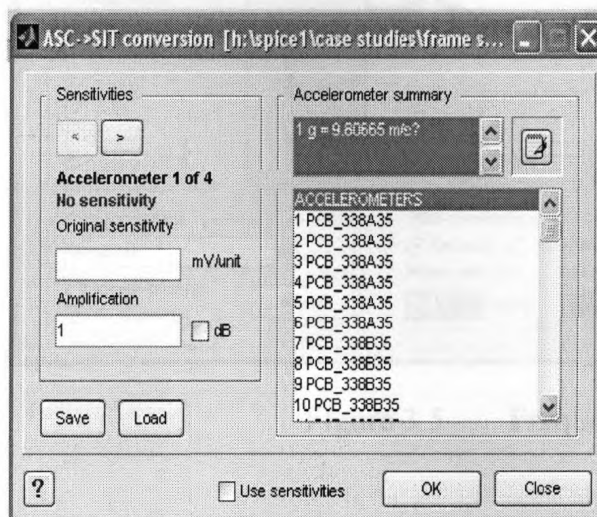


Figure 3.3 MACEC sensitivity window

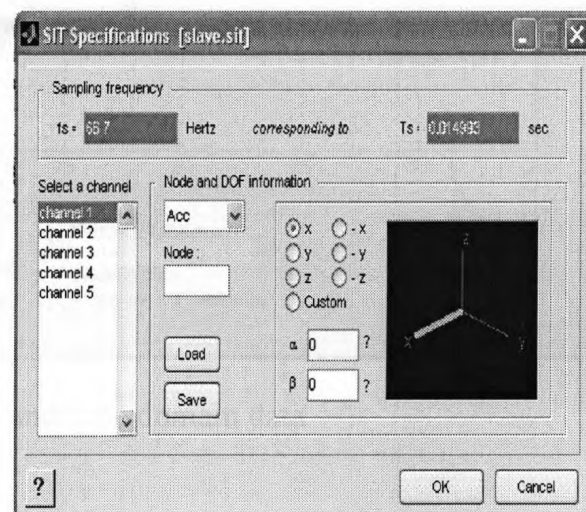


Figure 3.4 SIT specification window

If the data imported in MACEC is already in engineering units ( $m/s^2$ ), then there is no need to load sensitivities. Furthermore, the sampling frequency is entered followed by a

small confirmation dialog box for adding specifications to the created SIT files. A button “edit SIT” as illustrated in pre-processing section of Figure 3.1, creates, “SIT Specification” window. The “SIT specification” window stores information about node number, DOF for each channel, sampling frequency, and sampling time. If the sensitivity axis of a sensor does not coincide with one of the global axes it can be defined with two angles:  $\alpha \in [-180,180]$ , the angle in the x-y plane and  $\beta \in [-90,90]$ , the angle perpendicular to the x-y plane, as shown in Figure 3.4. After providing the specifications to the SIT file, the final step of the first stage, pre-processing, starts once the button, “pre-process SIT data” (Figure 3.1) is pushed to acquire the window that shows PSD spectrum.

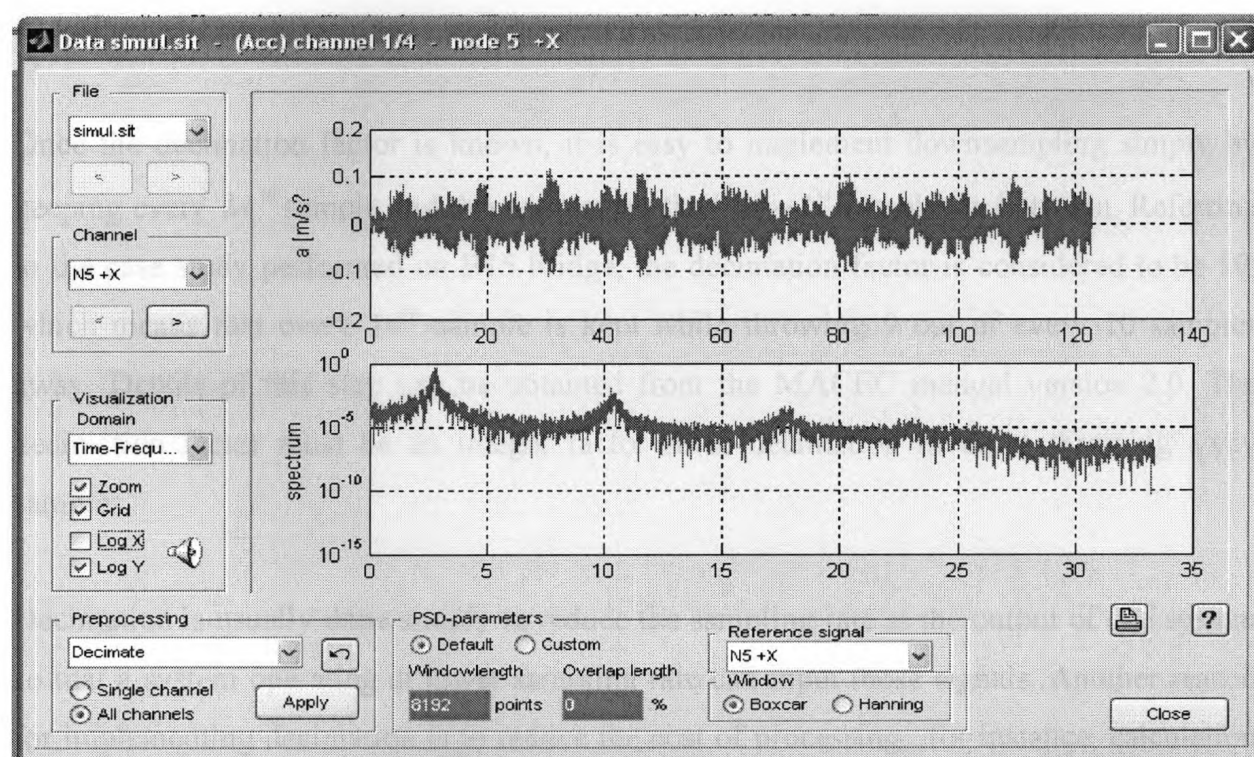


Figure 3.5 Frequency and time domain data

This window provides information about time and frequency domain data. There are three subdivisions under the headings of Visualization, Pre-processing, and PSD-parameters. The selection out of six options given in the drop down menu of “Visualization Domain” is based on the choice of visualizing the time and frequency domain data separately or in the same window. The other three options, coherence, transfer function and coherence



transfer function are not used in this thesis. Use of other check boxes such as zoom, grid, log x and log y under the same heading, illustrated by Figure 3.5, enhances the graphical representation of frequency and time domain data. There are eight options shown in drop down menu, “pre-processing,” out of which Decimation, Delete channel and Detrend are commonly used.

#### Decimation:

Decimation is performed by selecting “Decimate” in the drop down menu and then pushing the button “Apply.” MACEC inquires about the decimation factor by popping up the “Decimation factor” small dialog box. “Decimation factor” is required which is defined as the ratio of input rate to the output rate and usually symbolized by letter “M”, and  $M = \text{input rate/output rate}$ .

Once the decimation factor is known, it is easy to implement downsampling simply by keeping every  $M^{\text{th}}$  sample and throwing away the “ $M - 1$ ” samples in between. Referring to the case study performed on B15 bridge, the decimation factor is considered to be 10, which means that every 10<sup>th</sup> sample is kept while throwing 9 out of every 10 samples away. Details of this step can be obtained from the MACEC manual version 2.0. The decimation factor must be an integer factor since decimation involves throwing away samples.

Decimation is usually done simply to reduce the sampling rate at the output of one system so that a system operating at lower sampling rate can input those signals. Another reason for implementing decimation is to reduce the cost of processing, for instance, calculation of the memory required to implement a DSP (digital signal processing) system is generally proportional to sampling rate, so use of lower sampling rate results in computationally cheaper implementation.

#### Delete channel:

Sometimes data collected in one channel is more noisy and chaotic. In such cases, it is better to delete the complete channel for the improvement of identification results.

Detrend:

This action is mainly carried out in MACEC to remove DC offset components from the data. Mostly it is useful before a Fourier analysis is performed. In the case of a matrix of data this function removes the trend of each column. Generally speaking “Detrend” removes a constant linear or piecewise linear trend from a vector depending upon the command used. In the MATLAB environment we have the following three commands to use this function.

$Y = \text{DETREND}(X)$ : removes the best straight-line fit linear trend from the data in vector  $X$  and returns it in vector  $Y$ . If  $X$  is a matrix,  $\text{DETREND}$  removes the trend from each column of the matrix.

$Y = \text{DETREND}(X, 'constant')$ : removes just the mean value from the vector  $X$ , or the mean value from each column, if  $X$  is a matrix.

$Y = \text{DETREND}(X, 'linear', BP)$ : removes a continuous, piecewise linear trend. Breakpoint indices for the linear trend are contained in the vector  $BP$ . The default is no breakpoints, such that one single straight line is removed from each column of  $X$ .

PSD Parameters:

The Power Spectrum Density (PSD) simply shows the energy of a signal as a function of frequency. It can be computed directly by the FFT (Fast Fourier transform) or by computing the autocorrelation function and then transforming it. The purpose of spectral estimation is to describe the distribution (over frequency) of the power contained in a signal, based on a finite set of data. Estimation of power spectra is useful in a variety of applications, including the detection of signals buried in wide-band noise. As illustrated in Figure 3.5, different PSDs are calculated over the entire length of data with a selected window length and then averaged. Since the default data contains 8192 points, by adjusting the PSD parameters, from default to custom and then entering a window length of 1024 points, eight different PSDs of equal length (1024 points) are computed which are then averaged to give clean signals as depicted in Figure 3.7 from its noisy counterpart as shown in Figure 3.6.

For this example, the overlap is 0 % which means, if first of the eight PSD windows starts at the 1<sup>st</sup> and ends at 1024<sup>th</sup> point, and then the second window will take a successive start at the 1025<sup>th</sup> point covering the next 1024 points and so on.

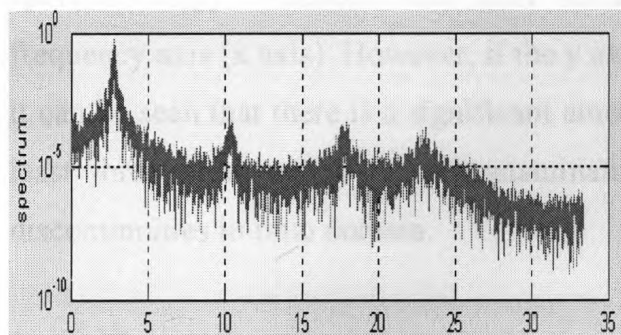


Figure 3.6 Default window length

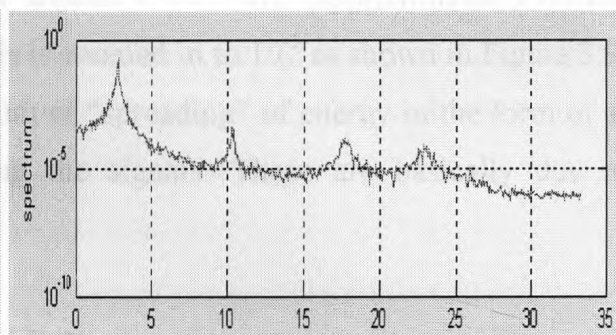


Figure 3.7 Customized window length (1024)

#### Window function:

It is known that in practice a signal is measured for a limited time, and the fact that the FFT only calculates results for certain discrete frequency values. The limit on measurement time is fundamental to any frequency analysis technique and the frequency sampling is peculiar to numerical methods like FFT. Since nothing can be known about the signal's behaviour outside the measured interval, it is the usual practice to assume something about the signal outside the measured interval, and the Fourier Transform makes an implicit assumption that the signal is periodic: i-e. The signal within the measured time repeats for all time.

Most real signals will have discontinuities at the ends of the measured time, and when the FFT assumes that the signal repeats it will sometimes assume discontinuities that are not really present there. Since the sharp discontinuities have broad frequency spectra, these will cause the signal's frequency spectrum to be spread out. The spreading means that signal energy which should be concentrated only at one frequency instead leaks into all the other frequencies. This spreading of energy is called 'spectral leakage'.



To check the spectral leakage in the reference data (Case study from MACEC manual 2.0), removal of the check mark from checkbox of “Log Y” in “visualization domain” as shown in Figure 3.8 is suggested. The spectrum looks like a well behaved single peak occupying a definite place. Although the peak is broad at the bottom (due to leakage), it seems that spectral energy is concentrated more about around  $k= 3.5$  Hz (approximately) on the frequency axis (x axis). However, if the y axis is zoomed in to  $10^{-3}$  as shown in Figure 3.9, it can be seen that there is a significant amount of “spreading” of energy in the form of at least three pronounced peaks contaminating the signals. These are basically due to discontinuities in time domain.

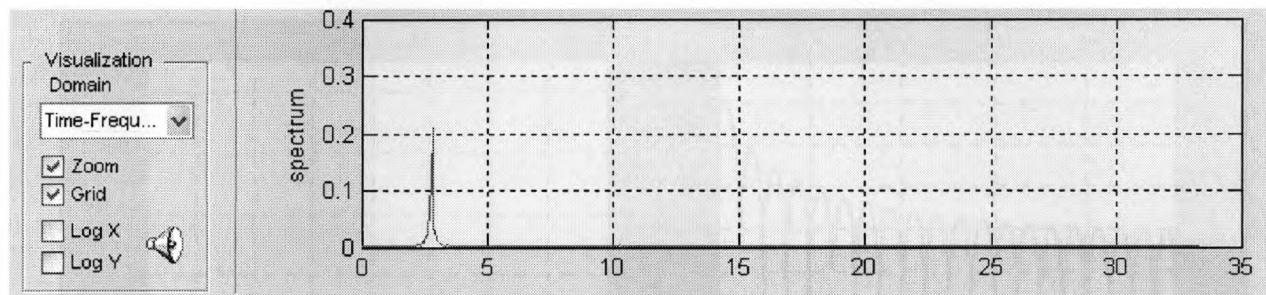


Figure 3.8 Amplitude spectrum of FFT with frequency on x-axis and amplitude on y-axis

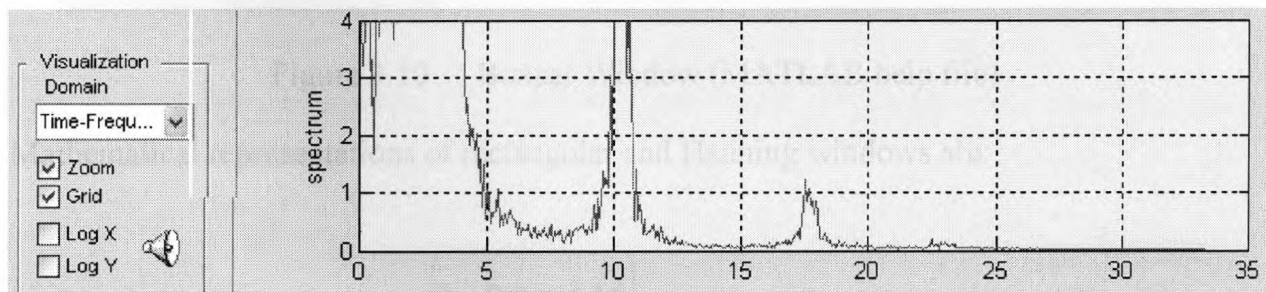


Figure 3.9 y-axis of figure 9 is zoomed in to  $4 \times 10^{-3}$  to show spectral leakage

The effects of spectral leakage can be reduced by reducing the discontinuities at the ends of the signal measurement time. This leads to the idea of multiplying the signal within the measurement time by some function that smoothly reduces the signal to zero at the end points, hence avoiding discontinuities altogether. The process of multiplying the signal

data by a function that smoothly approaches to zero at both the ends is called 'windowing' and the multiplying function is called a 'window function'.

Many different windows have been recommended for this purpose. The choice of suitable one depends on the nature of signal or data and on the type of information to be extracted from its spectrum. In general, a good FFT window has a narrow main spectral lobe to prevent local spreading of spectrum and low side lobe levels to reduce distant spectral leakage. The rectangular (boxcar) window has the narrowest possible main lobe but large sinc function (sine cardinal function) side lobes than the Hanning which has a wider main lobe but smaller side lobes.

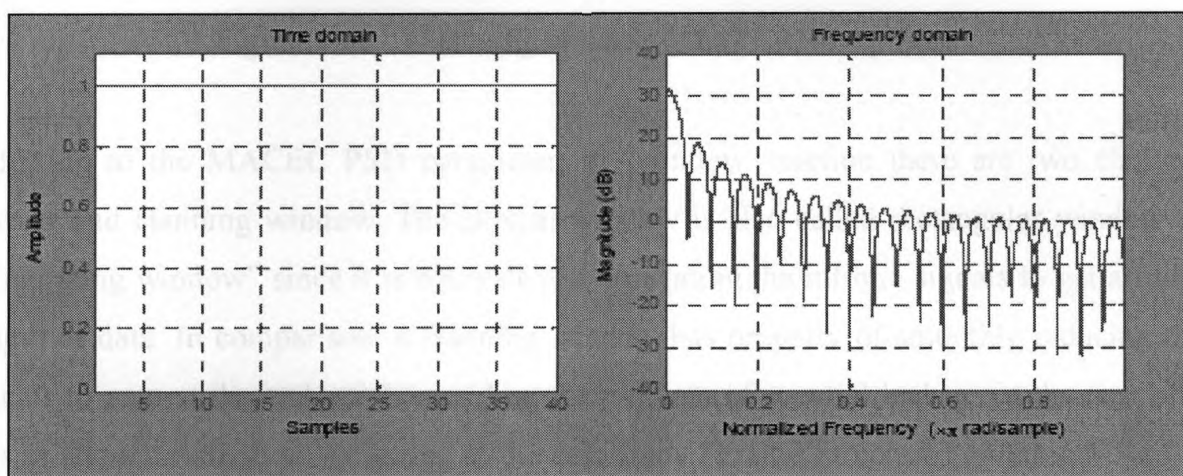


Figure 3.10 Boxcar Window (MATLAB help file)

Mathematical representations of rectangular and Hanning windows are:

$$W(n) = \begin{cases} 1, & 0 \leq n \leq M \\ 0, & \text{otherwise} \end{cases} \quad \text{Rectangular Window ,}$$

$$W(n) = 0.5 - 0.5 \cos\left(\frac{2\pi n}{M}\right) \quad \text{Hanning Window.}$$

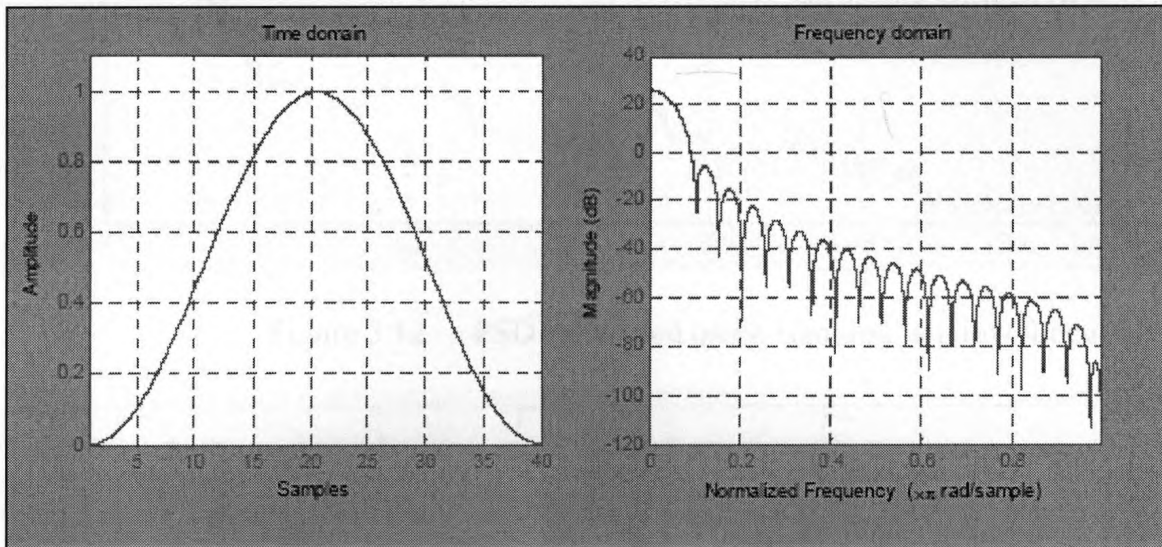


Figure 3.11 Hanning window (MATLAB help file)

Referring to the MACEC PSD parameter, in “window” section there are two choices, Boxcar and Hanning window. The Boxcar window is also called rectangular window or “do nothing window” since it is equivalent to truncating the infinite signals to get a finite length of data. In comparison, a Hanning window has property of smoothly reducing the signals to zero at the end points avoiding the problem of spectral leakage at the cost of a loss of some information. Referring to the case study “Frame Structure” given in MACEC manual 2.0, Figures 3.12 and 3.13 represent two power spectrums with application of Hanning and Boxcar window functions, respectively. It can be observed that there is no significant difference between two plots except that the plot with Hanning window function application as depicted in Figure 3.12 results in cleaner signals. However, it is suggested to check results with both the windows.

It is recommended to save the SIT file, so that it can be used later on, if the program has to stop for any reason. By the end of step 1, a SIT file is ready for system identification which is to be performed in step 2.

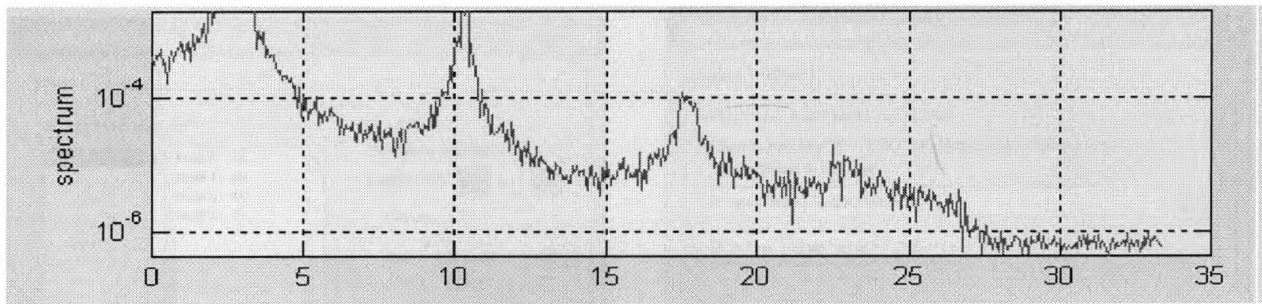


Figure 3.12 PSD calculated using Hanning window function

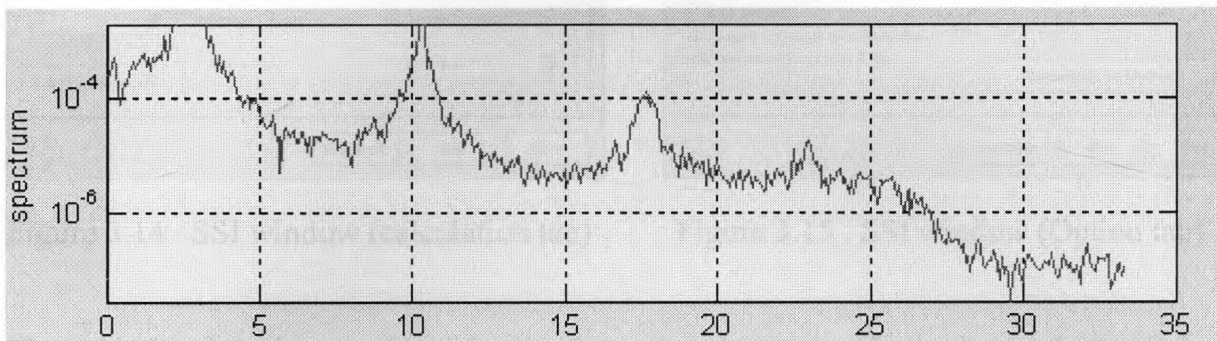


Figure 3.13 PSD calculated using Boxcar Window function

### 3.3.2 Section 2: Processing

The second section in MACEC's main window is "Processing". The Processing section starts with system identification, either by selecting Stochastic Subspace Identification Method (SSI) or Peak Picking Method in the drop down menu.

#### Stochastic Subspace Identification

In SSI, the user has to define some input parameters for the algorithm, such as one or more reference channels, expected model order, and a model order range. After some computation (QR factorization and singular value decomposition), a stabilization diagram is constructed which is then used to extract the modal parameters from identified state space model.



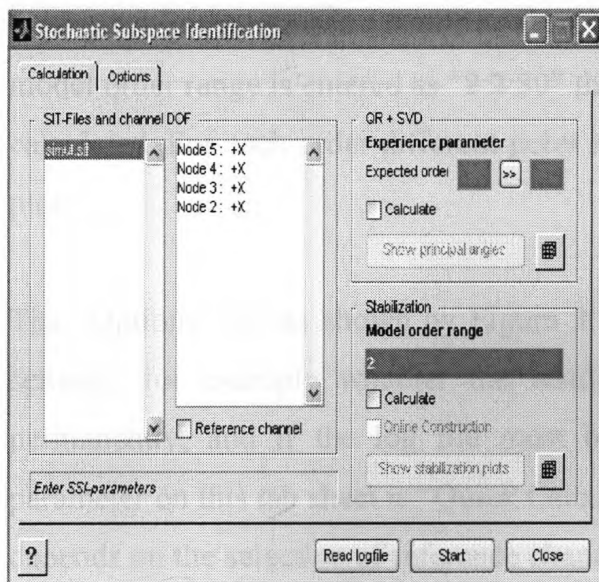


Figure 3.14 SSI window (calculation tab)

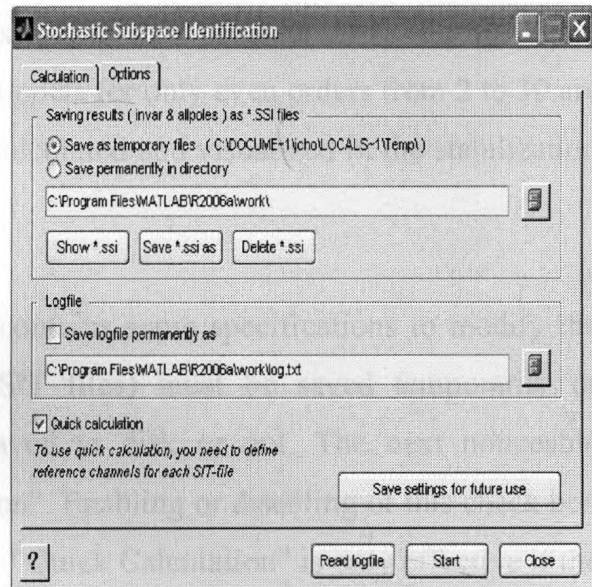


Figure 3.15 SSI window (Option tab)

The “Stochastic subspace Identification” window has two tab sheets: “calculation” and “options”. The Calculation tab sheet has three divisions: (a) “SIT files and channel DOF” section (b) “QR + SVD” section and (c) “Stabilization” section as shown in Figure 3.14. First section stores information regarding SIT files and their detail in terms of DOF. The operations, QR and SVD are two different methods of matrix decomposition. Subspace identification algorithms are as fast as the classical identification method such as PEM (Prediction Error Method), despite the fact they use QR and SVD. One of the important reasons for this could be that they are non-iterative.

The next input in second division of the ‘calculation tab’ is the experience parameter shown in Figure 3.14. The expected model order is 8 because four peaks can be seen in PSD plots illustrated by Figure 3.7, the expected model order being twice the number of peaks. Then the pass-over button can be used to calculate the experience parameter, which comes out to be 12. The formula behind the calculation of experience parameter is:

$$\text{Experience parameter} = (\text{expected order}) \times (6) / \text{number of reference channels}$$

$$8 \times 6 / 4 \text{ channels} = 12$$

One user input that needs to be provided in the stabilization section is the “Model order range”. If the model order range is “2:30”, the system model, calculated with an

experience parameter of 12 will be used to extract models of order 2, 3, 4... 30. If the model order range is entered as "2:2:30" then models for only even orders from 2 to 30 are calculated. For each order different poles are calculated and visualized in the stabilization plot.

The "Options" tab as shown by Figure 3.15, contains some specifications to modify the settings, for example whether the results (SIT files) must be saved temporarily or permanently, and if the log file must be saved to disk or not. The next noticeable parameter on this tab sheet is "Quick Calculation". Enabling or disabling of this check box depends on the selection of reference channels. "Quick Calculation" is only effective if the "reference channel" check box is selected in the "calculation" tab, otherwise all channels are considered to be references. By selecting some reference channels, the other channels, will be partly omitted in the identification process, resulting in faster computation without losing any accuracy provided that the references are well chosen.

Again considering the "calculation" tab sheet, the two "calculate" check boxes must be enabled and the start button must be pressed. Then "show principal angles" must be invoked. There is a remarkable discontinuity between order 8 and 9 which indicates that real model order is situated at 8 as seen from Figure 3.16. This gap is not as obvious in real life measurements so these plots are difficult to interpret and not always very useful, but in some cases they help to approximate the model order of measured data.

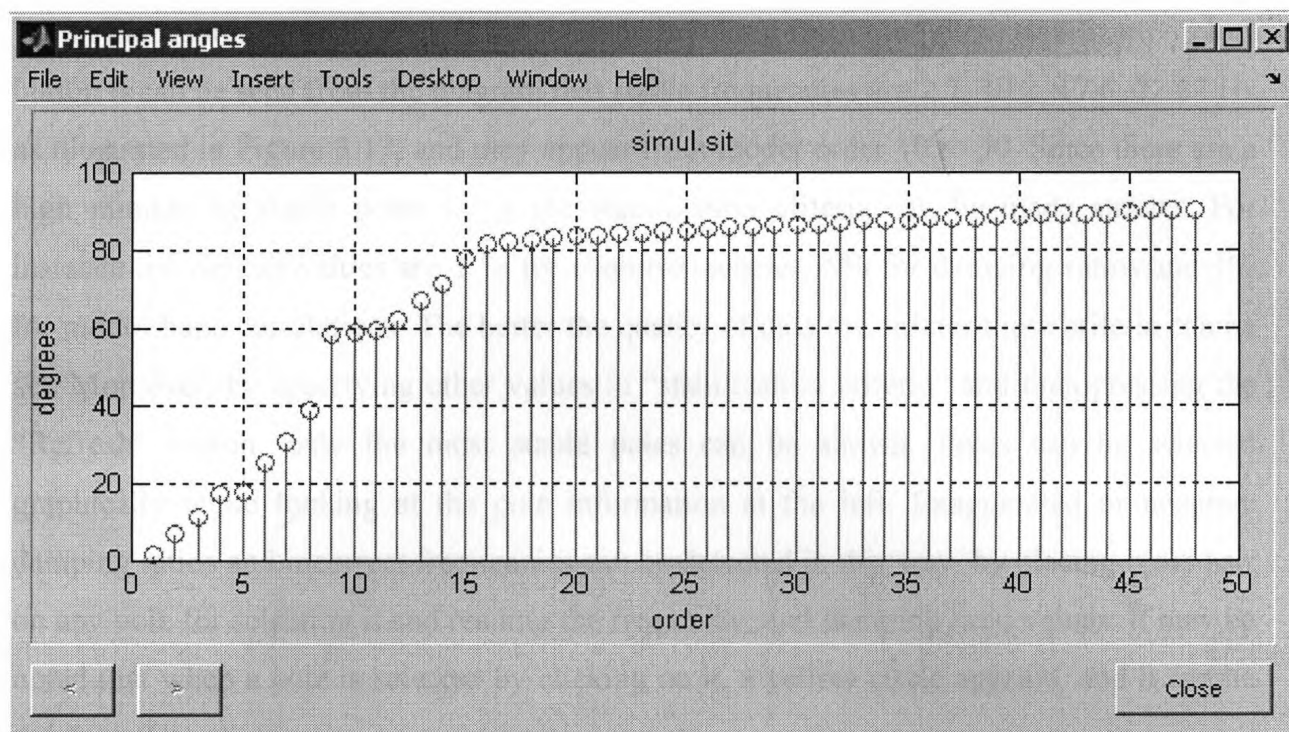


Figure 3.16 Principal angles illustration from MACEC

Since the criterion for estimating the model order by looking at the gap between two successive singular values is not very useful most of the time, as in most practical cases there is no gap, a stabilization diagram is needed as a tool to identify the real poles (modal frequencies) by visualization. It contains the poles identified by any identification algorithm and helps in distinguishing the real poles from the spurious ones. In this case repeated analysis of the same data set is performed, each time for a different model order resulting in poles corresponding to that order. The poles of the model of order  $n$  are compared to the poles of the model of order 1. If the differences in eigenfrequencies, damping ratios and mode shapes (or model participation factors) are within the preset limit of stabilization criteria, the pole is labelled a stable one. For instance the default stabilization criterion employed in MACEC suggests limits of 1% for eigenfrequencies, 5% for damping ratios and 1% for modal vectors. In the stabilization diagram shown in Figure 3.17, the pole values from each analysis are combined in one single plot, with the horizontal axis (X-axis) the pole frequency, and the vertical axis (Y-axis) the solution order. The pole is indicated by a symbol  $\oplus$  (blue colour), although not visible in this diagram. The idea behind the comparison is that the real poles corresponding to physical system appear at nearly identical locations for every analysis.



When the stabilization diagram is obtained by invoking from the “show stabilization plot” button it can be seen from the diagram that stable frequencies are 2.7, 10.2, 17.6, 22.87 Hz, as illustrated in Figure 3.17, and they appear from model order 10 to 30. Since there are a high number of stable poles ( $\oplus$ ), the stabilization criteria can be made stricter. For instance the default values are 1 % for eigenfrequencies, 5% for damping ratios and 1% for mode shape correlations. The better the quality of data the stricter these criteria can be set. Moreover, by specifying other values in “stabilization criteria” and then pressing the “Refresh” button, only the most stable poles can be shown. Poles can be selected graphically while looking at the pole information at the left. Exaggerated or negative damping ratios and incorrect frequencies can be detected in this way, by placing cross hair on any pole for selecting it and reading the frequency, and damping ratio values. It may be noted that when a pole is selected by clicking on it, a yellow circle appears, and it can be deselected by clicking it again.

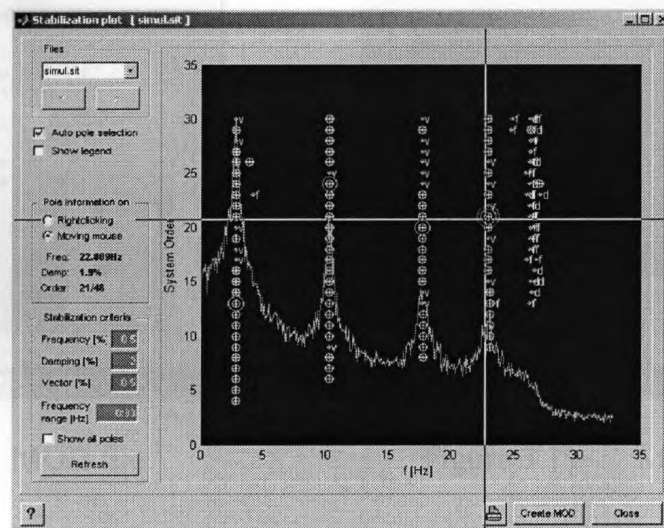


Figure 3.17 Stabilization diagram from MACEC  $\oplus$  stable poles,  $v$  stable vector,  $f$  stable frequency,  $d$  stable damping and  $o$  pole.

After selecting the stable poles, next step is to create a “MOD file. This file can be created by using “create MOD” shown in Figure 3.17 and a suitable name can be given to this file at this stage (which can be seen in file list box of MACEC’s main window). A quick check for satisfactory pole selection can be made by looking at the representation of mode shapes in the complex plane, as shown in the top right of the “MOD-view” window in



Figure 3.18. Real modes will always have same phase angles for all components. If the results are not good, some of the selected poles can be changed in the stabilization diagram and the MOD file can be overwritten.

The mode shapes of this MOD file can be viewed by clicking the “view MOD/SHP” button in the second section of MACEC’s main window. The “quick movie” feature of the “MOD-view” window facilitates viewing of the animated mode shape as illustrated in Figure 3.19. The “average MOD” button that is located next to “view MOD/SHP” button is used for averaging the MOD files of the same setup for ease and saving of time. The files which are needed to be averaged are selected first and then the “average MOD” is pressed to perform the averaging. A new name for the resulting averaged MOD file can now be typed.

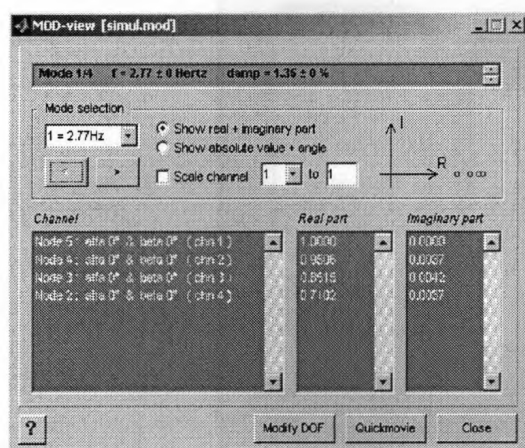


Figure 3.18. MOD file

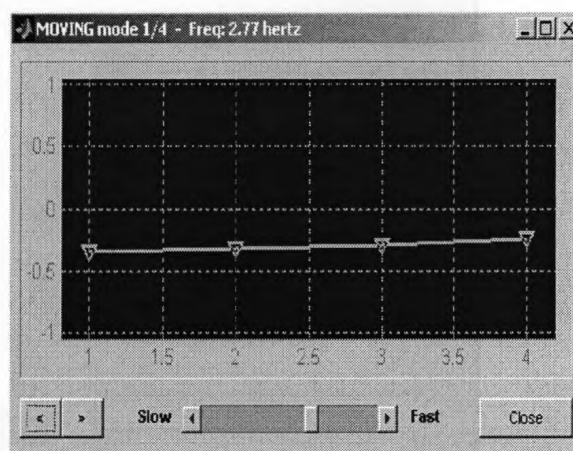


Figure 3.19 Moving Mode

### Peak picking Method:

This method has been briefly described in chapter two. As the name suggests the method identifies the eigenfrequencies as the peaks of spectrum plots. The “peak picking” window illustrated in Figure 3.20 is obtained by selecting the peak picking operation for system identification in MACEC’s main window. In this method it is necessary to select a “reference accel” (reference accelerometer) for every file, then select all the channels and press “calculate and show ANPSD” to get an “average normalized psd” window as shown in Figure 3.21. On this window, the mouse pointer changes into a cross-hair and user can

pick the peaks, then press “confirm frequencies”, to get “selected frequencies” in the main “peak picking” window.

Now the “start” button can be pressed under “calculate and show ANPSD”, in the main “peak picking” window to get a MOD file in the list box of MACEC’s main window. The MOD file can be selected and “calculate Mode shapes” can be invoked to view the results, after going through the post-processing operation which is described in section 3. The MOD files generated in the peak picking method contain no damping ratios because this property is not supported in peak picking window of the MACEC. The mode shape components are not complex but rather they are forced to represent real modes.

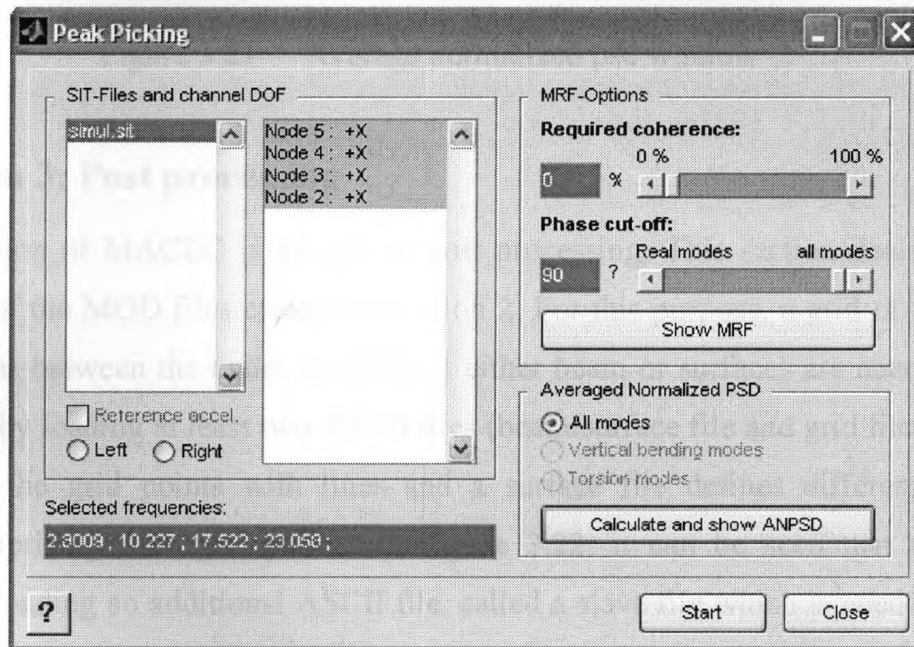


Figure 3.20 Peak picking method window

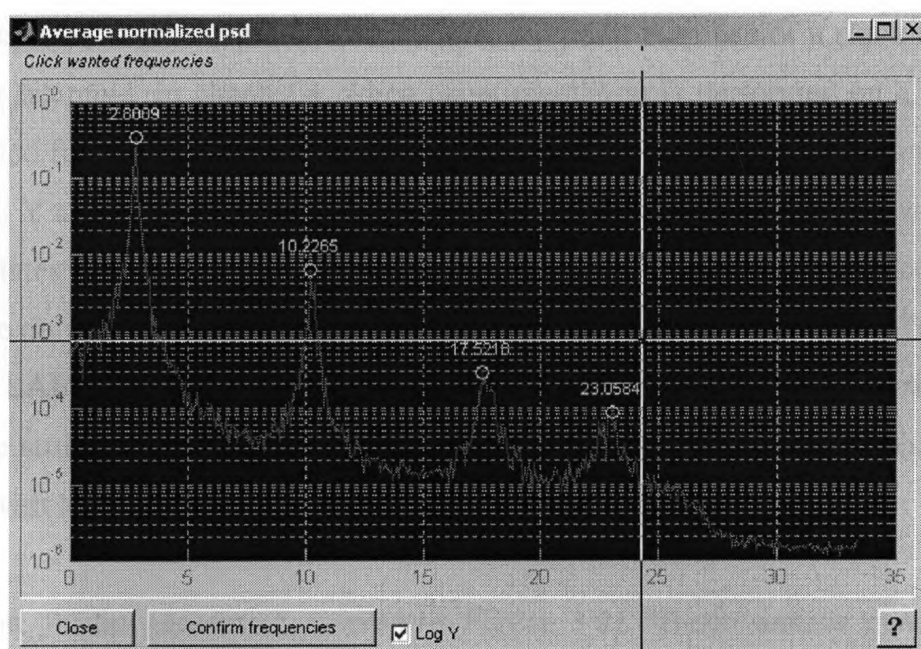


Figure 3.21 Average normalized psd window

### 3.3.3 section 3: Post processing

The third section of MACEC is known as post processing. This section deals with the visualization of the MOD files created in section 2. For this purpose, a grid of nodes and the connections between the nodes in terms of either beam or surfaces are needed. It can be performed by loading at least two ASCII files (beam/surface file and grid file). A beam file connects the grid points with lines and a surface file defines different surfaces (patches) comprising four grid points. In Figure 3.22, it can be seen that there is a provision for loading an additional ASCII file, called a slave file which is needed for 2-D representation of some structures. The unmeasured slave DOFs are related to measured master DOFs through a “slaving” procedure, for visualization of unmeasured DOFs. In the case study considered, a slave is created with five columns as depicted in Table 3.1. This table shows that node 7, X direction is one times X direction of node 2. The directions are 1, 2 and 3 for x, y and z axis:

Table 3.1 Structure of a slave file

Node # 1	Direction of Node # 1	Scaling factor	Node # 2	Direction of Node # 2
7	1	1	2	1

It may be noted that, if the data is measured at every point then use of a slave file is not necessary. For example, in chapter 4, when experimentation is performed on a beam, no slave file is used for visualization of the beam. The grid file contains four columns: node number and X, Y and Z coordinates. For example, [5 0 0 8] stands for node 5, with zero X and Y coordinates and eight as a 'Z' coordinate. The beam file contains two columns: a MATLAB line object is defined by two nodes; a surface file has four columns: four nodes define a MATLAB patch object. Selection between beam and surface files depends upon visualizing the structure as moving lines or moving surfaces. All of these files can easily be generated with MACEC beam/surface generator in the main manu bar.

By clicking on “beam generator” a window Figure 3.22 “Beam/surface generator for spice” appears which has three sections on its right hand side: “Manually entered” “Beams” and “surfaces”. Data can be entered manually in the first section. In the other two sections there is a provision to define two nodes, the first and the last nodes of any structure while the intermediate nodes will automatically be filled out by pressing the pass over button. After loading the three visualization files, selecting the MOD file and pressing the “calculate mode shapes” button, the mode shapes can be viewed. In the case of different MOD files corresponding to different setups, these are glued together to make one global file describing the whole structure with the help of reference sensors common to all setups. Common sensors are automatically detected by MACEC. The results can be saved by creating a SHP file which is performed by pressing “create SHP” button and giving an unused name to the specific file.

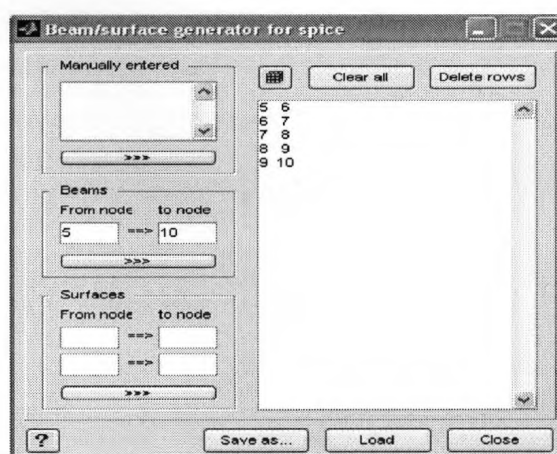


Figure 3.22 Beam Generator



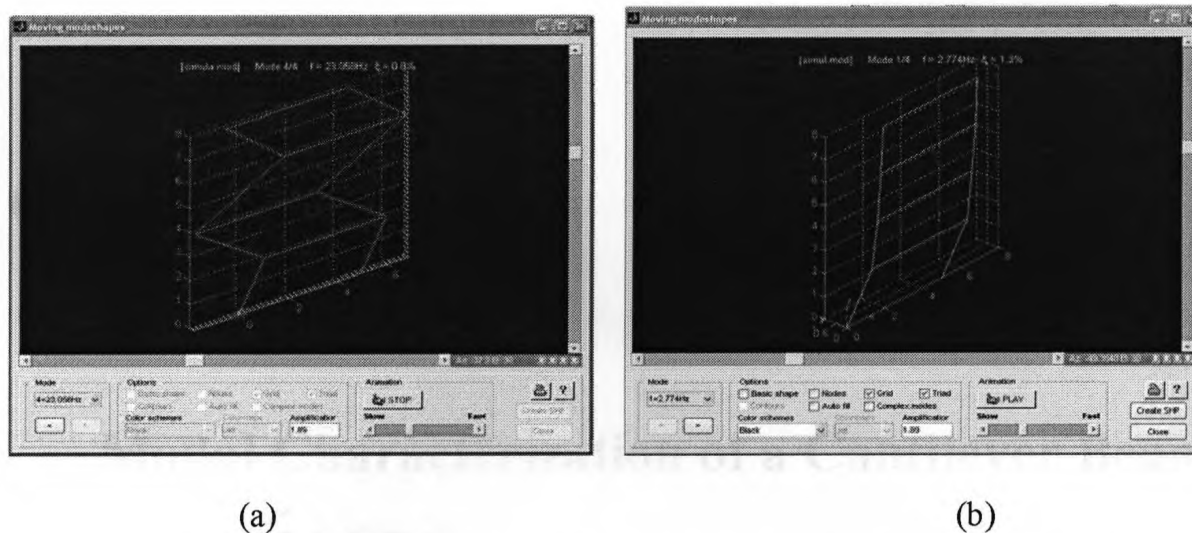


Figure 3.23 (a) Mode 1, (b) Mode 2 taken from SSI MACEC case study "Frame Structure" MACEC manual 2.0

### 3.4 Chapter Summary

In the context of system identification, the importance of GUI driven tool boxes is defined. Development of MACEC is defined briefly. Its implementation for identification of real data is also explained. An effort is made to clarify all of the functions and identification algorithms used in MACEC. An example is taken from a case study described in MACEC manual 2.0, to explain the functions involved in identification of frequencies and mode shapes. This chapter is envisaged to serve as a reference manual for the experiment to be performed on micron scale-structures, and are utilized in all of the experimentations described in the forthcoming two chapters.

# Chapter 4

## Modal Characterization of a Cantilever Beam using MACEC

### 4.1 Introduction

In the past, Modal Analysis on Civil Engineering Constructions (MACEC) has been primarily used for modal characterization of large-scale civil structures such as buildings and bridges. In the present chapter, application of MACEC would be validated for experimental modal identification of a meter long cantilever beam. This validation process is essential to ensure that the measurement process and equipment employed, yield suitable data that can work with MACEC. To this end, particular attention is given to the signal generation process and the non-contact Laser Doppler Vibrometry (LDV) measurements. This process is then used for experimentation on micron-scale structures which is presented in chapter 5. The methodology developed to perform experiments on macro-cantilever beam is composed of the following steps:

- Perform non-contact measurement for acquiring transverse velocity and Frequency Response Function (FRF) employing LDV.
- For output-only experiments, export time data (velocity) into MACEC for modal characterization of the beam via Stochastic Subspace Identification (SSI) and Peak Picking Method (PPM) and visualization of mode shapes.

- For input-output experiments, collect FRF from Polytec PSV software that controls LDV.
- Compare the results obtained from theoretical calculations, output-only experiment and input-output experiment.

For this purpose, a cantilever beam model was considered. First a numerical simulation was performed by means of the Finite Element Analysis (FEA COMSOL package). Four different sets of physical experiments were then conducted in the laboratory environment. A Laser Doppler Vibrometer (LDV) was employed as a data collecting device. Modal parameters (eigenfrequencies, mode shapes and damping ratios) were extracted via MACEC. To validate the LDV results, another experiment was performed on the same beam but with different conventional methods using accelerometer to acquire vibration data. The results obtained from simulation and physical experiments, were compared with analytical results obtained from the elementary beam, Euler-Bernoulli theory (differential equations representing transverse vibration of a cantilever beam).

## 4.2 Cantilever Beam Model

The theory of elasticity provides the basis for deriving the governing equations to describe the dynamic behaviour of beams. Several theories are presented for modelling the transverse vibrations of beams depending upon different assumptions. For instance, Timoshenko theory considers bending, shear deformation and rotary inertia and their joint contribution (Karnovsky and Lebed, 2004).

The beam model for the present thesis is based on Euler-Bernoulli Theory, which considers bending only (Karnovsky and Lebed, 2004). It takes into account the inertial forces due to the transverse translation and neglects the effect of shear deflection and rotary inertia (Clough and Penzien, 1975). The assumptions that compose the Euler-Bernoulli Theory of Beams are (Inman, 2001): (i) Uniform along its span or length and slender, (ii) Composed of a linear, homogeneous, isotropic elastic material without axial loads, (iii) plane sections remain plane, iv) plane of symmetry of the beam is also the plane of vibration so that the rotation and translation are decoupled and (v) rotary inertia

and shear deformation can be neglected. Under these assumptions the frequency equations used to calculate the analytical natural frequencies of a cantilever beam with fixed-free boundary conditions take the form (Inman, 2001):

$$\omega_n = \beta_n^2 \sqrt{\frac{EI}{\rho A}}, \quad n=1, 2, 3, \dots \quad (4.1)$$

where  $\beta_n l$  gives weighted natural frequencies. The first three values for  $\beta_n l$  are 1.87510407, 4.69409113 and 7.85475744. In Equation (4.1),  $E$  represents Young's modulus while  $I$  denotes the area moment of inertia and  $A$  the beam cross sectional area of the beam.

#### 4.2.1 Description of the Beam Model

The cantilever beam as shown in Figure 4.1, is selected for physical experiments and FEA simulation. The beam has been assumed to have following dimensions: Length ( $\ell$ )=0.996 m, Width ( $w$ )=0.0381 m, thickness ( $t$ ) = 0.0048 m and material properties: Young's modulus of elasticity for steel ( $E$ )=2.05 X 10<sup>11</sup> N/m<sup>2</sup>, density ( $\rho$ )=7850 kg/m<sup>3</sup> and area moment of inertia ( $I$ ) = 3.5113 X 10<sup>-10</sup> m<sup>4</sup>. A setup for a typical experiment is shown in Figure 4.2.

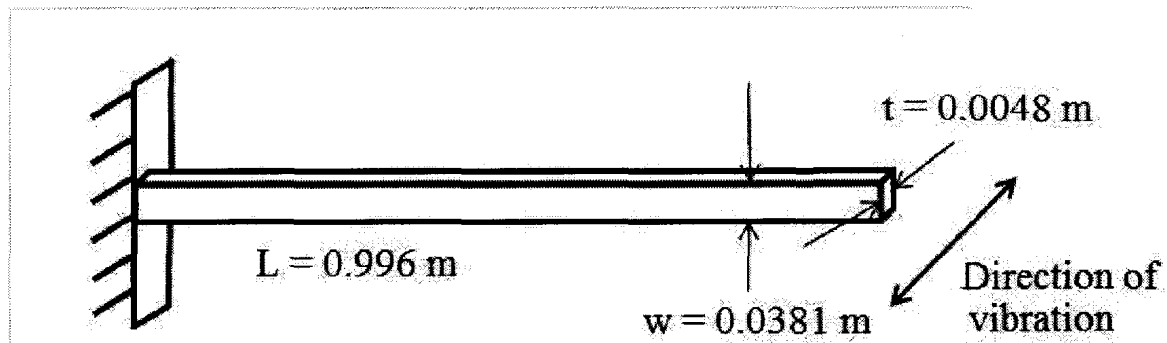


Figure 4.1 Cantilever beam used in experiments



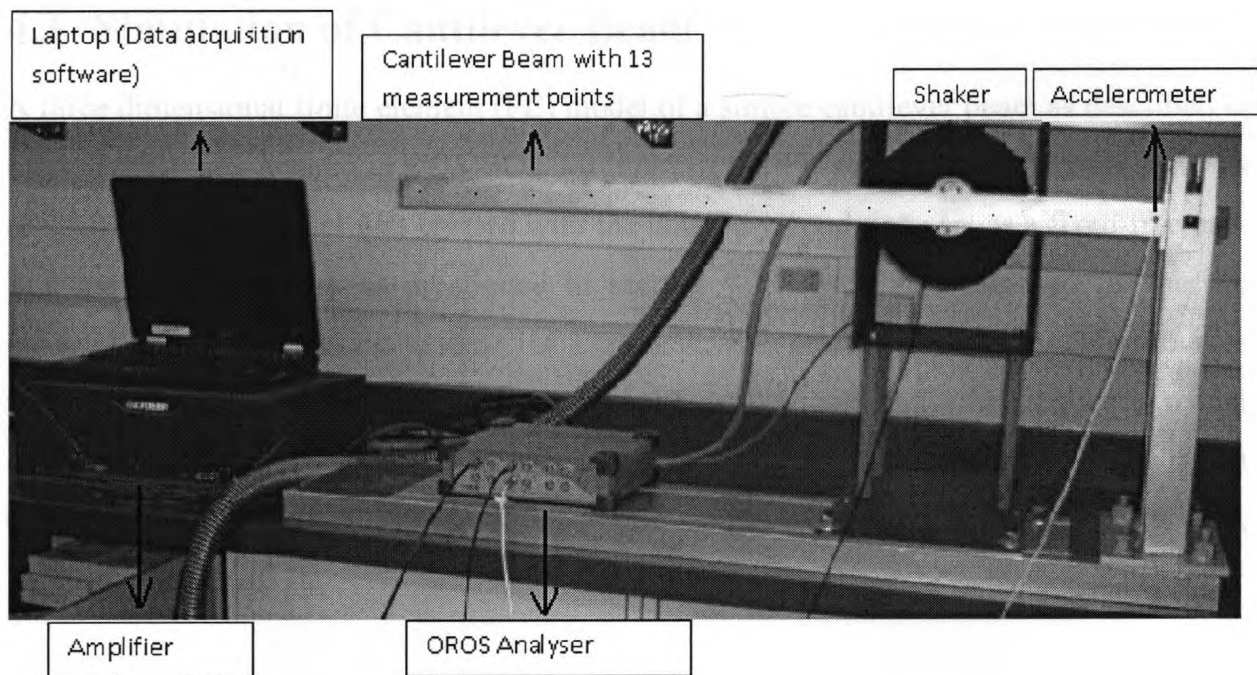


Figure 4.2 Setup for a typical experiment

### 4.2.2 Analytical Results

The first three natural frequencies of the beam, determined by substituting values in Equation (4.1) are: 4.0 Hz, 25.06 Hz and 70.18 Hz. It may be noted that these theoretical values may be subjected to some errors due to uncertainties in material, dimensions and boundary conditions, for example, non-uniformity in density ( $\rho$ ) of the beam material, imprecision in dimensions of the beam taken from vernier calliper and measuring tape, and, imperfect validation of boundary conditions. The fixed end of the beam is assumed to be clamped. Practically the clamp is not perfectly rigid, and there is a chance of deformation due to clamp loosening that can also bring error.

Owing to the above motioned errors, these theoretical values of natural frequencies may not exactly match those obtained from the experiments. However, these values can provide a meaningful comparison for the experimental results and to gain confidence on the experimental data analysis procedures as well as MACEC.

### 4.3 Simulation of Cantilever Beam

A three dimensional finite element (FE) model of a simple cantilever beam as described in section 4.2.1 was created in COMSOL Multiphysics, a FE software for dynamic analysis of structures. The model was created with the boundary conditions set as a fixed-free end. The material properties as mentioned in section 4.2.1 were also imposed. A specific module, 'structure dynamic module' of COMSOL was employed. This module provides tools for fundamental structural mechanics applications and performs frequency modal analysis. Different mode shapes are viewed by running eigenfrequency analysis in COMSOL. The first three natural frequencies obtained from COMSOL are: 3.90 Hz, 24.10 Hz and 69.40 Hz.

### 4.4 Physical Experiments on Beam

This section discusses four different experiments to develop a methodology for further work on submillimeter size cantilever beams and mechanoreceptor hair on insect's body which are of order of microns in size. In addition, MACEC is practically validated as a modal identification program for macro and micro size structural elements. Two different types of experiments are performed, i.e. input-output and output-only. One of the four experiments is output-only, based on time measurements while the other three are input-output and measurements taken during these three modal tests are based on frequency response function measurements (FRF).

A brief outline of these experiments is given below:

**Experiment 1:** The first experiment is based on the most conventional instrumentation and techniques available for acquiring frequency response measurements. This type of modal testing is known as frequency response function method, which measures the input excitation and output response simultaneously.

**Experiment 2:** It is also an input-output experiment where acceleration is measured with accelerometer mounted on the vibrating beam.

Experiment 3: It is an output-only experiment, where velocity of the vibrating beam is measured by LDV, while the beam was excited by approximate white noise created using random number generator within MATLAB.

Experiment 4: it is an input-output experiment where FRF is measured employing LDV.

## 4.5 Experiment 1

Experimental setup for the experiment is shown in Figure 4.3. In this experiment, FRF was collected based on transverse vibration measurements, at 13 different points marked on a cantilever beam. It is an input-output experiment.

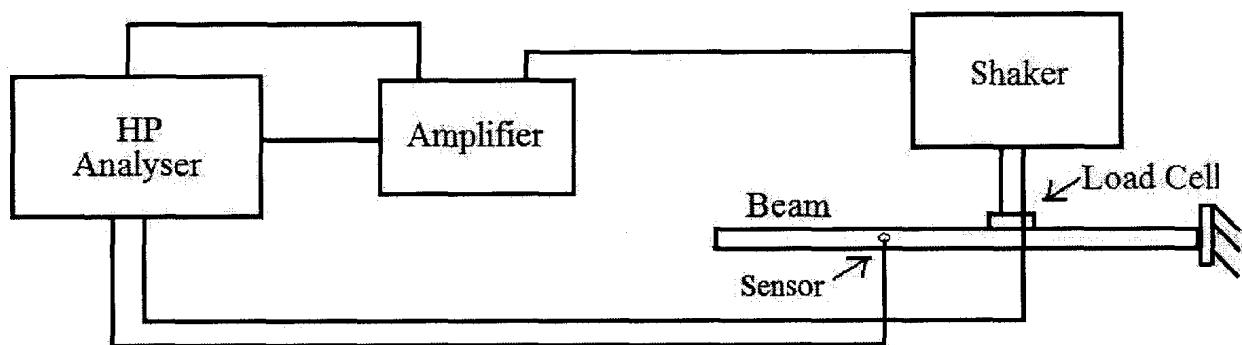


Figure 4.3 Schematic diagrams of the experimental setup for experiment 1

Various equipment used in the experimental procedure are described briefly:

### The signal generator and Analyser

Model HP 35670A Dynamic Signal Analyser is used for generating random signals so that shaker can excite the beam.

### The Signal Amplifier:

The Amplifier used in this experiment is a Crown CE 2000. It is used to amplify signals before they are fed into the shaker.

### The Shaker:

Model number VG65M-6 from Vibration Testing Systems (VTS) is used to vibrate a cantilever beam. It is placed at 270 mm from the fixed end of the beam.

### Load cell:

208CO2 (SN 20183) from PCB Piezotronics is mounted to the shaker with a threaded stud, that measures the force when subjected to vibration.

### The Sensor

A shear accelerometer, model number 353B68 with frequency range 1-10 KHz and sensitivity of 107.6m v/g is used.

### Cantilever Beam:

A 0.996 meter long cantilever beam as described in section 4.2.1 is fixed to the one side with clamps while the other side is kept free.

Random signals (approximate white noise) were generated in HP analyzer, which were then amplified to excite the beam using the shaker. The bandwidth of the signals was set to 200 Hz. The resolution was adjusted to 2 Hz with 400 of Fourier lines with number of averages fixed to 10 averages. Thirteen different sets of FRF were obtained, which were then averaged to create the average FRF spectrum.

The plot shown in Figure 4.4 shows the FRF as a function of velocity and force. The first three natural frequencies extracted from experiment 1 are: 4.50 Hz, 25.0 Hz, and 67.50 Hz. The first three resonance peaks of the vibrating beam are identified approximately at the same frequencies acquired from FEM and analytical results. Similar predictions can also be made from Figure 4.5 which shows the FRF between the acceleration and force.

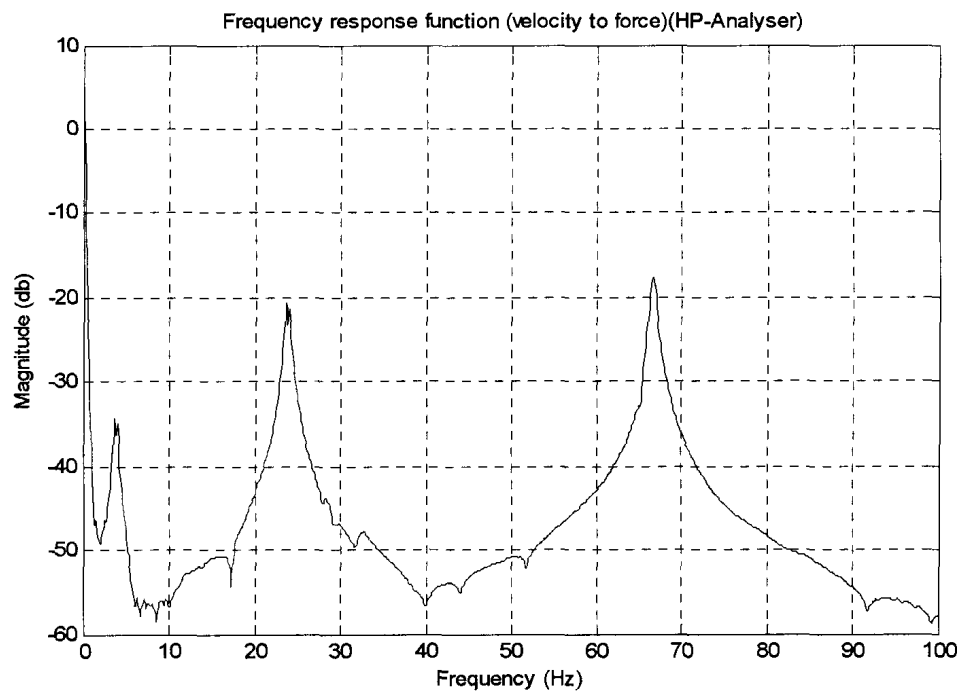


Figure 4.4 FRF from experiment 1, velocity vs Force

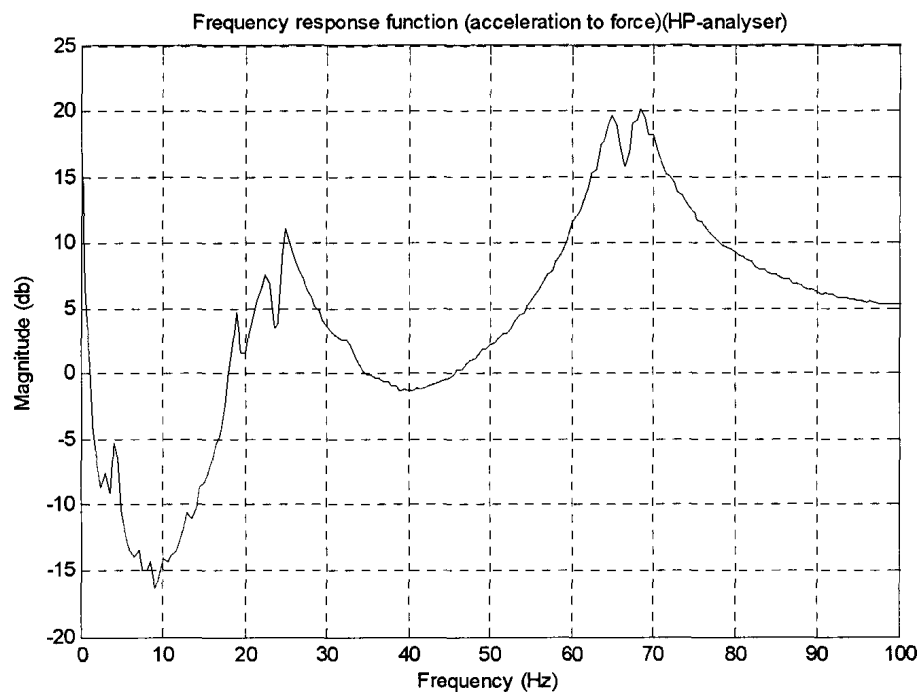


Figure 4.5 FRF from experiment 1, Acceleration vs Force

## 4.6 Experiment 2

In this experiment acceleration is measured with accelerometer mounted on a vibrating beam and the data is collected by data acquisition software NV Gate which works in conjunction with OROS-35. It is also an input-output experiment and Figure 4.6 illustrates the setup used for this experiment.

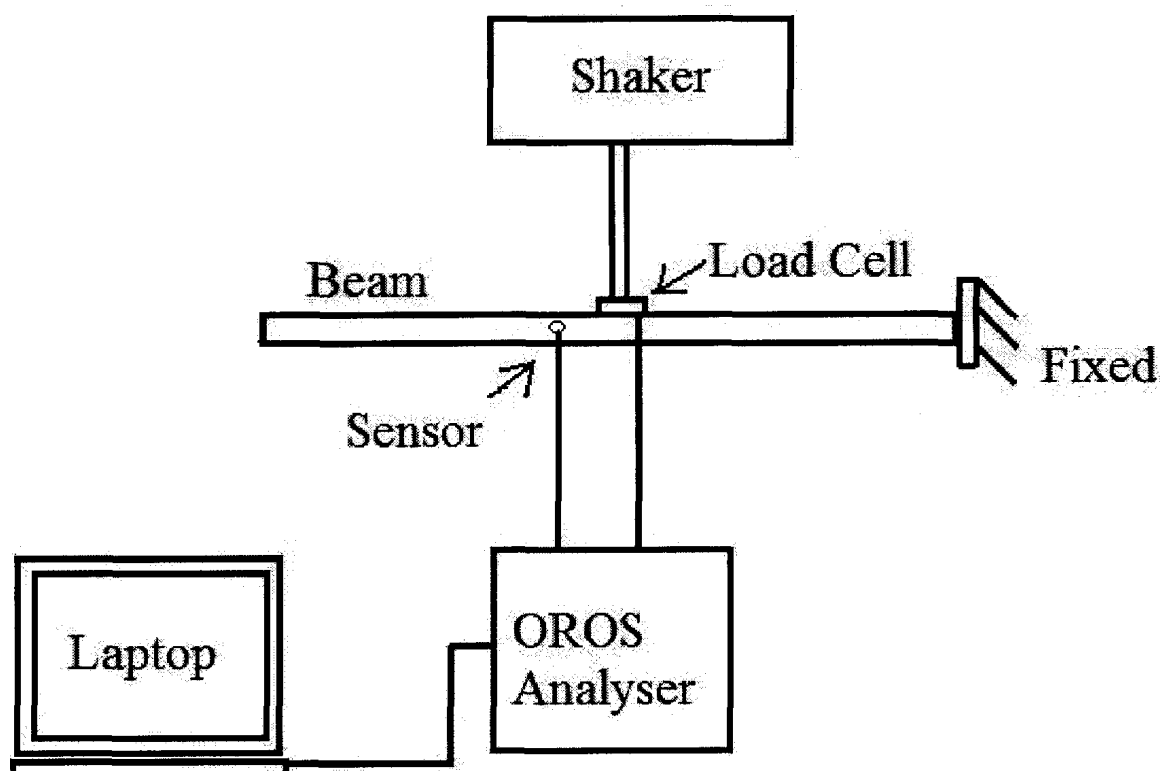


Figure 4.6 Schematic diagram of the experimental setup for experiment 2

The components used in this experiment are same as those used in experiment 1. The additional component used in this setup is given below:

### Data Acquisition Software

NV Gate which works in conjunction with OROS, a PC-based dynamic analyser used for collecting data. The signal amplifier, shaker, load cell, and beam are the same as used in previous experiments.

A band limited approximate white noise was generated using the random number generator within MATLAB. The noise was sampled at 2.048 kHz. It was then low pass filtered at 90 Hz by applying a chebyshev type II filter of order 14. The noise was created for 10 seconds and repeatedly applied on each scan point for 8 seconds to collect time data. The skewness and kurtosis of the noise were calculated as 0.0517, and 2.9406 respectively which are in good agreement with the values for a Gaussian white noise (skewness 0, kurtosis 3). It is further detrended and finally scaled before it is saved as a .txt file. This text file is imported as an input signal in NV Gate software. Figure 4.7 illustrates the time and frequency domain plots of white noise signals.

The signals were amplified and fed to the shaker to generate random input forces to excite the beam. The data acquired from data acquisition software was sampled at 512 Hz which was measured for 8 seconds resulting in 5120 data points. The bandwidth was set to 200 Hz and resolution was 500 mHz with 401 Fourier lines. The position of the sensor was changed for 13 different points on the beam to collect the data. To compare the results obtained from previous experiment, same points were considered on the beam as previously marked in experiment 1. Finally, 13 different data sets were collected which were then averaged to create an average FRF plot shown in Figure 4.8.

The first three modal frequencies of the cantilever beam, obtained in experiment 2 are: 4.0, 24.0 and 67.50 Hz, which match with those determined from the previous experiment.

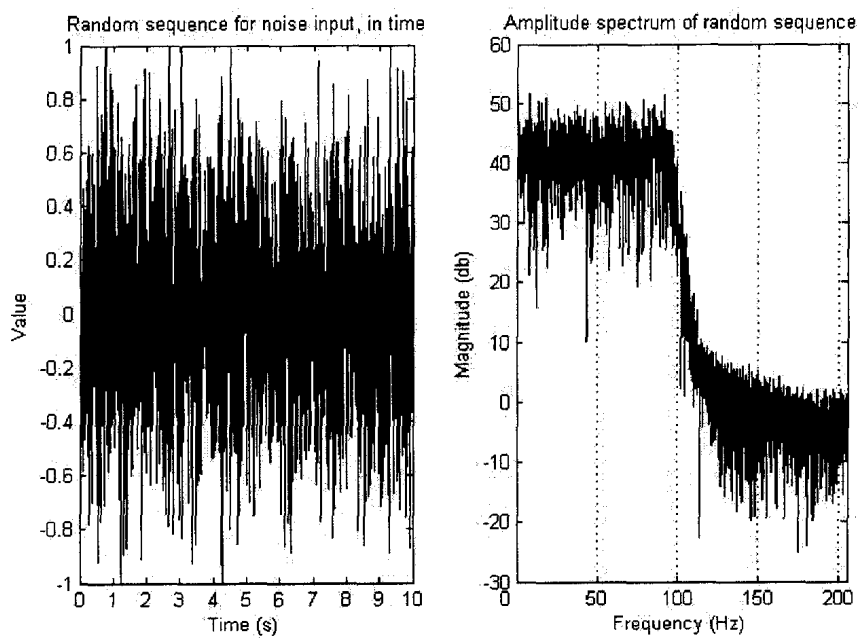


Figure 4.7 Signals generated in MATLAB using random numbers

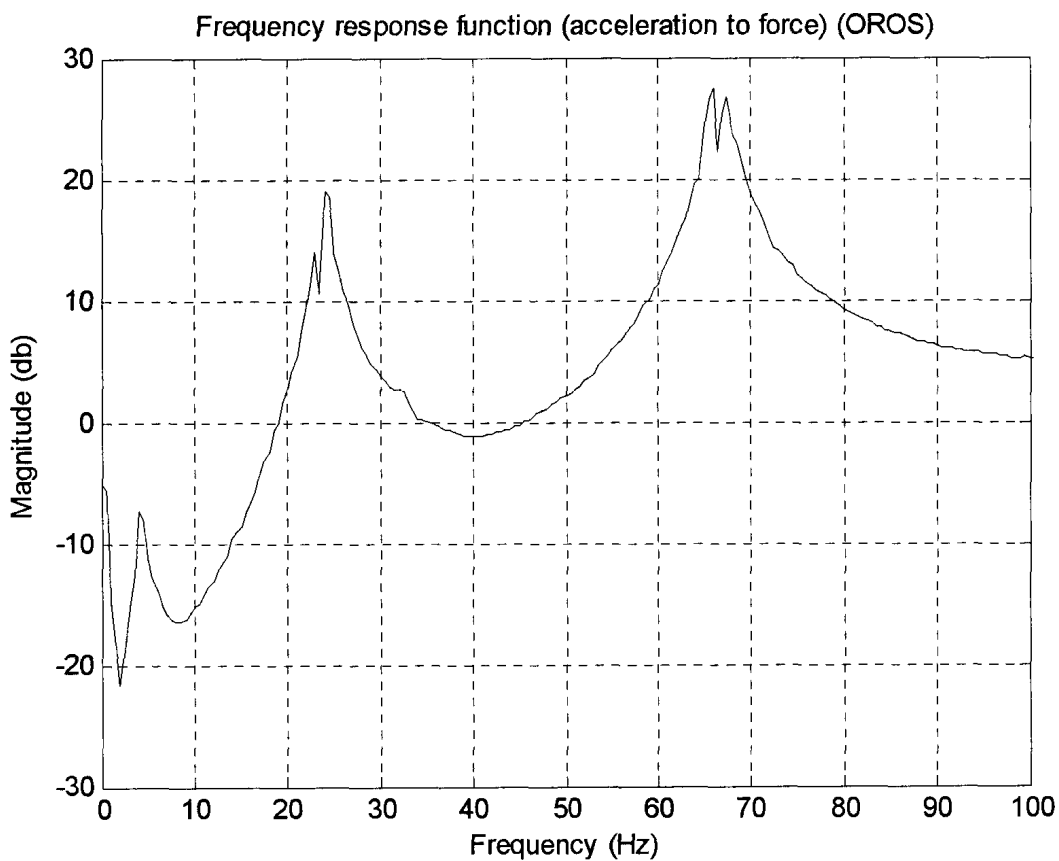


Figure 4.8 FRF obtained in experiment 2-Aceleration vs Force



## 4.7 Experiment 3

Experiment 3 is an output-only experiment where the input is a MATLAB generated approximate white noise and output is a transverse velocity measured by LDV on the vibrating beam. Laser Doppler Vibrometry has been a valuable technique for non-contact vibration measurements on large, macroscopic and microscopic structures. The time data collected from the experiment is used in MACEC for modal analysis.

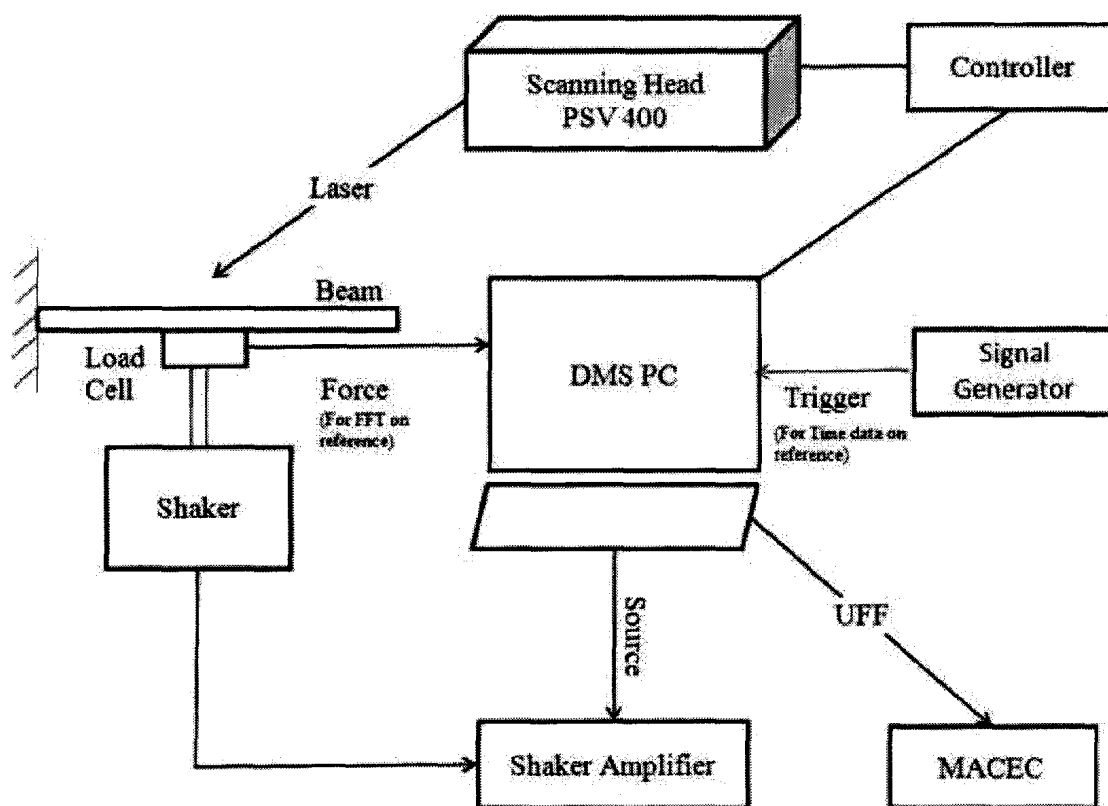


Figure 4.9 Experimental layout for experiment 3

Figure 4.9 shows the experimental layout for experiment 3. A brief description of the components used in this experiment is given below.

### Polytec Scanning Vibrometer (PSV 400 scanning Head):

A PSV-400 Scanning Vibrometer is used in this experiment. It focuses a laser beam on the structure, which scatters or reflects light from laser beam. The Doppler frequency shift/phase is used to measure out-of-plane velocity/displacement in a direction along the

axis of this laser beam. It is provided with integrated laser interferometer, scanning unit and a video camera.

#### Polytec DMS (Data management system):

The PSV-400 is controlled by PSV software which is installed on the DMS PC. The software performs following major functions: Controls the scanner, performs data processing, provides intuitive and animated data visualization and provides interfaces to modal, FEM and other software.

#### The Controller:

OFV 5000 vibrometer controller is a part of PSV workstation besides DMS. The controller provides signals and power for the sensor head, and processes the vibration signals. These are electronically converted by specially developed decoders within the controller to obtain velocity and displacement information about the test structure. This information is provided by OFV-5000 in either analog or digital form, for further data evaluation. The analog output is provided at standard BNC connectors. Both analogue and digital decoders are available, giving a frequency range from near DC to 24 MHz, with velocities to  $\pm 10$  m/s and displacements from the sub-nanometer to meter range.

#### The Signal generator:

Model number DS345, synthesized Function Generator is used for trigger in collecting time data using LDV setup. User defined function is used in PSV software to make use of white noise created in MATLAB as a signal that allows the shaker to vibrate the beam. The other components such as signal amplifier, shaker, load cell and cantilever beam are same as those used in previous experiments.

The beam was set with a shaker fixed at a distance of 27 cm from the fixed end. PSV 400 scanning head was fixed to a tripod and placed roughly two meters away from the beam facing towards it, as shown in Figure 4.9. The same band limited approximate white noise with same properties was used as an input source of excitation as used in previous experiment. It was imported in PSV software as a txt file.

The laser beam was set parallel to the plane of motion of the vibrating cantilever beam with the lens approximately 2 meter directly on in front of the beam. Before starting the scan, the laser beam was focused automatically and coordinates were aligned properly. There were 13 defined scan points connected by a line on the live video image of the beam in PSV software. These points were defined to acquire complete and better visualization of the beam. Once the fine positioning of laser beam was performed, then some of the acquisition settings were made, such as the range of vibrometer and reference was set to 10 volts with impedance of 1 Mohm. Reference was connected to the function generator for pre-triggering the signals. Then signals were generated using pre-defined band limited approximate white noise created in MATLAB as described above. Signals are then band pass filtered with first cut-off frequency of 0.05 Hz and second cut-off frequency of 180 Hz. Finally the velocity measurement employing LDV was obtained with a sensitivity of 10mm /s/V on each point for 8 seconds. The output signals were then low pass filtered at 100 kHz with a sampling frequency of 1.024 kHz giving 8192 samples for each measurement.

The time-domain data (velocity) measured at each point was exported in a universal file format with extension 'uff' which is compatible with modal analysis program used in present thesis i.e. MACEC. As described in chapter 3, MACEC needs at least two files (a grid file and a patch file) for the complete visualization of modes shapes. Different subroutines are written in MATLAB to separate a grid and a path file from the data obtained from LDV and to save the three files in an ASCII format for further use in MACEC. Now these files, a data file which contains time data (measured velocity), a patch file and a grid file are ready to feed in to MACEC for modal identification of the structure.

#### **4.7.1 Modal characterization in MACEC**

##### Preliminary Signal Processing:

The velocity data file was converted into SIT file format, which is the internal format of MACEC. Nodes were specified from 1:13 according to the number of channels (there

were 13 points considered on beam). The reference direction was selected as positive z-axis and node 6 was taken as the reference node in accordance to match with the reference of the vibrometer. The data originally sampled at 1.024 kHz was decimated by factor '2' to reduce the sampling frequency to 512 Hz and the number of samples to 4096 per channel during pre-processing. It was further detrended and the window length of 512 selected to produce 8 averages of the total length of data points ( $4096/512=8$ ). Finally Hanning window was applied to the data. These specifications were made to make the data cleaner since the interest was in the first three modes of the vibrating beam which lie within the frequency range of 4 Hz to 90 Hz. Once the data was pre-processed, employing techniques identified in chapter 3, it can undergo the identification process. Identification was carried out by using SSI and Peak picking techniques and the results are tabulated in Table 4.1.

#### Stochastic subspace identification (SSI) Technique:

The important feature to discuss in SSI technique is the selection of model order. A key problem of the system identification process is the selection of the correct model order and related to this, the selection of valid system poles. A Stabilization diagram is used as a tool to differentiate physical poles from the spurious ones. Here models of increasing order are compared and poles that are repeatedly found in these models with about the same characteristics are considered to be physical. Expected model order is selected as '6', as the interest is in the first three modes of the vibrating beam. It can be observed from Figure 4.10, that there is a jump between orders 5 and 6 which also suggests that the expected system order is 6. This gap indicates the points where singular values become zero. Now consider stabilization diagram as shown in Figure 4.11 with default stabilizing criteria (1% frequency, 5% damping, and 1% vector). It can be seen that three frequencies (5 Hz, 25 Hz and 70 Hz) have appeared in higher order. Although the system poles are stabilizing at a little higher order with default stabilization criteria, but it has been observed during modal analysis of the data, that system poles are there at lower orders as well, and those can be stabilized by increasing the default stabilization criteria to 5%.

Inspection of stabilization diagram shows that there are five well organized columns of

stabilized poles around 5 Hz, 25 Hz, 32 Hz, 70 Hz and 90 Hz. From the analytical and FEM results, it is known that 5 Hz, 25 Hz and 70 Hz are the first three natural frequencies of the vibrating beam. The presence of unavoidable columns of extra poles (stabilized like physical poles) in the vicinity 32 Hz and 90 Hz may be attributed to two possible reasons. Firstly, the peak around 32 Hz is due to the vibration transmitted from vertical support and base of the beam stand. Further details on this are provided in discussion section 4.9. Secondly, the strong vertical column of stable poles around 90 Hz is definitely a spurious poles column which could be the effect of low pass filtering of the noise at 90 Hz, as from previous results we know that beam doesn't have any mode at this frequency.

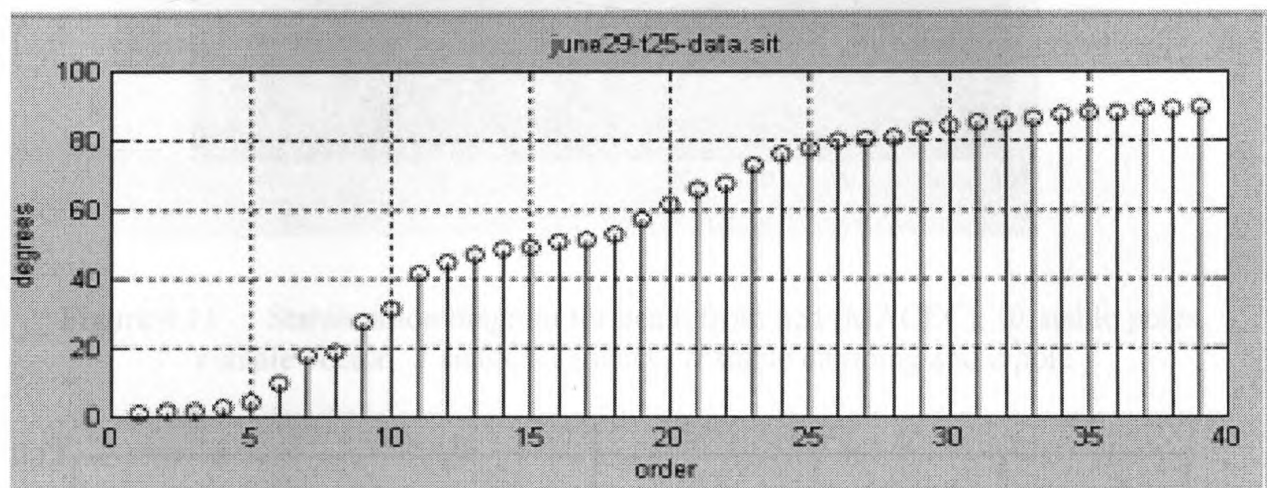


Figure 4.10 Principal angle diagram from MACEC

#### Peak Picking Method:

Figure 4.12 shows the peaks selected to identify the modal frequency of the vibrating beam via peak picking method where node 6 is considered as a reference channel in this method. Again, a remarkable peak can be seen around 32 Hz which is not a genuine peak but the result of vibration transmitting outside the beam system.

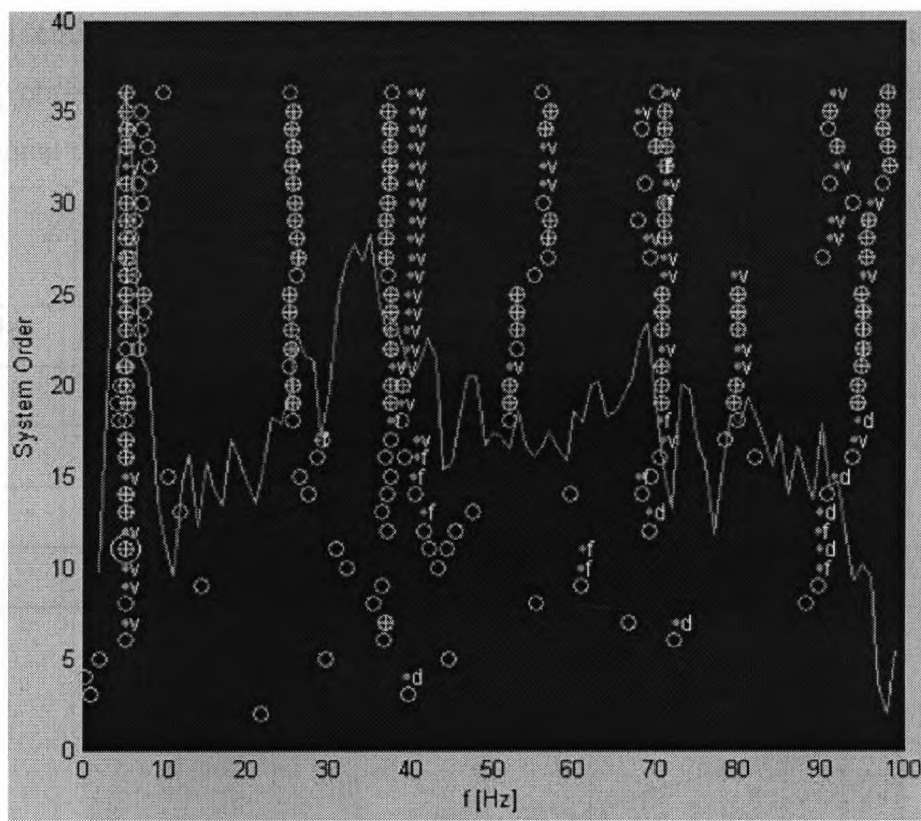


Figure 4.11 Stabilization diagram for beam from SSI (MACEC),  $\oplus$  stable poles,  $\otimes$  stable vector,  $f$  stable frequency,  $d$  stable damping and  $o$  pole.

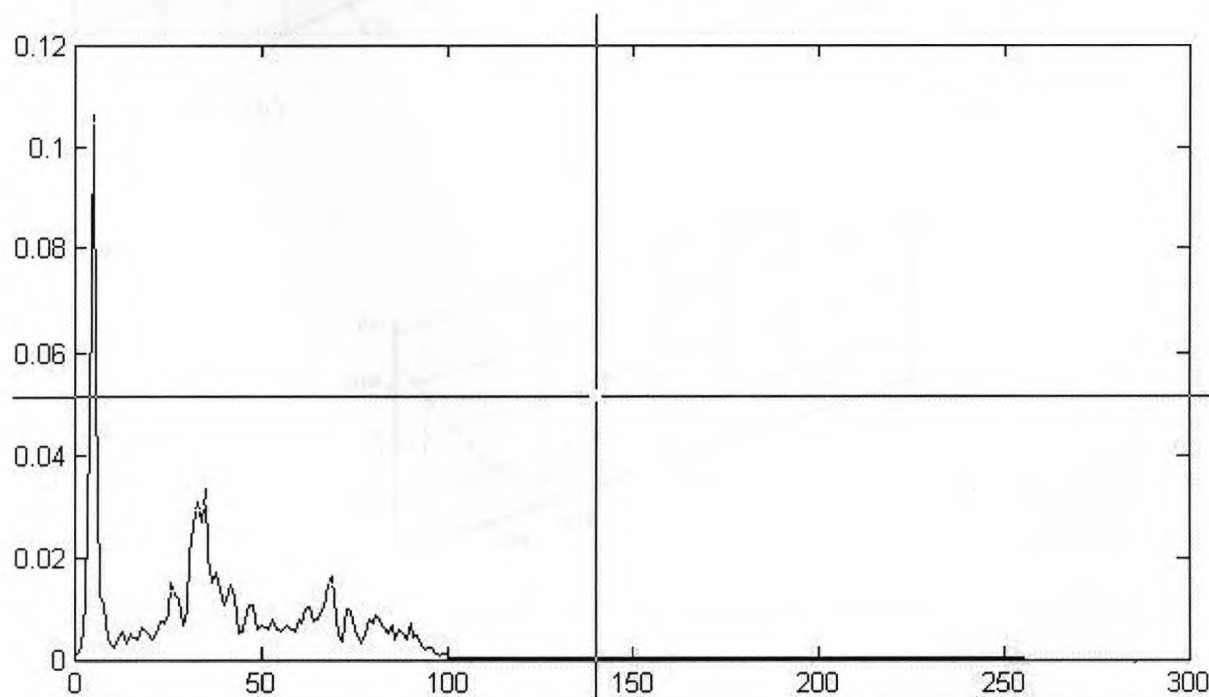


Figure 4.12 ANPSD from PPM (MACEC). (MACEC presents this plot without units for the y-axis and the values are normalized for easier peak identification)

Modal identification results obtained from SSI and PPM are tabulated in Table 4.1. Mode shapes obtained from SSI are illustrated in Figures 4.13 (a), (b) and (c) while the operational deflection shapes obtained from PPM are given in Figures 4.14 (a), (b) and (c).

Table 4.1 Results obtained from MACEC (SSI and PPM)

Mode	Stochastic Subspace Identification (SSI)		Peak Picking Method
	Natural Frequency (Hz)	Damping Ratio (%)	Natural Frequency (Hz)
1	5.20	7.70	4.99
2	25.20	11.90	26.09
3	70.50	3.60	69.93

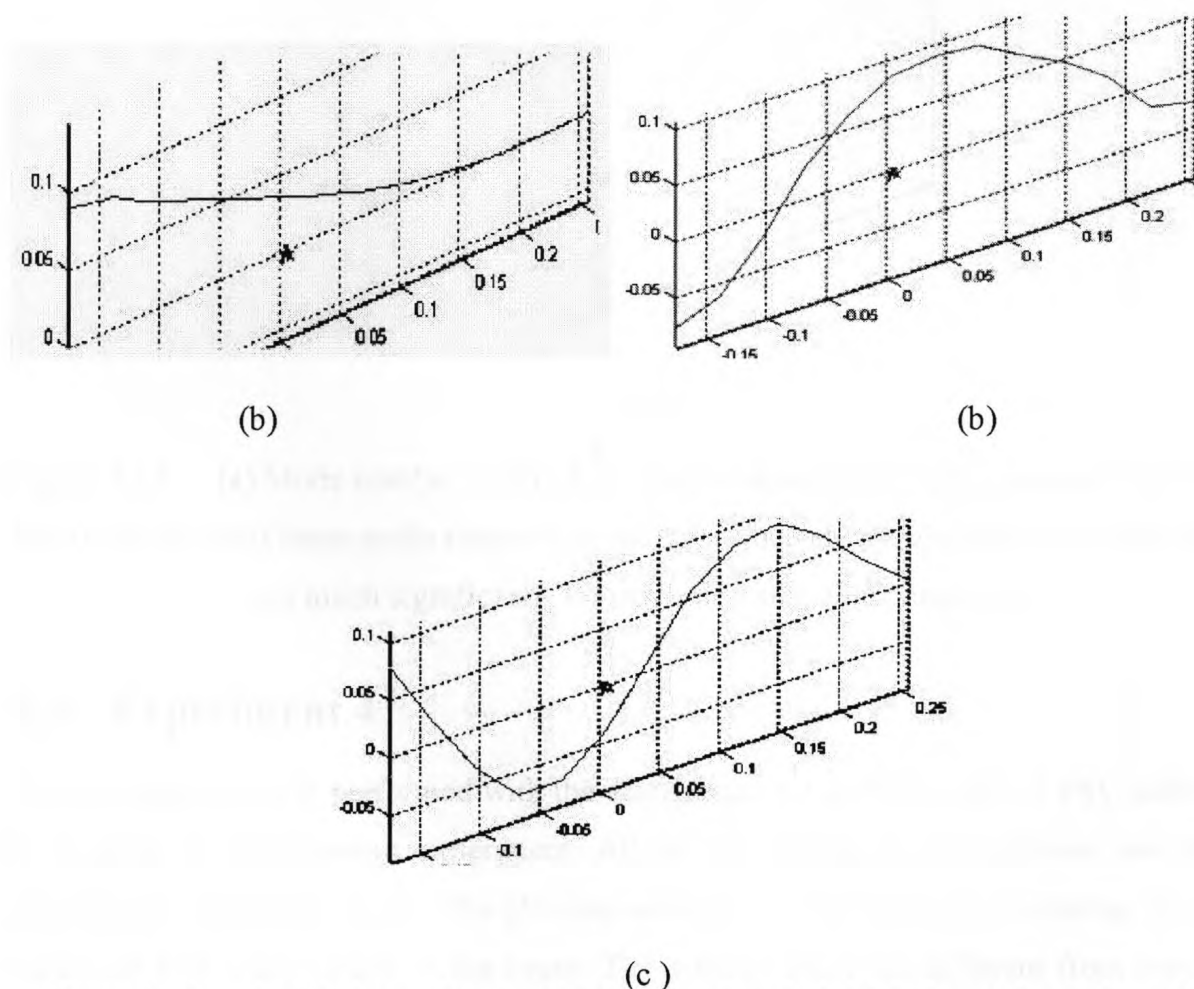


Figure 4.13 (a) Mode number 1, (b) Mode number 2, (c) Mode number 3 from SSI MACEC (MACEC presents these mode shapes without units since absolute numerical values are of not much significance for extracting shape information)



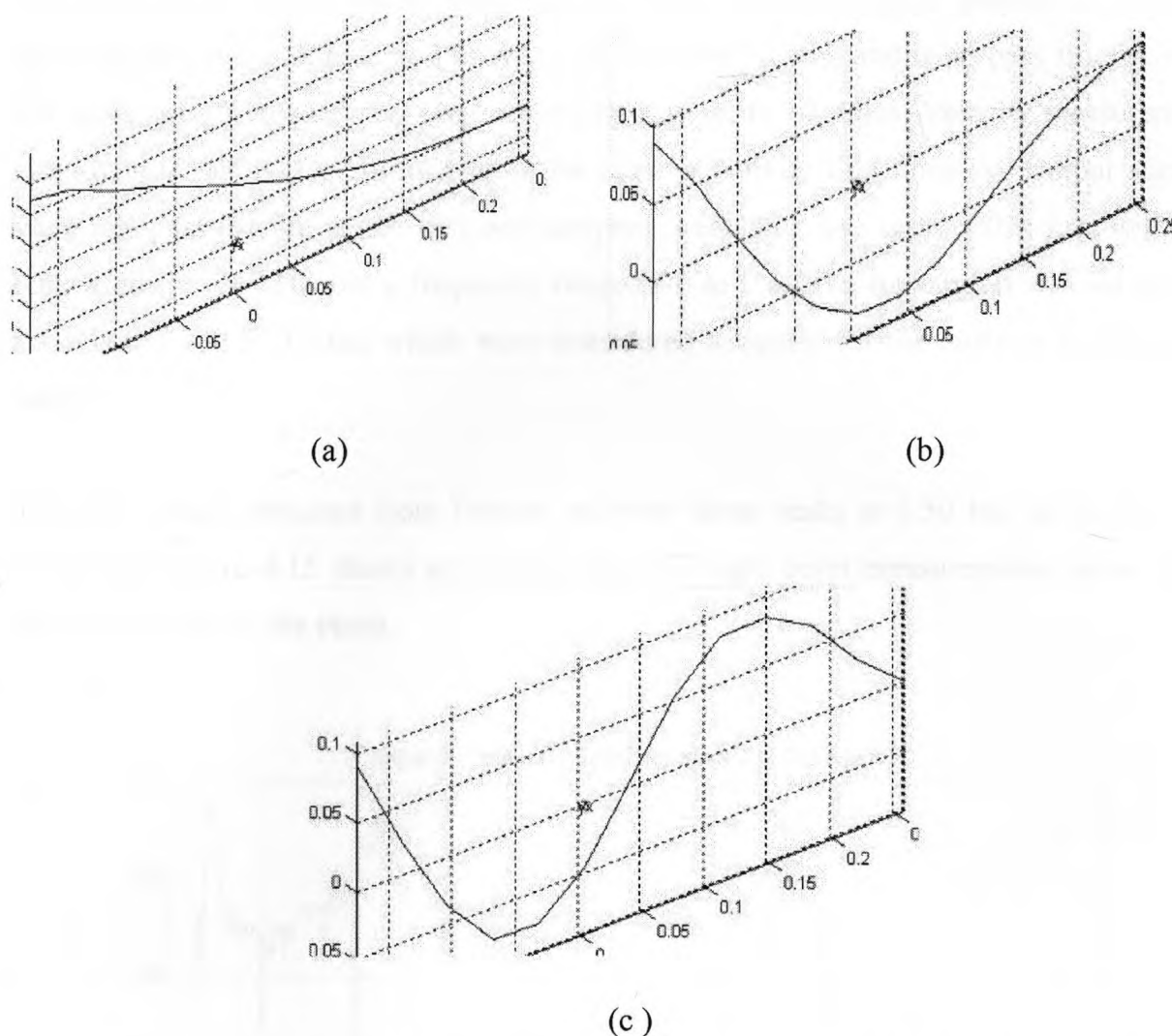


Figure 4.14 (a) Mode number 1, (b) Mode number 2 and, (c) Mode number 3 via PPM. (MACEC presents these mode shapes without units since absolute numerical values are of not much significance for extracting shape information)

## 4.8 Experiment 4

The last experiment is performed with the same setup but in FRF mode of PSV software. It is again an input-output experiment. All of the settings in the software are made according to frequency mode. The physical settings are kept the same including the scan points on live video image of the beam. The settings those are different from previous experiments are discussed here briefly. In this experiment, single point measurements are taken unlike experiment 3 where scanning is performed.



The same band limited white noise was used as a source of signal generation with the same properties (amplitude and offset is set to 1 and 0 volts) and band pass filtered with the same cut-off frequencies. Here averaging was set to 10 times. Velocity measurement employing LDV was performed with the same sensitivity i.e.10mm/s/v. Output signals were low pass filtered at 100 kHz and sampling frequency was set to 1.024 kHz with the bandwidth of 0.4 kHz and a frequency range of 0 to 0.4 kHz. Resolution was set to 125 mHz with 3200 FFT lines which were considered adequate for the analysis in the given range.

The FRF results obtained from Polytec software show peaks at 4.50 Hz, 24.25 Hz, and 67.62 Hz. Figure 4.15 shows an average plot of single point measurements taken at 13 different points on the beam.

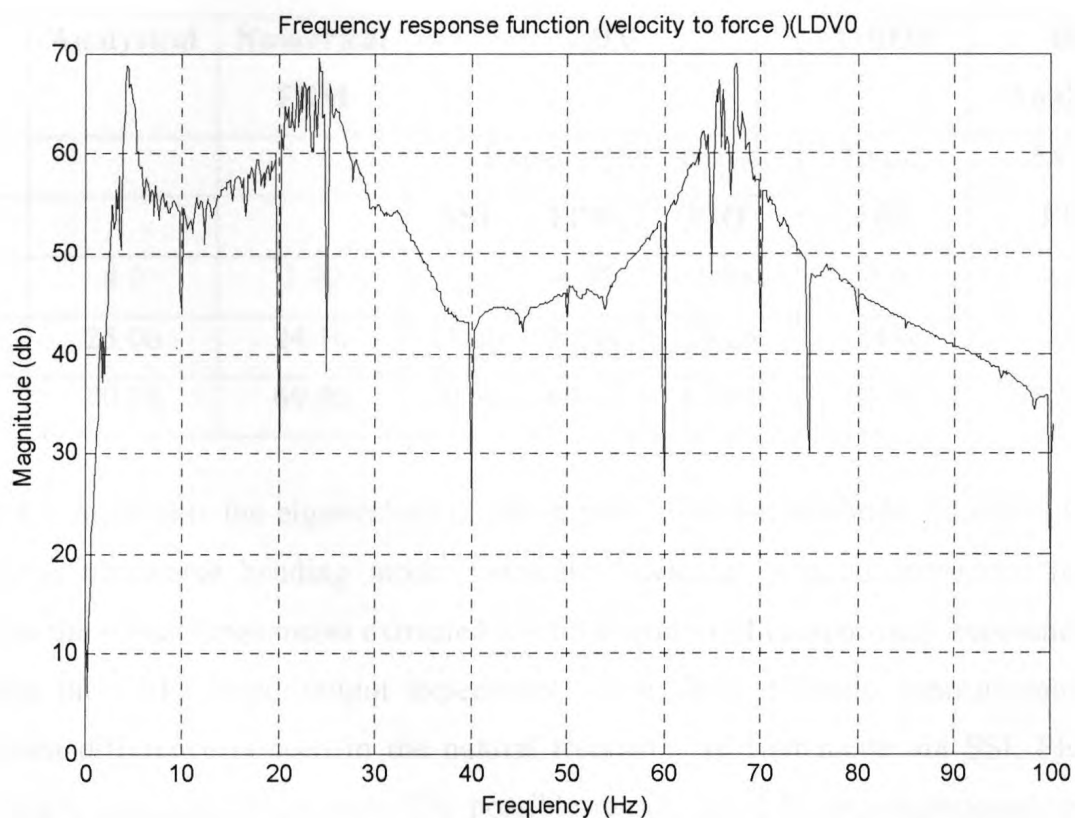


Figure 4.15 FRF obtained from Polytec software Velocity vs Force

## 4.9 Comparison and Discussion of Results

Results and comparison of modal frequencies of cantilever beam is presented in this section mode by mode. Table 4.2 shows all three modal frequencies obtained employing four different methods. In general, all of the methods seem to agree with each other very well on the natural frequency estimates of first three modes. The damping ratio estimates from SSI, lie within the reasonable limits. The damping ratios have not been estimated by PPM. The comparison does not include the mode shapes comparison, as PPM and FRF (frequency response function) from LDV show operational deflection shapes (ODS), while only SSI estimates the true mode shapes. However, the ODS seem to approximate the mode shapes reasonably well.

Table 4.2 Comparison of the results obtained from different experiments.

Mode	Eigenfrequency (Hz)						
	Analytical	Numerical FEM	LDV		OROS	HP Analyzer	
			Exp-3		Exp-4	Exp-2	Exp-1
			SSI	PPM	FRF	FRF	FRF
1	4.0	3.90	5.18	4.99	4.50	4.0	4.50
2	25.06	24.10	25.20	26.09	24.25	24.0	25.0
3	70.18	69.40	70.50	69.93	67.62	67.50	67.50

Table 4.3 represents the eigenvalues obtained from different methods for mode 1 which represents transverse bending mode. Generally speaking, a good agreement is found between the modal frequencies extracted from SSI and PPM (output-only experiment) and between the FRFs (input-output experiment) from three different measurements. The maximum difference is seen in the natural frequency of first mode via SSI, FEM and analytically calculated frequency. The possible reason could be, non-homogeneous beam material which can effect the assumption of considering ( $E$ ) value a constant ( $2.05 \times 10^{11} \text{ N/m}^2$  for steel), which may vary in reality. Therefore the first mode being at lower frequency is effected significantly. A check on FRF results from OROS and HP analyser

has also been made by changing the random input to sine sweep and similar results have been noted. i.e. 3.9 Hz (HP analyser) and 4.5 Hz (OROS analyser).

Table 4.3 Results for mode from SSI and FRF from Polytec

<b>Methods</b>	<b>SSI</b>	<b>PPM</b>	<b>FRF</b>
<b>LDV</b>	5.18	4.99	4.50
<b>OROS</b>			4.0
<b>HP Analyser</b>			4.50

The results for mode 2 are tabulated in Table 4.4. The results from SSI and PPM show good agreement with those obtained from different FRFs. The FRF with sine sweep input gives similar results i.e. 23.9 Hz (HP analyser) and 23.5 Hz (OROS analyser). Table 4.4 shows results for mode 2 obtained from different experiments.

Table 4.4 Results for mode 2 from SSI and FRF from Polytec

<b>Methods</b>	<b>SSI</b>	<b>PPM</b>	<b>FRF</b>
<b>LDV</b>	25.20	26.09	24.25
<b>OROS</b>			24.0
<b>HP Analyser</b>			25.0

Referring to the FRF plot from LDV and PPM, a remarkable peak around 32 Hz has been noted. A simple experiment is performed similar to experiment 1 with the same setup but this time an impact hammer was used to excite structures other than the experimental beam, for example, the fixed support and base of the beam stand, and measured the frequency response. The measurement on beam support and beam stand base is taken under ambient condition. And surprisingly a peak around 16 and 32 Hz appeared from those two structures. For this reason the peak in PPM plot is not selected for identification as it is known that this is the structural frequency results from the support structure. Further peaks around 16 and 32 Hz have also been observed when the measurement on two different structures is taken using LDV.

Table 4.5 shows the results tabulated for mode 3. Third mode results also show a good agreement. The FRF with sine sweep input yield similar results .i.e. 66.8 Hz (HP analyser) and 69.0 Hz (OROS analyser).

Table 4.5 Results for mode 3 obtained from different experiments

<b>Methods</b>	<b>SSI</b>	<b>PPM</b>	<b>FRF</b>
<b>LDV</b>	70.50	69.93	67.62
<b>OROS</b>			67.50
<b>HP Analyser</b>			67.50

## 4.10 Chapter Summary

In the present chapter MACEC has been validated for moderate size structure such as a meter long cantilever beam. To this end different experiments are conducted in that context with input-output as well as output-only methods. LDV is employed for acquiring vibratory response. The measurements obtained from LDV are analysed in MACEC and results obtained has shown good agreement with the analytically calculated frequencies. The motivation behind the validation process was to develop a methodology to work with micron-size mechanoreceptor hair as described in chapter 5. For further confirmation of the accuracy of equipment and procedure, the results achieved through LDV are further compared with the modal frequencies obtained through different conventional methods such as HP Analyser and PC based Acquisition analyser. A good agreement is seen between the results obtained through LDV and through conventional methods.

# Chapter 5

## Modal Characterization of Smaller Structures

### 5.1 Introduction

The methodology and measurement process developed in chapter 4, for acquiring suitable data for MACEC, is employed to characterize one and two dimensional micron-size structural elements such as: (a) submillimeter size cantilever beam (b) mechanoreceptor hair on insect's sensory organ and (c) diaphragm of microphones. Modal characterization is carried out using SSI algorithm via MACEC. A Microscope Scanning Vibrometer (MSV) is used to measure the structural vibration. A copper wire of  $37 \mu\text{m}$  diameter with different lengths was selected as a micron-size cantilever beam which is structurally similar to a mechanoreceptor sensory hair on cercus of an insect. An attempt is also made to characterize a typical two dimensional structure, a microphone diaphragm. Modal frequencies extracted from MACEC via stochastic subspace identification (SSI) and Peak picking method (PPM) for one dimensional micron-size structures show good agreement with the analytical natural frequencies and those acquired from MSV. The mode shapes determined via MACEC for micron-size structure are not distinguishable owing to limitations of the equipment; however some of them show correct behaviour.



## 5.2 Micron-size Cantilever Beam Model

A copper wire of diameter ( $d$ ) =  $37 \mu\text{m}$  is selected for experiment with three different lengths ( $\ell_1$ ) = 9mm, ( $\ell_2$ ) = 7.5mm and ( $\ell_3$ ) = 6.4mm. The wire has been assumed to have material properties: Young's modulus of elasticity for copper ( $E$ ) =  $1.10 \times 10^{11} \text{ N/m}^2$ , density ( $\rho$ ) =  $8970 \text{ kg/m}^3$  and area moment of inertia ( $I$ ) =  $9.199 \times 10^{-20} \text{ m}^4$ .

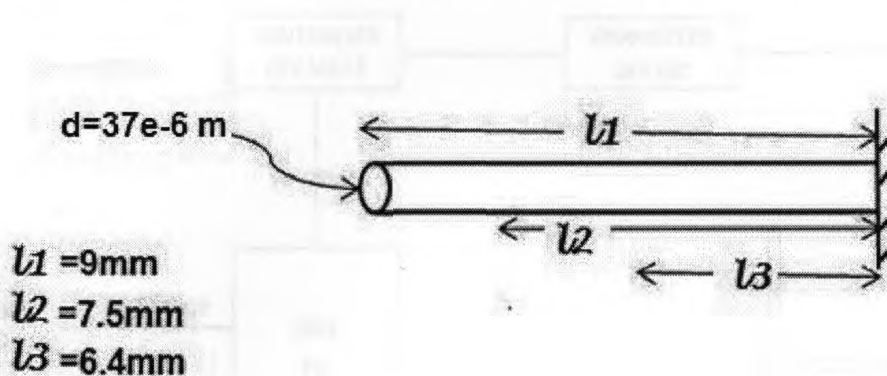


Figure 5.1 Different lengths of submillimeter size cantilever beam

The first and second natural frequencies of the wire with three different lengths, calculated using Equation (4.1) are given in Table 5.1.

Table 5.1 Analytical results for micron- size cantilever beam

Mode	$\ell_1 = 9\text{mm}$	$\ell_2 = 7.5\text{mm}$	$\ell_3 = 6.4\text{mm}$
1	223.78 Hz	322.25 Hz	442.54 Hz
2	1.402 kHz	2.019 kHz	2.773 kHz

## 5.3 Physical Experiment on Micro Cantilever Beam

The schematic drawing of the MSV measurement setup used to perform velocity measurements on micron-size cantilever beam is shown in Figure 5.2. Here modal frequencies of a copper wire with dimensions described in section 5.2 are determined by performing FFT measurements in Polytec software and by collecting the time-domain data

and analysing it in MACEC. In experiment 3, discussed in chapter 4, the PSV setup was employed to measure the transverse vibration of a meter long cantilever beam. In the present experiment, Microscope Scanning Vibrometer (MSV) setup has been employed to measure the vibratory velocity of a vibrating beam. The scanning feature allows measurements to be performed along the length of the beam.

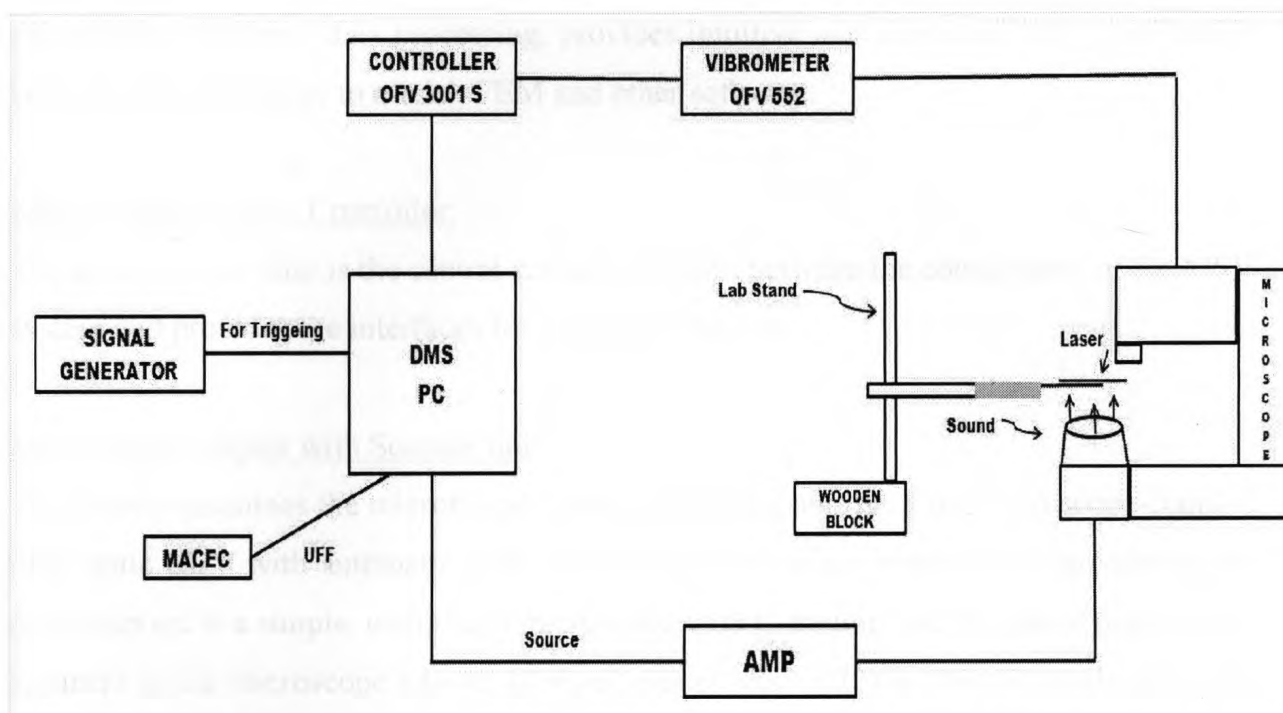


Figure 5.2 Experimental setup for measuring velocity on micron- size beam and hair on insect's cercus

A brief description of the components used in this experiment is given below.

#### Fiber Vibrometer OFV 552/ Sensor Head:

The sensor head contains the interferometer which is linked by a fiber to scanner unit. The interferometer signals from the sensor head is decoded in the controller. An analog voltage signal is thus generated which is proportional to the vibrational velocity.

#### Controller OFV 3001-S:

The controller provides power for the scanning head, controls the rotation of two mirrors in the OFV-552 and the scanning of the laser beam, and processes the interferometry created by back-scattered laser beam and the reference laser beam in the sensor head.

Polytec DMS (Data management system):

The MSV Data Management System (DMS) consists of a Windows 2000 based PC in an industrial housing, hardware for scanner control, video and data acquisition. The instrument is controlled by PSV software, which also analyses the data, and displays it in the form of colour maps and animations. MSV is controlled by PSV software which is installed on the DMS PC. The software performs the following major functions: Controls the scanner, performs data processing, provides intuitive and animated data visualization and provides interfaces to modal, FEM and other software.

MSV-Z-040 Scanner Controller:

The scanner controller is the central connection point between the components of the MSV system and provides the interfaces for peripheral devices.

Microscope Adapter with Scanner unit:

The system combines the micron-scale measurement capability of the microscope-coupled, fiber optic LDV with automatic scan acquisition. The optical platform for supporting the measurement is a simple, compound microscope with C-mount, and the use of piezo based scanners in the microscope adapter (Polytec model MSV-072) is used for positioning the laser beam over the microscope field view. The sensing element of this system is (OFV-300 S, and OFV-552) coupled into a microscope through the MSV-072 adapter.

The Signal generator:

Model number DS345, synthesized Function Generator is used for providing a trigger in collecting time data using MSV setup.

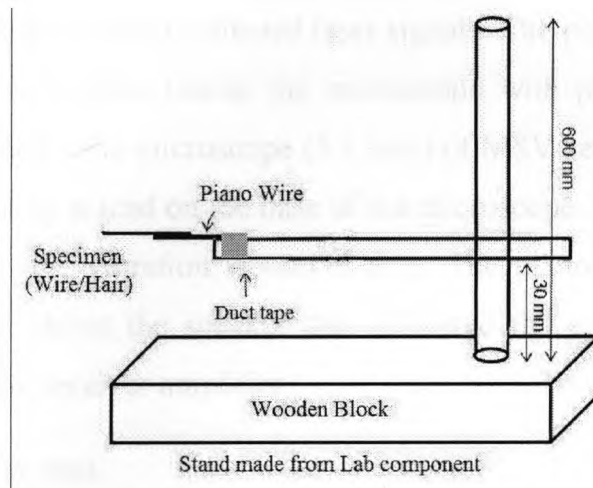
### **5.3.1 Preparation and Positioning of the Specimen**

Preparation of a specimen:

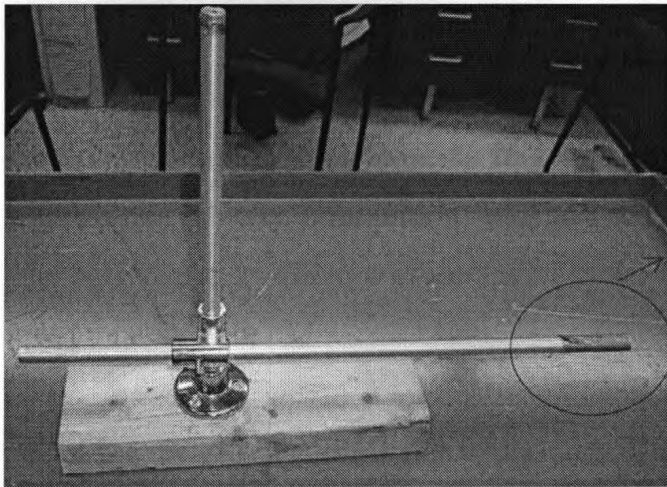
A copper wire as described in section 5.2 was cut into three different lengths i-e.  $\ell_1=9\text{mm}$ ,  $\ell_2=7.5\text{mm}$  and  $\ell_3=6.4\text{mm}$ , respectively. Under the dissection microscope the wire with length  $\ell_1=9\text{mm}$  was glued to the top surface of a thin metallic piano wire made of steel



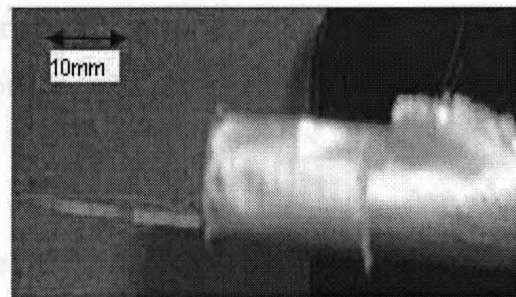
(modulus of elasticity for steel ( $E$ )= $2.05 \times 10^{11} \text{ N/m}^2$ ) as shown in Figure 5.3(b),(c). It was then left for 8 to 15 minutes to ensure the proper bond between two wires (a piano wire and a copper wire). The same procedure was repeated for other wires with lengths  $l_2=7.5\text{mm}$  and  $l_3=6.4\text{mm}$ .



(a) Schematic diagram of stand carrying wire specimen



(b)



(c)

Figure 5.3(a), Aluminum stand made from lab frame elements mounted on wooden block of 3 x 11 in, (b) real photo of the stand holding wire specimen (c) zoom in view of piano wire glued with copper wire beam, is fixed to horizontal component of stand with duct tape.

### Positioning of the Preparation:

The piano wire with copper wire glued on free end was positioned on the horizontal lever of a metallic stand which is made by joining the lab frame elements, made of aluminum ( $E = 69 \times 10^9 \text{ N/m}^2$ ), mounted on a wooden block as shown in Figure 5.3(a). The wooden block was placed on the adjustable positioning micrometer stage that allows x and y direction movement of the wooden block to make the fine spatial adjustments necessary to optimize the strength of reflected laser signals. The positioning stage was placed on the vibration isolation table beside the microscope with piano wire holding the specimen directly underneath the microscope (5 x lens) of MSV setup. A speaker was positioned on a wooden housing placed on the base of the microscope. The speaker and wooden housing were bolted to the vibration isolation table. The piano wire holding the specimen was positioned just above the speaker that delivered the acoustic stimuli. The speaker was connected to the receiver amplifier.

### Measurement system

The system consisted of sensor head (OFV 552), controller (OFV 3001-S), DMS, Scanner controller (MSV-Z-040), Microscope adapter with scanning unit (OFV 072). Coaxial to the laser beam was the video camera which captured an image of the scanning area. In the acquisition mode, the system software (PSV 8.4, Polytec) allows user to calibrate and control the position of laser beam, to generate the acoustic stimuli via signal generator, to acquire the velocity information from the sensor head and to monitor the image on PC. The software also offers a presentation mode for the evaluation and visualization of the measurement data.

All of the measurements for this experiment were performed on a vibration isolation table. The specimen was positioned between the speaker and microscope (Mitutoyo 5X). The fiber interferometer generated the input laser beam and received the resulting interference optical signal through a microscope adapter (OFV 072). The resulting optical signal was converted into an electrical signal by the photo detector inside fiber interferometer and subsequently decoded by a vibrometer controller (OFV 3001 S) to generate the velocity.

### Sound stimuli

Stimuli were approximate white noise created using random number generator within the MATLAB. It was generated for 10 seconds. The sound stimuli were repeatedly applied by passing through a stereo receiver amplifier and finally delivered from a 6.5 in dual cone full range speaker placed underneath the specimen at distance of roughly 1 in from it. The speaker has the specified frequency range of 45-16 kHz and impedance of 4 ohms.

## **5.4 Transverse Vibration Measurements on Beam Type Structures**

In this section time and frequency measurements on the microstructure cantilever beam have been described.

### **5.4.1 Time Measurements**

All of the measurements in this experiment were carried out using two-beams method. For the two-beams method, a part from the beam focused onto the measuring spot, a reference beam was also focused onto the surface and this beam did not move when the measuring beam was scanning over the surface.

Before starting the scan, both the laser beams were focused and coordinates were aligned properly. To acquire the highest possible quality for the measurement signals, the laser beam has to be optimally focused which was achieved by decreasing the diameter of the laser beam target area on the object as small as possible (Polytec manual). The signal level was shown on display of the controller. When the signal level is higher, a better focus of the laser beam is obtained.

The scan point definition was done by the grid layout of measurement points over the live microscope video image. The coordinate system for positioning the laser spot and video image are kept independent. These were overlapped by alignment of optical axis of the microscope with axis of the micro scanning mirrors. Exact alignment was attained by

manually moving the laser to points on the structure to confirm the pixel location on the video image with angular orientation of the mirrors.

- i) For 9 mm long beam there were 7 scan points selected on the image of the beam that went through scan sequence measurements. These 7 points covered  $1169.565 \mu\text{m}$ , approximately in the mid, of the total length of the wire.
- ii) For 7.5 mm long beam there were 9 scan points covering  $1206.381 \mu\text{m}$  approximately in the mid of the total length of the wire.
- iii) For 6.4 mm long beam there were 8 points that covered  $1162.299 \mu\text{m}$  of the total length of the wire approximately in the mid.

These points were defined to get better visualization of the beam. Once the fine positioning of laser beam was performed, then some of the acquisition settings were made, such as the range of vibrometer and reference was set to 5 volts with impedance of 1 Mohm. Reference was connected to the function generator for triggering the signals. Then acoustic signals were generated using predefined band limited approximate white noise created in MATLAB as described earlier. Finally, the velocity measurements from LDV were acquired with a sensitivity of  $10\text{mm /s/V}$  on each point for 6.4 seconds. The sampling frequency was set to 10.24 kHz giving 65536 samples for each measurement. The time-domain data (velocity) measured at each point was exported in a universal file format with extension 'uff' to be further used in MACEC for modal analysis.

#### Modal characterization in MACEC:

##### **Preliminary Signal Processing:**

The data was sampled at 10.24 kHz with 65536 samples per channel during pre-processing. The window length was selected as 1024 to provide 64 averages of the total length of the data points ( $65536/1024=64$ ) and after that Hanning window was applied to the data before it was finally detrended. This signal processing was performed to make the data cleaner. Once the data was pre-processed, employing techniques outlined in chapter 4, it

was ready to undergo the identification process. Identification was carried out by using SSI and Peak picking techniques and the results are tabulated in Table 5.2.

#### **Stochastic subspace identification (SSI) Technique:**

The expected model order was entered as '4' considering node 7 for 9 mm long beam (node 9 for 7.5 mm and node 8 for 6.4 mm long beam) as a reference channel which are the fixed points on respective beams. The principal angle diagram for this case is illustrated in Figure 5.4, which shows a discontinuity between orders 3 and 4 suggesting that order of the system could be '4'. Although not shown, but a similar behaviour was observed in the principal angle diagrams for 7.5 mm and 6.4 mm long beams. Inspection of stabilization diagram which is shown in Figure 5.5 depicts four distinct peaks around 214.69 Hz, 360 Hz and 1.36 kHz and 3.84 kHz with default stabilizing criteria (1% frequency, 5% damping, and 1% vector). It is seen that the stabilized poles have appeared in almost all orders. A comparison with the analytical results shown in Table 5.1 reveals that the frequencies 214.69 Hz, 1.36 kHz and 3.84 kHz show good agreement for the first three modal frequencies of 9mm long vibrating beam. Since this is the preliminary experiment to find the modal frequencies of micron-size cantilever beam, the main interests would only be in the first two modes of the vibrating beam.

Similarly, the stabilization diagrams for the other two experimental beams are illustrated in Figures B.1 and B.2 in appendix B, which show resonance peaks with stabilized poles at appropriate frequencies. For the 7.5mm long beam the poles tend to stabilize at 304.0 Hz and 1.870 kHz and for 6.4 mm long beam poles tend to stabilize around 432.0 Hz and 2.89 kHz. These identified frequency values show good agreement with the calculated frequency values. However, the presence of a peak around 360 to 370 Hz in all three stabilization diagrams is not the modal frequency but the result of electrical noise from the vibrometer. Further details on this are included in the discussion section 5.9.

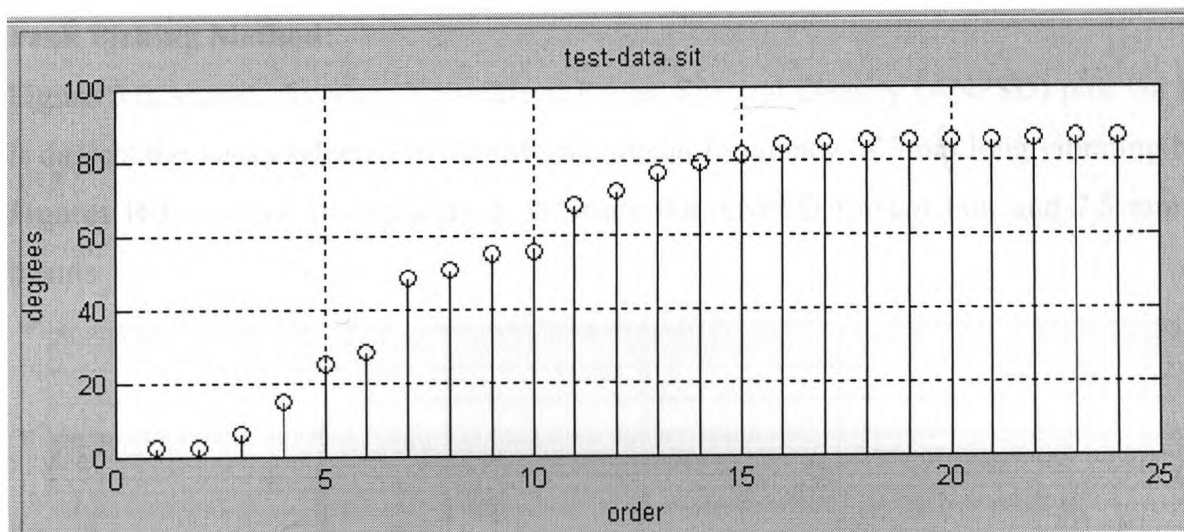


Figure 5.4 Principal angle diagram from MACEC for 9mm long beam

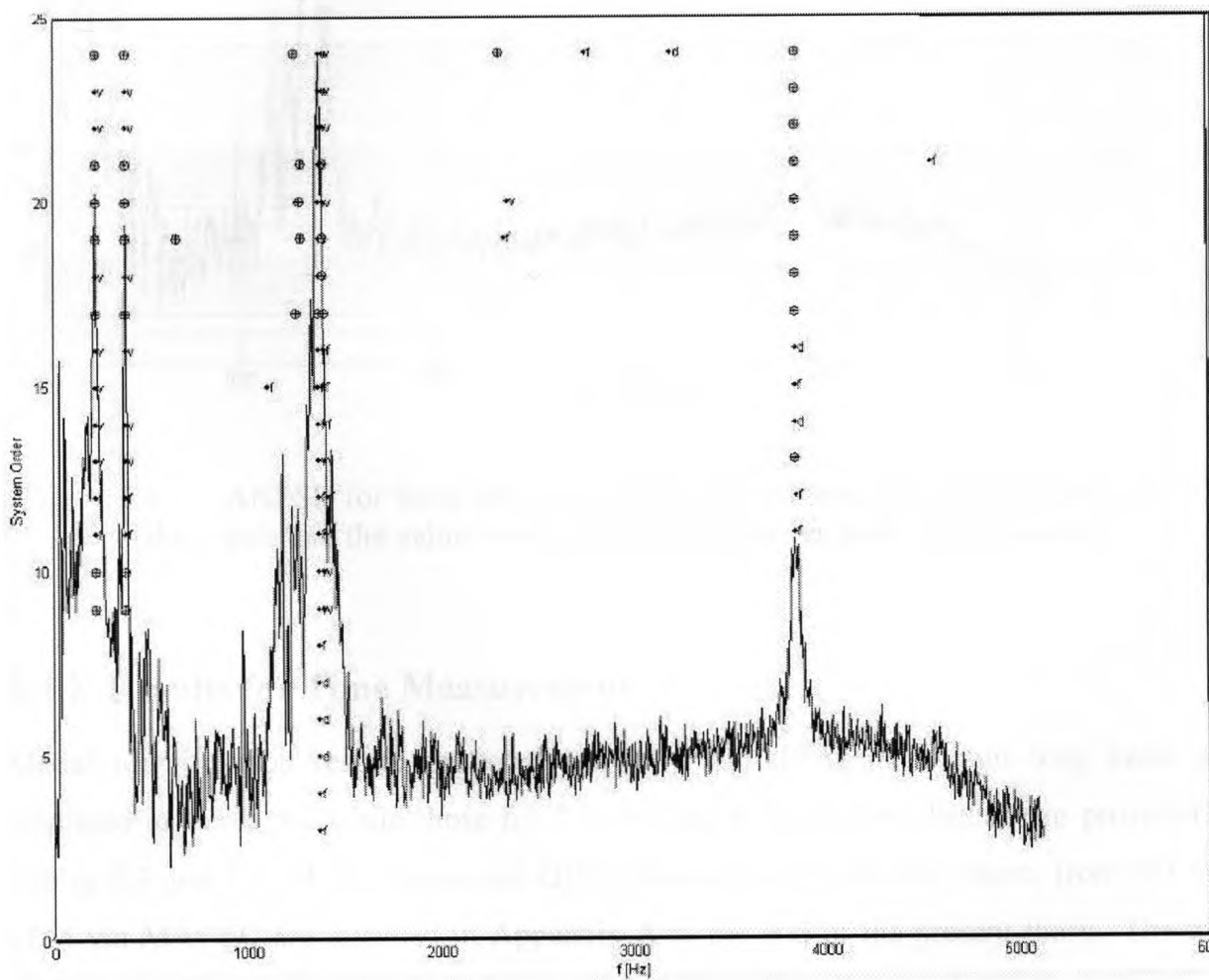


Figure 5.5 Stabilization diagram for 9 mm long beam.,  $\oplus$  stable poles,  $v$  stable vector,  $f$  stable frequency,  $d$  stable damping and  $o$  pole.

### Peak Picking Method:

Figure 5.6, shows, Average Normalized Power Spectral Density (ANPSD) plot via PPM. It depicts the peaks selected to identify the modal frequency of 9mm long vibrating beam. Figures B.3 and B.4 in appendix B illustrate the ANPSD for 6.4 mm and 7.5 mm long beams.

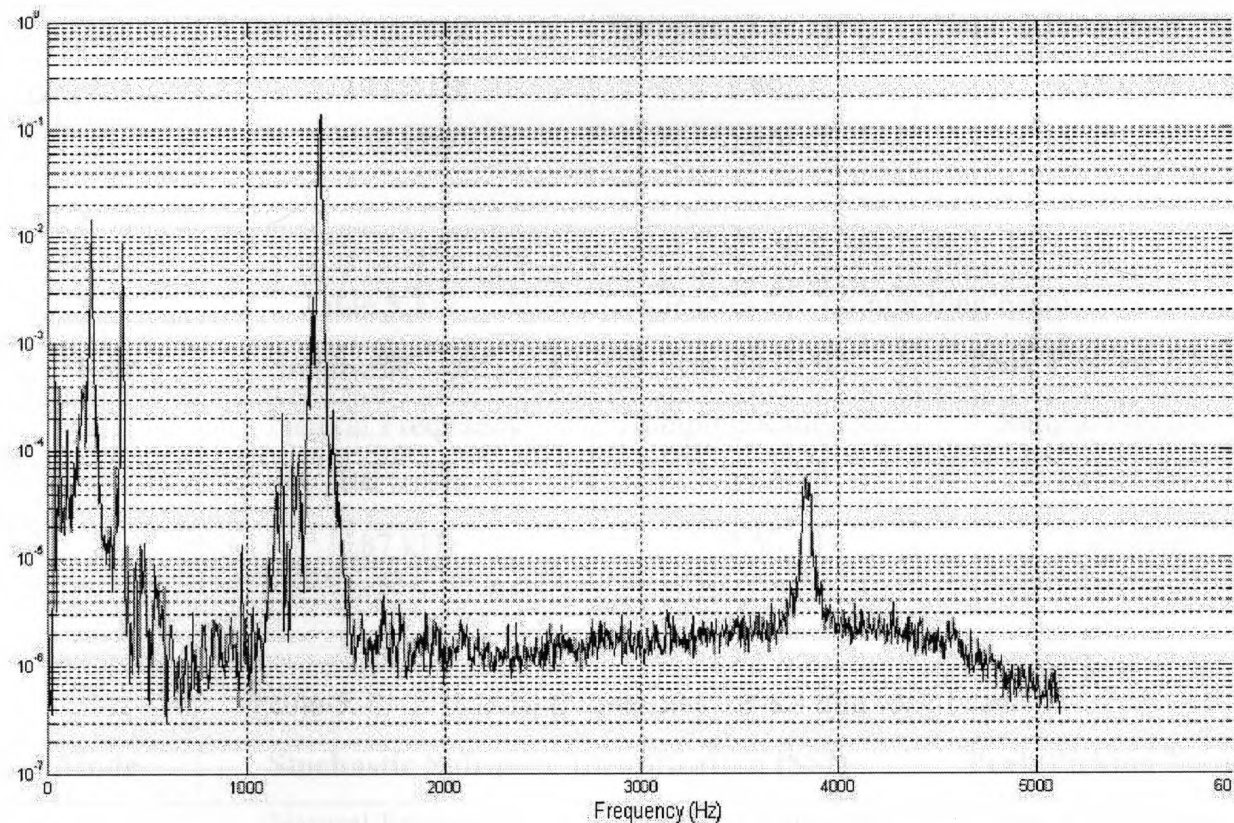


Figure 5.6 ANPSD for 9mm long beam (MACEC presents this plot without units for the y-axis and the values are normalized for easier peak identification)

### 5.4.2 Results for Time Measurement

Modal identification results extracted from SSI and PPM for 9 mm long beam are tabulated in Table 5.2 while those for 7.5 mm and 6.4 mm long beams are provided in Tables 5.3 and 5.4. Mode shapes and ODS obtained for 9 mm long beam, from SSI and PPM via MACEC are attached in Appendix A at the end of the present thesis. The first mode behaves reasonably well while the second mode is unclear and indistinguishable. It is hard to predict the behaviour of the unclear mode which deviates from the right general behaviour of a second mode for a cantilever beam. Although not shown but the mode



shapes obtained for 7.5 mm and 6.4 mm long beams follow the same pattern. Further details on this discrepancy are provided in the discussion section.

Table 5.2 Modal frequencies for 9 mm long beam

Mode	Stochastic Subspace Identification (SSI)		Peak Picking Method
	Natural Frequency	Damping Ratio (%)	Natural Frequency
1	214.69 Hz	1.80	215.0 Hz
2	1.36 kHz	0.20	1.37 kHz

Table 5.3 Modal frequencies for 7.5 mm long beam

Mode	Stochastic Subspace Identification (SSI)		Peak Picking Method
	Natural Frequency	Damping Ratio (%)	Natural Frequency
1	304.70 Hz	0.70	297.50 Hz
2	1.87 kHz	2.50	1.95 kHz

Table 5.4 Modal frequencies for 6.4 mm long beam

Mode	Stochastic Subspace Identification (SSI)		Peak Picking Method
	Natural Frequency	Damping Ratio (%)	Natural Frequency
1	432.30 Hz	3.0	445.0 Hz
2	2.89 kHz	0.60	2.85 kHz

### 5.4.3 Frequency Measurements on Beam

In this experiment “FFT” acquisition is performed to obtain frequency response measurements using the same acoustic signals. All of the settings in the software were made according to the frequency mode. The physical settings were kept the same including the scan points on live video image of the beam for each case. MSV measured the velocity again with the same sensitivity i.e. 10mm/s/v and sampling frequency was set



to 10.24 kHz with the bandwidth of 4 kHz and a frequency range of 0 to 4 kHz. Resolution is set to 6400 FFT lines and is considered to be adequate for analysis in the given range.

#### 5.4.4 Results for Frequency Measurements

Following plot shows an average FFT spectrum obtained from frequency measurement of 9mm long beam employing MSV. The numerical values of frequency measurements are tabulated in Table 5.5.

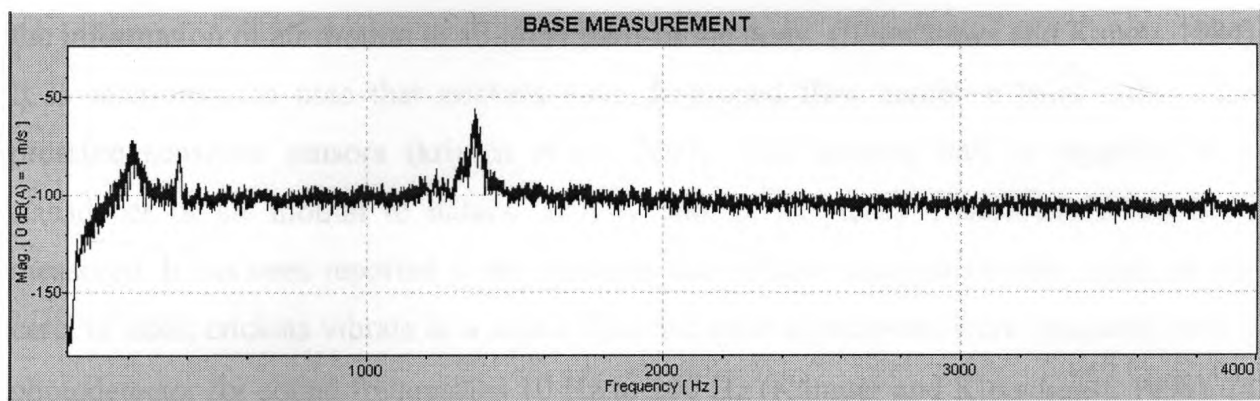


Figure 5.7 Average spectrum of frequency measurements from MSV for 9mm long beam

Table 5.5 FFT results obtained from Polytec for three different lengths of beam.

Mode	Length=9mm	Length=7.5mm	Length=6.4mm
1	211.0 Hz	299.0 Hz	445.0 Hz
2	1.32 kHz	1.80 kHz	2.90 kHz

In addition to resonance peaks around tabulated frequency values, it can be noted from the plots illustrated in Figure 5.7 that a peak appears at 369.40 Hz for 9 mm long beam, at 370.61 Hz for 7.5 mm long beam and at 368.10 Hz for 6.4 mm long beam. The supplementary plots for 7.5 mm and 6.4 mm long beams are illustrated in Figures C.1 and C.2 in appendix C. A possible reason, for the frequency peak between 360-370 Hz in three cases, can be the noise in electrical component of the vibrometer. Further details on this are provided in discussion section.

## 5.5 Background for Insects

Crickets and cockroaches bear a pair of outgrowths, cerci, at the rear end of their bodies. The cerci have hundreds of filamentous hairs, which under dissection microscope can be seen to deflect when touched by a gentle flow of medium air, Figure 5.8. When a hair is deflected by air motion, the sensory cell at the base of the hair generates nerve impulse and sends them out to central nervous system (CNS) along its nerve axon. These structures form a functional unit referred to as a sensory hair or sensillum. In the CNS the sensory nerve fibres connect to other nerve cells which in turn process the signals and distribute the information of air motion to all other parts of the body. (Shimozawa and Kanou, 1984). It is interesting to note that crickets have developed flow sensitive hairs rather than pressure sensitive sensors (krijnen *et al*, 2007). The sensory hair is regarded as a transducer of air motion to natural activity and its frequency characteristic has been measured. It has been reported in the literature that filiform hairs of various length on the cerci of adult crickets vibrate in a sound field and their movements were measured with a photodetector for sound frequencies 10 Hz to 200 Hz (Kämper and Kleindienst, 1990). In the present thesis a different experimental setup, MSV, is used to perform preliminary experiments for finding the modal frequency of filiform hair.

Current development in biomimetic flow-sensors is based on flow sensitive mechano-sensors of crickets. There seems to be a favourable size match between the primary sensing part (e.g. mechanoreceptor hair on cricket's cercus with lengths roughly between 100-1000  $\mu\text{m}$ ) and what can be made by MEMS technology. It allows bio-mimicking of biological sensory systems such as flow sensitive hairs on cricket's cercus. Crickets are amongst the most energy sensitive sensors known (krijnen *et al*, 2007). Fabrication of biomimetic flow-sensors based on mechanoreceptive sensory hair has recently gripped the momentum in bio-robotics area.



Figure 5.8 Female crickets under the dissection microscope  
at DASSL

## 5.6 Experiment on Insect's Sensory System

### 5.6.1 Materials and Method:

#### Dissection and Preparation of specimen:

All of the experiments were performed on adult crickets of both the sexes obtained from a commercial supplier. The insects were briefly anaesthetised by cooling them on ice cubes in an ice cooler for 15 minutes. The experiments were performed within an hour of anaesthetising the animals. Only crickets with undamaged cerci were used. The animals head, thorax, ovipositor, and anterior part of abdomen were removed so that only the posterior three or four abdominal segments remained. To prevent movement of the remaining abdominal segments the insect was pinned on a balsa wooden block of 50 cm x 70 cm of size. The preparation was then placed under the dissection microscope. It was carefully examined under the microscope for any damage caused to the cercus before gluing it to the wire, and was documented by photograph. The top surface of the cercus was then glued to the same piano wire used before, under the microscope. A special care was taken to ensure that the wire does not stick to the bottom surface of cercus that contains filiform hair. Once the wire was properly glued on the top surface of the cercus, it

was then cut with scissors from the base. The edge of the cercus that was cut from the base was then waxed to reduce drying out as shown in Figure 5.9.

#### Positioning of the Preparation:

Positioning of the preparation was performed in a manner similar to that carried out for the micro-scale cantilever beams. The piano wire with cercus glued on free end was positioned on the horizontal lever of a metallic stand mounted on a wooden block. The wooden block was placed on the adjustable positioning micrometer stage that allows x, and y direction movement of the wooden block to make the fine spatial adjustments necessary to optimize the strength of reflected laser signals. The positioning stage was placed on the vibration isolation table besides the microscope housing with metallic wire holding the cercus directly underneath the microscope (10 x lens). A speaker was positioned on a wooden housing mounted on the stage of the microscope. The speaker and wooden housing were bolted to the vibration isolation table. The piano wire holding the cercus was positioned just above the speaker that delivered the acoustic stimuli. The speaker was connected to the receiver amplifier.

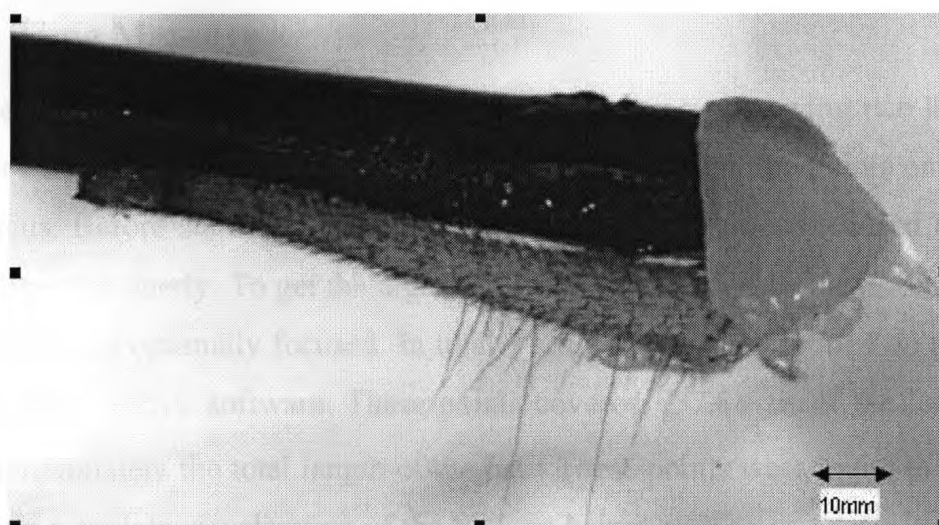


Figure 5.9 Mechanoreceptor hairs on cercus of an insect (cercus is glued to 1.6mm thick piano wire made of steel)



### Measurement system

MSV was employed to investigate the dynamic behaviour of insects' sensory hair. The experimental setup for measurements on mechanoreceptor hair was same as used for the micron-scale beams.

### Sound stimuli

Stimuli were a wide band approximate white noise created by random number generator within MATLAB. The noise was sampled at 44100 Hz. It was created for 10 seconds. The sound stimuli were repeatedly applied by passing through a stereo receiver amplifier and finally delivered from a 6.5 in dual cone full range speaker placed underneath the specimen at distance of roughly 25 mm from it. The speaker has the frequency range of 45-16kHz and impedance of 4 ohms.

## **5.7 Transverse Vibration Measurements on Hair of the Insect**

In this section time and frequency measurements taken from MSV on the cercus of an insect is described.

### **5.7.1 Time Measurements**

The measurements were taken from a differential vibrometer owing two laser beams, one was set as a reference beam and other moved for measuring the points on sensory hair of the cercus. Before starting the scan, both the laser beams were focused and coordinates were aligned properly. To get the highest possible quality for the measurement signals, the laser beam was optimally focused. In total 7 scan points were defined on the image of the insect's hair in PSV software. These points covered 757.88  $\mu\text{m}$  of the hair length which was approximately the total length of the hair. These points were found to be adequate for obtaining complete visualization of the filiform hair.

After the scan point definition was performed, and beams were focused, some of the acquisition settings were made, such as the range of vibrometer and reference was set to 10 volts with impedance of 1Mohm. Reference was connected to the function generator

for triggering the signals. Then acoustic signals were generated using predefined band limited approximate white noise as described in section 5.6.1. Finally the velocity measurements from MSV were obtained with a sensitivity of 125 mm /s/V on each point for 800 ms. The sampling frequency was set to 2.56 kHz producing 16384 samples for each measurement. The time-domain data (velocity) measured at each point was exported in a universal file format with extension ‘uff’ to be further used in MACEC for modal analysis.

#### Modal characterization in MACEC:

##### **Preliminary Signal Processing:**

The data was sampled at 2.56 kHz with 16384 per channel during pre-processing. The window length of 1024 was selected to provide 16 averages of the total length of data points ( $16384/1024=16$ ), then Hanning window was applied to the data and finally it was detrended. Once the data was pre-processed it was ready to undergo the identification process employing the techniques outlined in chapter 3. Identification was carried out by using SSI and Peak picking techniques via MACEC and results are tabulated in Table 5.6.

##### **Stochastic subspace identification (SSI) Technique:**

The expected model order was entered as ‘4’ as the primary interest was in first two modes of vibrating structure. Now consider the following principal angle diagram.

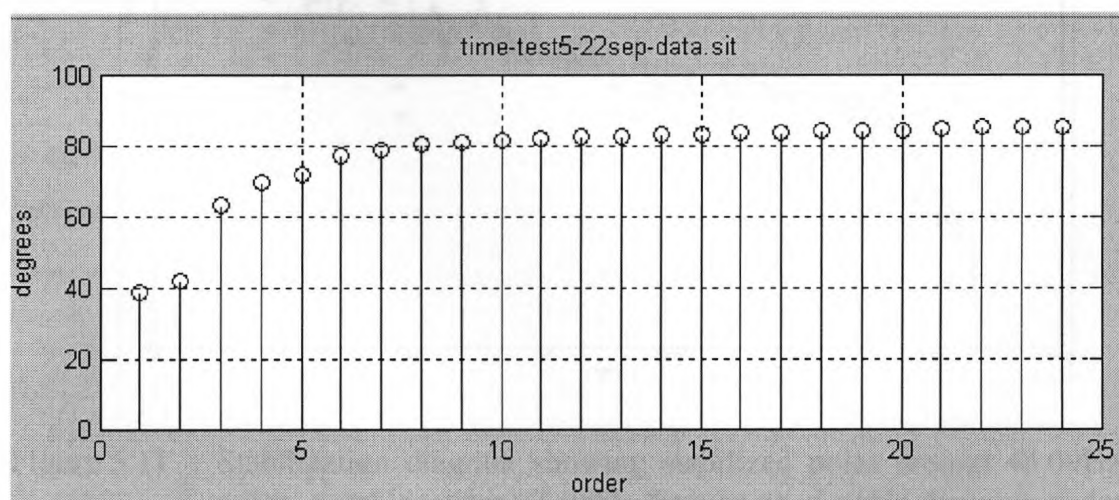


Figure 5.10 Principal angle diagram that shows a gap between 4th and 5th order of the system.

It can be observed from the Figure 5.10 that there is a gap between orders 2 and 3 and a smaller gap is also observed between orders 4 and 5. The expected order is selected as 4 since the stabilization diagram with expected order '2' went high up to order 12 which gave insufficient information about stabilized poles, however as shown in Figure 5.11 the stabilization diagram with expected order '4' went up to order 25 and showed that the poles are stabilizing around 48.12 Hz and 166.70 Hz. It can be observed from the stabilization diagram with default stabilizing criteria (1% frequency, 5% damping, and 1% vector) that the pole around 48.12 and 166.70 Hz has appeared in almost every order. Another important observation is that, the system poles are present at lower order as well, which can be stabilized by increasing the default stabilizing criteria. A peak around 360 Hz which has been found in previous results of the micron-size beam can also be seen here. Further details on this are provided in discussion section.

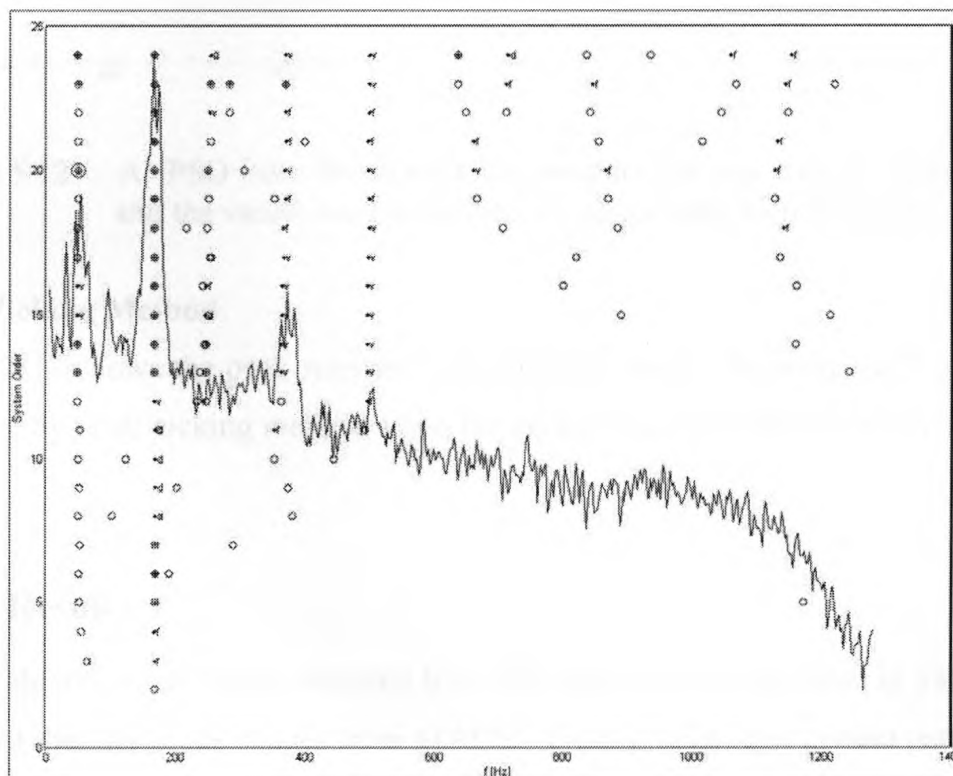


Figure 5.11 Stabilization diagram showing stabilized poles around 48.09Hz  $\oplus$  stable poles,  $v$  stable vector,  $f$  stable frequency,  $d$  stable damping and  $o$  pole.

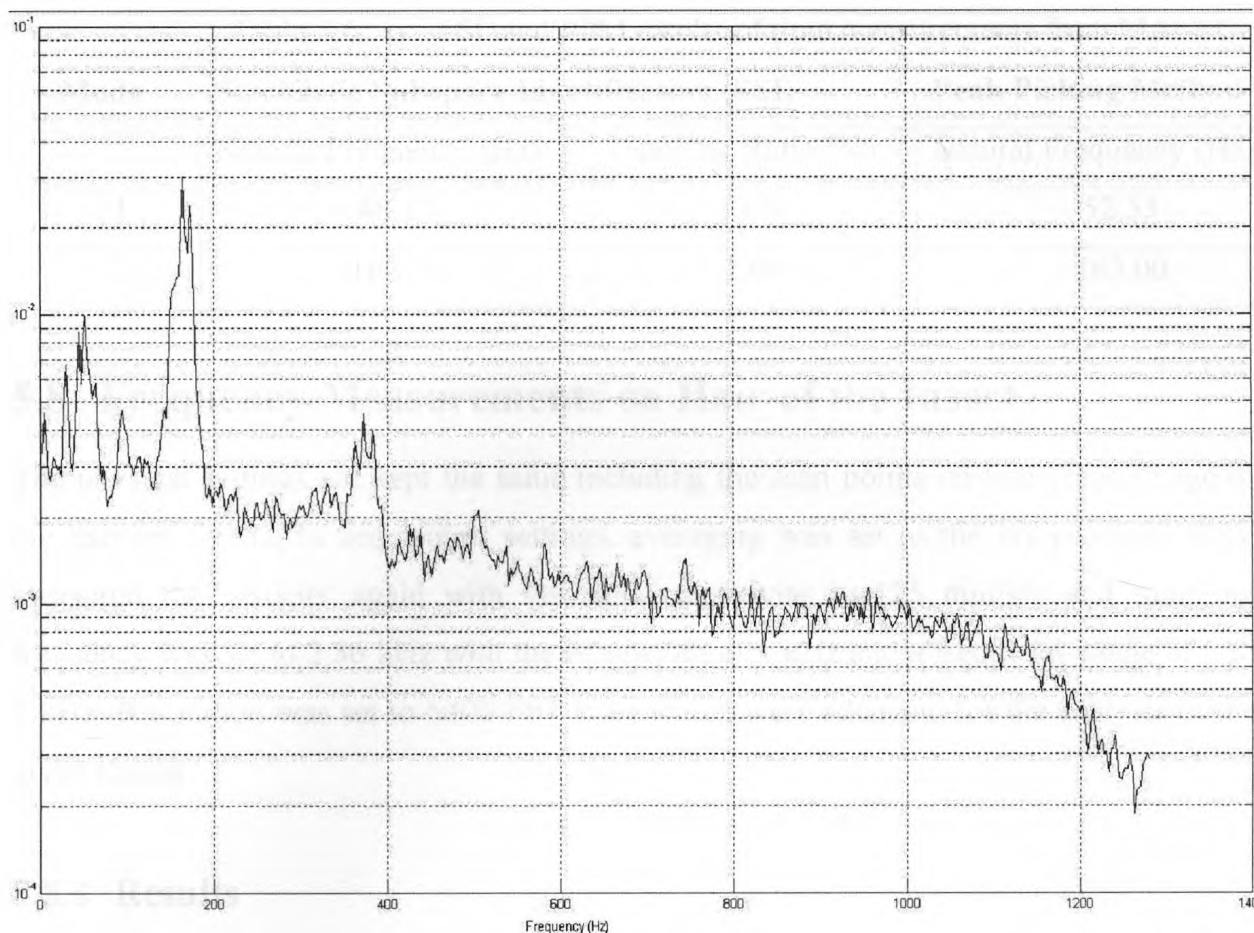


Figure 5.12 ANPSD from PPM (MACEC presents this plot without units for the y-axis and the values are normalized for easier peak identification).

### Peak Picking Method:

Figure 5.12 shows the peak selected to identify the modal frequency of the vibrating hair of insect by peak picking method while the peak around 370 Hz can also be noticed in the plot.

### 5.7.2 Results

Modal identification results obtained from SSI and PPM are tabulated in Table 5.6. It may be noted that the mode shapes from MACEC did not behave in correct pattern. A further detail on this is provided in discussion section.



Table 5.6 SSI and PPM results of time measurements from MACEC

Mode	Stochastic Subspace Identification (SSI)		Peak Picking Method
	Natural Frequency (Hz)	Damping Ratio (%)	Natural Frequency (Hz)
1	48.12	12.70	52.53
2	166.70	2.00	165.00

### 5.8 Frequency Measurements on Hair of the Insect

The physical settings are kept the same including the scan points on live video image of the hair on cercus. In acquisition settings, averaging was set to the off position. MSV measured the velocity again with the same sensitivity i.e.125 mm/s/v and sampling frequency was set to 2.56 kHz with the bandwidth of 1 kHz and a frequency range of 0 to 1 kHz. Resolution was set to 6400 FFT lines which were adequate for the analysis in the given ranges.

#### 5.8.1 Results

Figure 5.13 shows the average FFT spectrum obtained from MSV. The FFT spectrum shows peaks around 49.69 and 167.19 Hz and further confirms the results acquired via SSI.

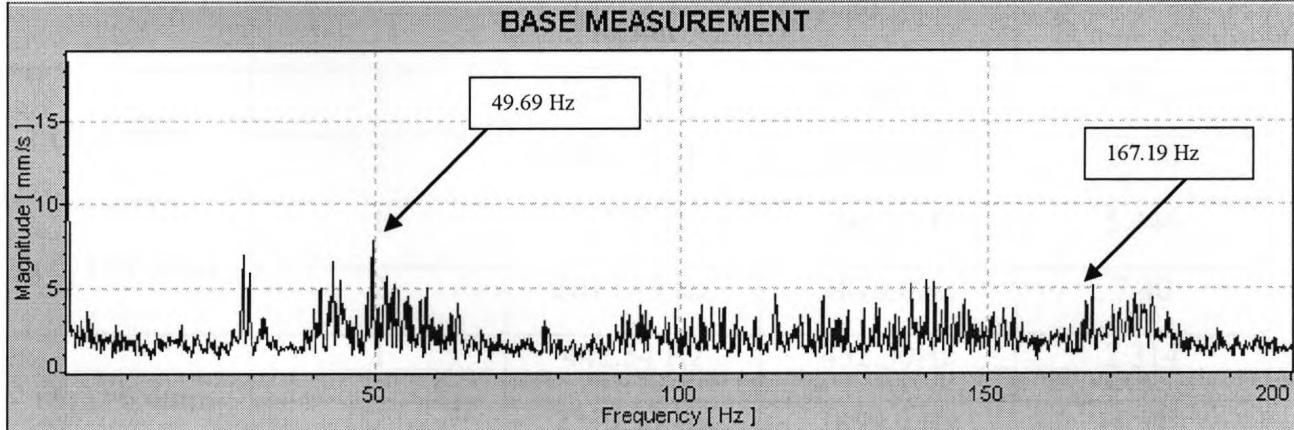


Figure 5.13 FFT results for hair from PSV Polytec (linear scale). (The peaks are selected by selecting a frequency band in Polytec software which automatically selects the highest peak in the selected band).

## 5.9 Discussion of the Results

- Preliminary experimental testing was carried out on micron-scale structural elements for example submillimeter size beam and micron-size hair on cricket's cercus, which are considered as one dimensional structures. Table 5.7 shows analytically calculated frequencies, the frequencies of submillimeter size beam identified by SSI via MACEC, and the percent difference calculated between the two frequencies. It is seen that the modal frequencies of the same beam with three different lengths has shown an expected trend of increase in frequencies with decrease in length of the beam.
- The modal frequencies identified by SSI via MACEC have also shown good agreement with analytical frequencies of the beam. It can be noticed from Table 5.7 that the maximum percent difference between calculated and identified frequencies of the beam is about 7.4 percent, which points towards taking an initiative to use MACEC as a modal identification tool for micron-scale structures.

Table 5.7 Percent difference between calculated and identified frequencies

Beam	Mode Number	Calculated Result	SSI Result	% Difference
$(l_1)=9\text{mm}$	1	223.78 Hz	214.69 Hz	4.062
	2	1402.43 Hz	1364.0Hz	2.740
$(l_2)=7.5\text{mm}$	1	322.25 Hz	304.70Hz	5.446
	2	2019.49 Hz	1870.0Hz	7.40
$(l_3)=6.4\text{mm}$	1	442.54 Hz	432.30Hz	2.314
	2	2773.35 Hz	2899.0 Hz	-4.530

- The SSI results have also shown a good agreement with FFT results obtained from Polytec software for modal frequencies of the beam tabulated in Table 5.8. The FFT results from Polytec software also show the similar trend of increase in

frequencies with decrease in length of the beam as revealed by frequencies identified in MACEC.

Table 5.8 Comparison of FFT results from Polytec and identified frequencies ( SSI) from MACEC

Beam	Mode Number	SSI Result	FFT Result
$(\ell_1)=9\text{mm}$	1	214.69 Hz	211.0 Hz
	2	1.36 kHz	1.33 kHz
$(\ell_2)=7.5\text{mm}$	1	304.70 Hz	2.99 kHz
	2	1.87 kHz	1.80 kHz
$(\ell_3)=6.4\text{mm}$	1	432.30 Hz	445.0 Hz
	2	2.89 kHz	2.91 kHz

- As mentioned in section 5.4.1, the measurements were only managed to be taken on approximately 1.2 mm of the total length of each beam in the mid of the beam. The reason for considering a millimeter long section of the total length was primarily to work around the limitation in field of view of the camera. The field of view of the camera for 5x lens ranges from 1650 X 1330  $\mu\text{m}$  approximately, therefore it was not possible to measure the total length of each beam.
- Based on the measurement technique employed on submillimeter size beam, the measurements performed on approximately 750  $\mu\text{m}$  long mechanoreceptor hair has shown a reasonable number in terms of frequency. The frequencies identified in MACEC using SSI technique are 48.12 Hz and 166.70 Hz. These frequencies show a good agreement with those obtained from FFT measurements in Polytec software as tabulated in Table 5.7.
- Kämper and Kleindienst (1990) have shown a correlation between measured best frequencies and the length of the hair. They revealed a trend of decreasing frequencies with increase in hair length. Based on their correlation they reported a

preliminary range for the first mode of the hair which is between 30 Hz to 100 Hz. In the present case, the measured and identified frequencies for the first mode of the sensory hair show a reasonable agreement with that reported in the literature.

- The first mode shape for submillimeter size beams extracted via MACEC employing SSI technique, show the correct expected behaviour. However, the second mode shape for these beams are unclear and hard to predict as shown by MACEC. The similar observation is made for ODS obtained from Polytec software except for the second mode for 9mm long beam which shows more or less a correct general behaviour. One of the reasons for getting unclear mode shapes can probably be that the measurements are taken only on a millimetre long section of the whole beam, due to limitation of the equipment. This can be one of the considerations for future work.
- For the sensory hair, the first two ODS obtained from Polytec software are clearly distinguishable. The first ODS, as shown in Figure 5.14 around 49.69 Hz, is behaving like a first mode except point 1, which shows off track behaviour. The second ODS clearly shows the deflection starting from point 4 to point 7 as illustrated in Figure 5.15. The mode shapes obtained in MACEC using SSI technique are indistinguishable and unpredictable.

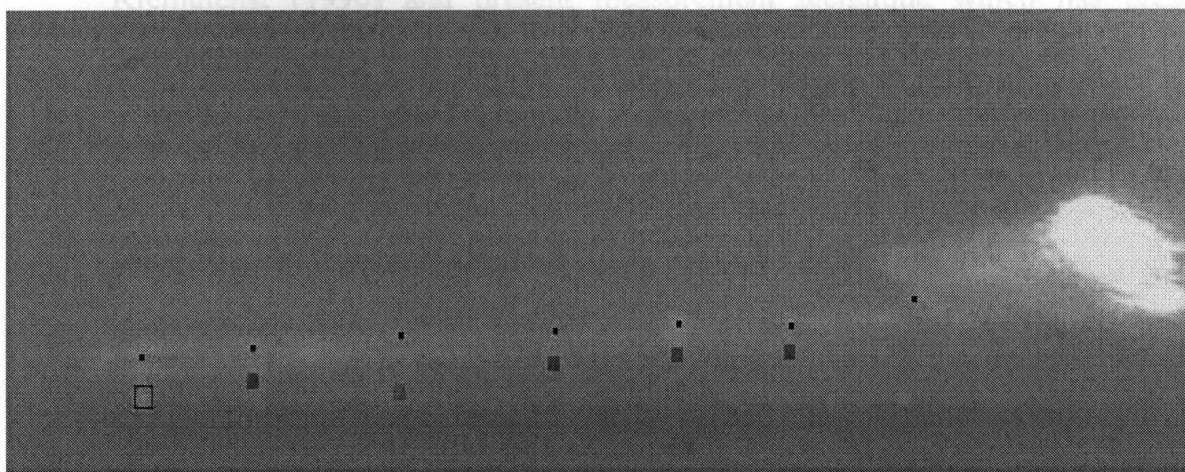


Figure 5.14 First ODS of sensory hair from Polytec software (point 1 to point 7 starting from right to left)



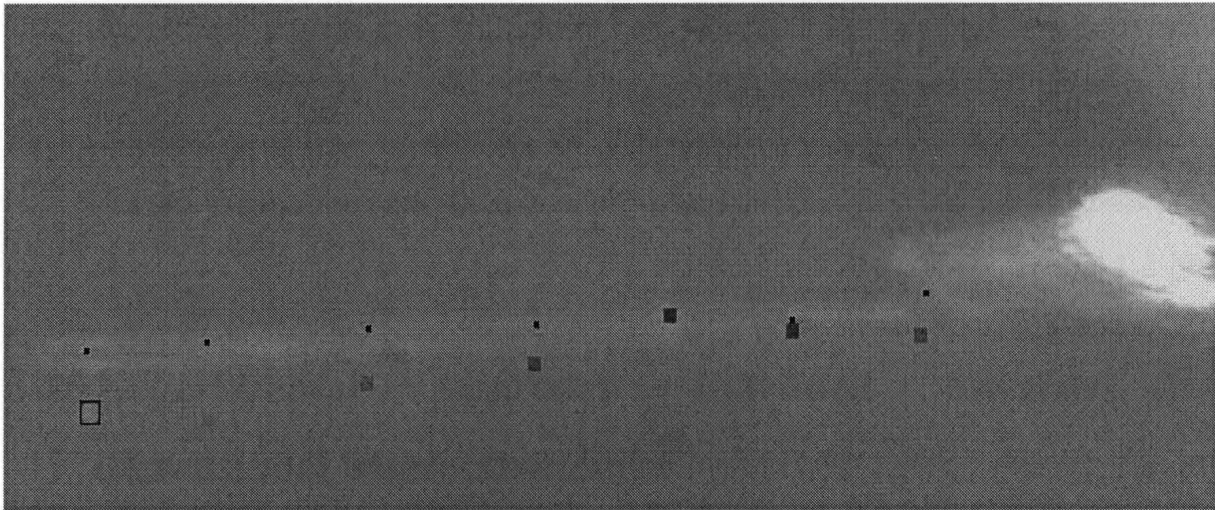


Figure 5.15 Second ODS of sensory hair from Polytec software (point 1 to point 7 starting from right to left)

- There is a possibility that, owing to the lateral motion of the hair, some of the points may go off the edge of the hair during measurement. Therefore those points show totally different movement compared to those which are measured on the hair surface. This can be the reason for getting indistinguishable mode shapes in MACEC as well.
- Based on the previous literature on sensory hair system by Kämper and Kleindienst (1990) and present measurement technique which has presented satisfactory results for a meter long cantilever beam and for a micron-scale beams, it can be said that the first modal frequency of a  $750 \mu\text{m}$  long sensory hair can probably be around 49.69 Hz as its ODS behaves like a first mode in Polytec software.
- A peak between 360-370 Hz has been showing up in all of the measurements taken for the three different cases of the beam and the mechanoreceptor hair. Some checks were performed to isolate that specific frequency. Firstly, the amplifier was replaced with another amplifier but the peak still appeared, secondly, the input signals to the Polytec software were checked, and finally the sound from the speaker was stopped and a single point FFT measurement was taken under ambient

conditions and the peak still showed up. Hence, it was concluded that the peak at this frequency is a result of the noise in vibrometer or any element in the vibrometer system or from the PC. Therefore, it can be concluded that this peak has no association with the system being measured.

## 5.10 Experimental Approach Extended towards two-dimensional Micro-structures

Micro electro mechanical systems (MEMS) microphones are being increasingly used in applications such as cellular phones. These microphones typically include a thin diaphragm electrode and a fixed sensing electrode that is positioned along the diaphragm electrode. In short Microphones are type of transducer which converts energy from one form to another. They convert acoustical energy (sound waves) into electrical energy (the audio signal).

In section 5.7, laser based measurement technique was successfully applied on micron-size one dimensional structures. In this section, a similar approach has been extended towards two dimensional micron-size structures. The experiment was performed on diaphragm of a condenser type microphone with flat frequency response between the range 20 Hz to 16 kHz and 20 Hz to 200 kHz.

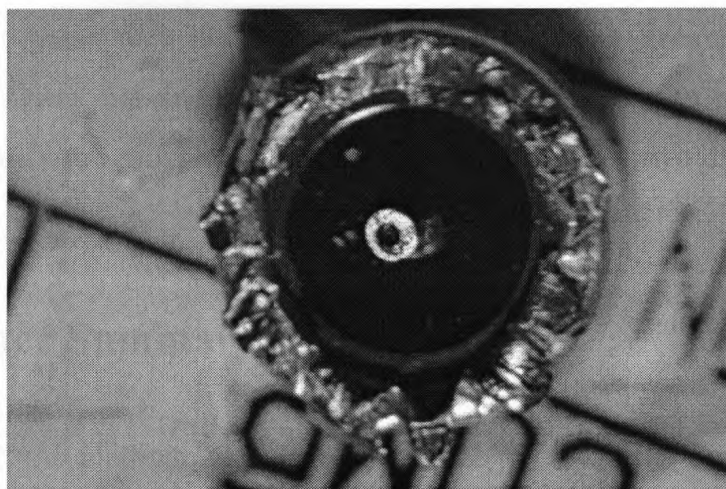


Figure 5.16 Diaphragm of microphone with two metal bits on top surface of it

The experiment was performed on the same experimental setup employed for one dimensional structure, except for the different sound stimuli which was delivered from the loud speaker placed roughly at a distance of 2 meter from the diaphragm. The motivation was to reveal a trend of decrease in frequencies with increase in mass on the diaphragm. Three experiments were performed with three different cases:

Case 1: experiment was performed on a diaphragm without any mass on it. Case 2: a single metal piece was glued to the top surface of the diaphragm and Case 3: two metal pieces were glued on the top of each other and finally on the surface of the diaphragm as shown in Figure 5.16. The results did not show any resonance peak at higher frequency. Although SSI and FFT results show some low frequency peaks but there was not significant change observed in the frequencies with increasing the mass on diaphragm.

The low frequency peaks could be the speaker characteristic, receiver amplifier characteristic or the characteristic of microphone itself. The uncertainty prevails because of unavailability of proper hardware to make certain checks. For example speaker and receiver amplifier with proper specifications and wider frequency range are required to check if the microphone is not excited properly with the present equipment. Another possibility of not exciting the specimen can be the microphone mountings itself which prevent the diaphragm to excite properly.

The mode shapes from MACEC are unpredictable and tough to understand, and ODS in Polytec do not match with the mode shapes of a vibrating circular membrane. Therefore the experiment was not successful for accomplishment of the results, however it was fruitful to identify the problems that can be encountered for two dimensional elements for future work.

## **5.11 Chapter Summary**

In this chapter, the methodology developed in chapter 4 based on LDV has been applied on submillimeter and micron-size one dimensional and two dimensional structures

respectively. The modal frequencies of a submillimeter size beam, with three different lengths have shown a good agreement between the FFT results obtained in Polytec software and the frequencies identified in MACEC. The mode shapes obtained in MACEC has shown a reasonable expected behaviour for the first mode of the beam with three different sizes. However, the second mode shapes has been indistinguishable and unpredictable and tough to observe in some cases. The first two frequencies obtained for a sensory hair fall in the reasonable range indicated by a previous study presented by Kämper and Kleindienst (1990). The ODS for the mechanoreceptor hair obtained from Polytec software showed the expected behaviour for the first two modes of the hair. The preliminary attempt to employ the developed methodology on insects was successful in accomplishing the reasonably correct modal frequencies.

An attempt towards measurement on two dimensional micron-scale structures is made to the preliminary extent which was not successful; though it was fruitful in terms of getting an acquaintance with the type of problems that can be encountered in future work on two dimensional elements using the same methodology.



# Chapter 6

## Conclusions and Recommendations

### 6.1 Summary

An overview of system identification is given with special emphasis on output-only techniques. Different models often taken into consideration in the system identification context are discussed. Algorithms available for identification from the output data are also discussed briefly. Stochastic subspace algorithm (SSI) with its application is briefly studied for the purpose of extracting dynamic characteristics of small-scale structural elements. Different methods of output-only system identification are discussed. The output-only data dynamics has an advantage of being inexpensive since no equipment is needed to excite the structure. The modeling of output-only data obtained from naturally excited structure is particularly interesting because test structure remains in its normal in-operation condition during the test. Since it is impossible to measure the ambient excitation sources, deterministic knowledge of the input is replaced by the assumption that the input is a realization of a stochastic process (white noise). There has been several output-only data modal parameter techniques developed over the past decades and Peak picking (PP) Method, Complex Mode Identification Function (CMIF), Instrumental Variable (IV) Methods and Stochastic Subspace Identification (SSI) are some of them.

In the context of system identification, operation of a Graphical User Interface (GUI) based program called Modal Identification on Civil Engineering Structures (MACEC) is described along with its implementation for identification of real data. An effort is made to

clarify all of the functions and identification algorithm used in MACEC. For the purpose of validating MACEC as a modal parameter extraction program for large and micron-scale structures, data collected during measurements on smaller structures, ranging from a meter long beam to submillimeter size beams and micron-size mechanoreceptor hair has been analysed in MACEC using SSI algorithm and PPM.

SSI algorithm was applied based on data obtained on moderate structures such as a cantilever beam. The experiments have been conducted employing a meter long cantilever beam and its response due to broad band approximate white noise excitation has been measured. The primary purpose of the experiment was to develop a methodology employing a Laser Doppler Vibrometer (LDV) setup, and to test the suitability of this equipment for performing further experiments on micron-size structures. The time-domain data (velocity) obtained from LDV on the beam was then fed into MACEC for modal characterization via SSI and PPM. The results obtained from LDV were compared to the results obtained from different conventional methods such as, HP Analyser, and PC based data acquisition system (OROS Analyser). A good agreement between laser based measurements and the measurements taken by conventional methods has been found. The mode shapes obtained from MACEC showed the correct expected behaviour.

Based on the methodology developed on a meter long cantilever beam, further experiments were performed on one dimensional micron-scale structure such as a sub-millimeter size cantilever beam with three different lengths. Motivation was to use a structure similar to the structure of a sensory hair on the cercus of insect, which was one of the central focus for future research. The measurements were taken on Microscope Scanning Vibrometer (MSV) setup for submillimeter size beam and the micron-size hair.

The modal frequencies of a submillimeter size beam, with three different lengths have shown a good agreement between the Fast Fourier Transform (FFT) results obtained in Polytec software and the frequencies identified in MACEC via SSI. The mode shapes acquired in MACEC have shown a reasonable expected behaviour for the first mode of the beam with three different sizes. However, the second mode shape has been difficult to

visualize and unpredictable in some cases. The first two frequencies obtained for a sensory hair have been found to lie in the reasonable range reported in a previous study presented by Kämper and Kleindienst (1990). The ODS for the hair obtained from Polytec software showed the expected behaviour for the first two modes of the hair. A preliminary attempt to use the developed methodology on insects was successful in acquiring the reasonably correct frequencies.

An attempt towards measurement on two dimensional microstructures is made and was found to be unsuccessful, though was fruitful in terms of getting an acquaintance with the type of problems that can be encountered in future work with two dimensional elements employing the same methodology.

## 6.2 Thesis Contribution

- SSI algorithm in MACEC has been validated for modal characterization of smaller structures which has been used in the past for modal identification of larger structures.
- SSI in MACEC has provided accurate modal frequencies and mode shape for a meter long cantilever beam that has been used for output-only identification experiment, performed on LDV.
- MSV has been used to measure velocity on submillimeter size cantilever beam. The expected identified frequencies via SSI in MACEC provided confidence in validity of this method for frequency measurement on insect sensory hair.
- MSV was applied to a micron-size mechanoreceptor hair for velocity measurements. The identified frequencies via SSI in MACEC showed good agreement with those, obtained from frequency domain measurements on MSV and with those reported in previous literature, providing validation for frequency measurement on one dimensional micron-scale structures.
- The present method employing MSV and SSI can be extended to two dimensional structures, can extract damping ratios and is able to determine multiple mode

shapes which are advantages over the method reported in a study by Kämper and Kleindienst (1990).

- Another advantage is the use of output-only system identification technique employing excitation input of approximately wide band white noise. The excitation was delivered as air velocity to which the sensory organs respond in nature.

### 6.3 Recommendations for Future Work

- The mode shapes identified for submillimeter beam were unclear and sometimes unpredictable. This may be attributed to measurements being taken only on a millimeter (approximately) long section in the middle of the whole beam rather than measuring the complete length of the beam owing to the limited field of view of the camera which has led to only a partial scan of the beam. Possibly, better mode shapes can be obtained by scanning the full length of the beam. This can be achieved by providing PSV-400 with close-up attachment, allowing it to zoom in for smaller and closer objects. Secondly, the full length scan of the beam can be achieved by marking common measurement points on the beam and taking multiple measurement sets as MACEC is provided with the ability of stitching the modes to show the complete visualization of the beam.
- Another possible reason for the unclear mode shapes may be attributed to shifting of the measurement points on the structure, during the test. That can be overcome by determining the source of motion and suppressing it.
- The ODS obtained from Polytec showed the correct expected behaviour for the mechanoreceptor hair, however the mode shapes obtained from MACEC have been difficult to understand. One of the possible ways to overcome this difficulty is to decrease the bandwidth during measurements. A similar problem was faced when the experiment was performed on a meter long cantilever beam which was resolved by lowering the bandwidth during measurements.
- If required in future research, specialized subroutines can be rewritten in MATLAB to improve the quality of animation of mode shapes in MACEC.

- Once the methodology and measurement technique is validated on two dimensional structures, other insect sensory organs of more general shapes can be studied.

# References

- Ali, S., 2006, "Modal Identification of Structures with Output-only data," Masters Thesis, University of Western Ontario.
- Byard, D., 1992, "An algorithm for state-space frequency domain identification without windowing distortions," Proceedings of 31<sup>st</sup> IEEE conference on Decision and Control, Tucson, AZ, USA, December 16-18, pp. 1707-1712.
- Butler, R., 2005, Biomimetics technology that mimics nature, At Mongabay.com [.http://news.mongabay.com/2005/0711-rhett\\_butler.html](http://news.mongabay.com/2005/0711-rhett_butler.html).
- Clough, R., and Penezien, J., 1975, Dynamics of Structures, McGraw-Hill, USA.
- Chalmers, P., 2000, Lobster special, In Mechanical Engineering Magazine, publication of ASME. [http://memagazine.asme.org/Issues/Back\\_Issues.cfm](http://memagazine.asme.org/Issues/Back_Issues.cfm).
- Cock, K.D., Peeters, B., Veechio, A., Auweraer, H.V., and Moor, B.D., 2002, "Subspace identification for mechanical engineering," Proceedings of International conference on Noise and Vibration engineering, Leuven, Belgium, September 16-18, pp. 1332-1352.
- Dumpert, K., and Gnatzy, W., 1997, "Cricket combined mechanoreceptor and kicking response," Journal of Comparative Physiology, 122 (1), pp. 9-25.
- Gopinath, B., 1969, "On the identification of linear time-invariant systems from input/output data," Bell System technical journal, 48(5), pp. 1101-1113.
- Gnatzy, W., and Tautz, J., 1980, "Ultra structure and mechanical properties of an insect mechanoreceptor: stimuli-transmitting structures and sensory apparatus of the cercal filiform hairs of gryllus," Cell and Tissue Research, 213(3), pp. 441-463.
- Ho, B., and Kalman, R., 1966, "Efficient construction of linear state variable models from input/output functions," Regelungstechnik, 14, pp. 545-548.
- Inman, J., 2001, Engineering Vibration, Prentice Hall, Upper Saddle River, NJ.

Ivan, G., and Moor, D.B., 2003, "Subspace identification combined with new mode selection techniques for modal analysis of an airplane," Proceedings of the 13<sup>th</sup> IFAC symposium on system identification (SYSID), Rotterdam, The Netherlands, pp. 695-700.

Kirkegaard, P.H., and Andersen, P., 1997, "State space identification of civil engineering structures from output measurements," Proceedings of the 15th International Modal Analysis Conference, Orlando, Florida, USA, February 3-6, pp. 889-895.

King, A., Desai, U., and Skelton, R., 1988, "A generalized approach to q-markov covariance equivalent realizations of discrete systems," *Automatica*, 24(4), pp. 507-515.

Karnovskii, I.A., Lebed, O., I., 2004, *Free vibrations of beams and frames : eigenvalues and eigenfunctions*, McGraw-Hill, New York.

Kämper, G., and Kleindienst, H., 1990, "Oscillation of cricket sensory hairs in a low-frequency sound field," *Journal of Comparative Physiology*, 167(2), pp. 193-200.

Ljung, L., 1999, *System Identification: Theory for the user*, Prentice-Hall, Upper Saddle River, NJ.

Ljung, L., 2005, *System identification toolbox for use with MATLAB user's guide, version 6*, MathWorks, Inc, Natick, MA.

Ljung, L., 1998, *Signal processing toolbox for use with MATLAB user's guide, version 4*, MathWorks, Inc, Natick, MA.

Mevel, L., Benveniste, A., and Basseville, M., 2006, "Input/output versus output-only data processing for structural identification-Application to in-flight data analysis," *Journal of Sound and Vibration*, 295(2-3), pp. 531-552.

Overchee, P.V., and Moor, B.D., 1993, "Subspace Identification for the stochastic for the stochastic identification problems," *Automatica*, 29(3), pp. 649-660.

Peeters, B., and Roeck, G.D., 1999, "Reference based stochastic subspace identification for output-only modal analysis," *Mechanical Systems and Signal Processing*, 13(6), pp. 855-878.

Peeters ,B., and Roeck, G.D., 2001, “Stochastic system identification for operational modal analysis,” *Journal of Dynamic Systems, A review, Measurement and Control*, 123(4), pp. 659-667.

Peeters ,B., and Ventura, C.E., 2003, “Comparative study of modal analysis techniques for bridge dynamics and characteristics,” *Mechanical Systems and Signal Processing*, 17(5), pp. 965-988.

Peeters ,B., Branden, B.V.D., Laquiere, A., and Roeck, G.D., 1999, “ Output-only modal analysis: development of a gui for matlab,” *Proceedings of 17<sup>th</sup> International Modal Analysis Conference*, Kissimmee, FL, USA, pp. 1049-1055.

Peeters, B., 2000, “System Identification and Damage Detection in Civil Engineering,” PhD Thesis, Katholieke Universiteit Leuven.

Polytec Scanning Vibrometer, “Theory manual”, Polytec inc.

Skordosy, A., and Chanz, P.H., 2002, “A novel strain sensor based on campaniform sensillum of insects,” *Philosophical Transactions of Royal Society of London*, 360(1791), pp. 239-253.

Shimozawa, T., and Kanou, M., 1984, “Varieties of filiform hairs: range of fraction by sensory afferents and cercal interneurons of a cricket,” *Journal of Comparative Physiology* 155(4), pp. 485-493.

Tusker, F., Bosse, A., and Fisher, S., 1998, “Real time modal parameter estimation using subspace methods Theory,” *Mechanical Systems and Signal Processing* 12(6), pp. 797-808.

Overchee, P., and Moor, B., 1996, *Subspace Identification for Linear Systems: Theory – Implementation-Applications*, Kluwer Academic Publishers Dordrecht, The Netherlands.

Viberg, M., 1995, “Subspace-based methods for the identification of linear time-invariant systems,” *Automatica*, 31(12), pp.1835-1851.

Zieger, H., and Mcewen, A., 1974, “Approximate linear realizations of given dimensions via Ho’s algorithm,” *IEEE transactions on Automatic Controls*, 19(2), pp.153-153.



# Appendix A

## Supplementary Mode Shapes Figures

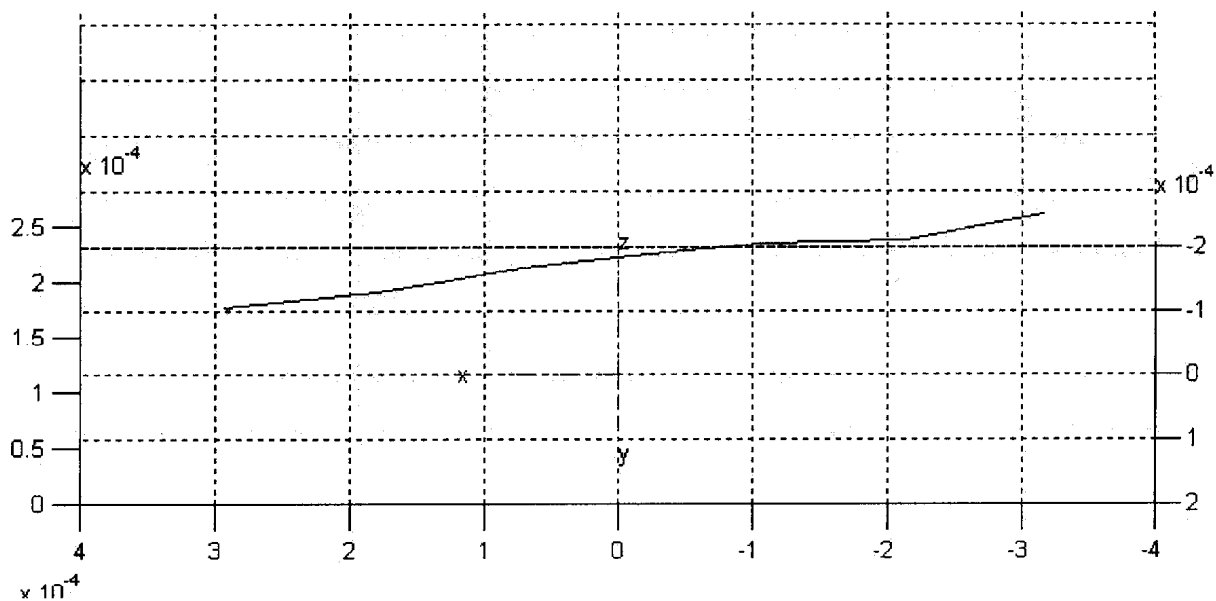


Figure A.1 First mode from SSI for 9mm long beam

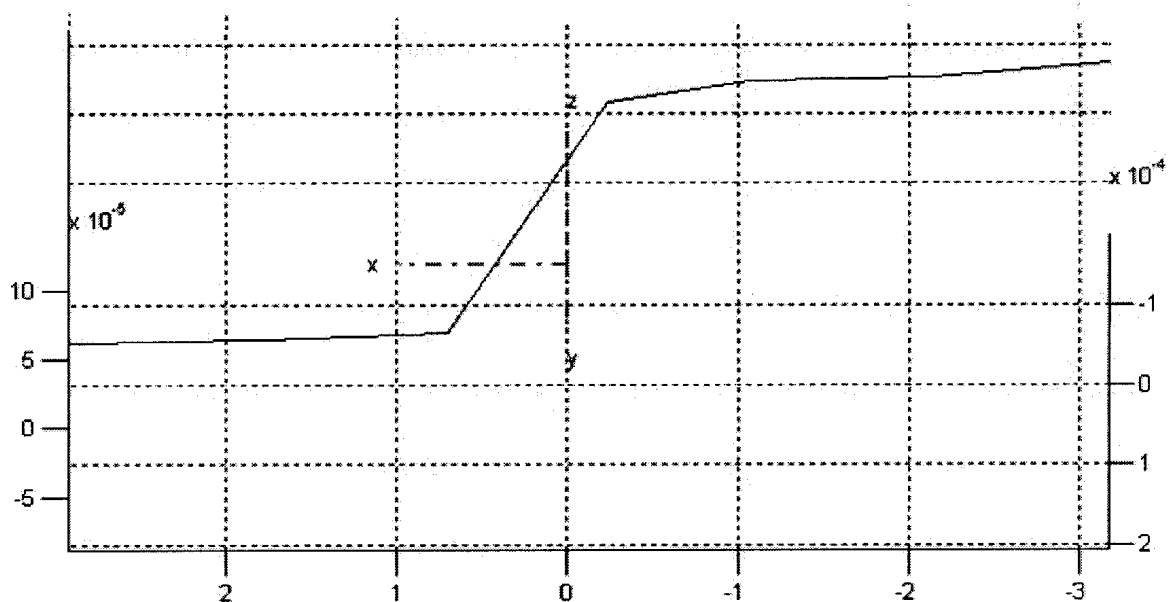


Figure A.2 Second mode from SSI for 9mm long beam

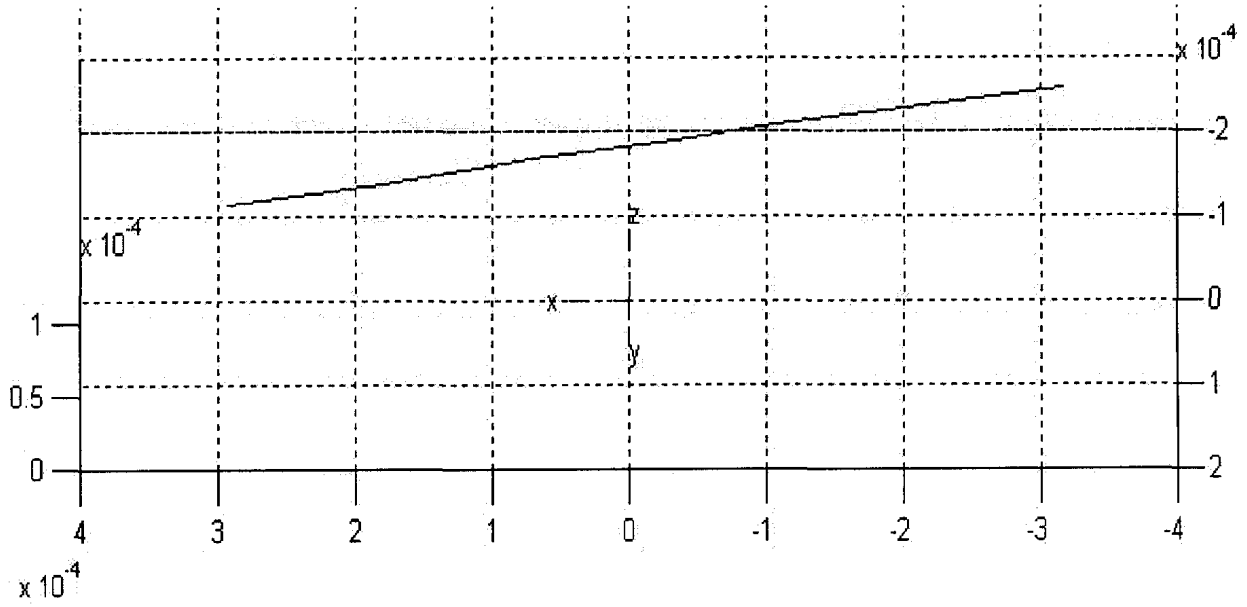


Figure A.3 First mode from PPM for 9 mm long beam

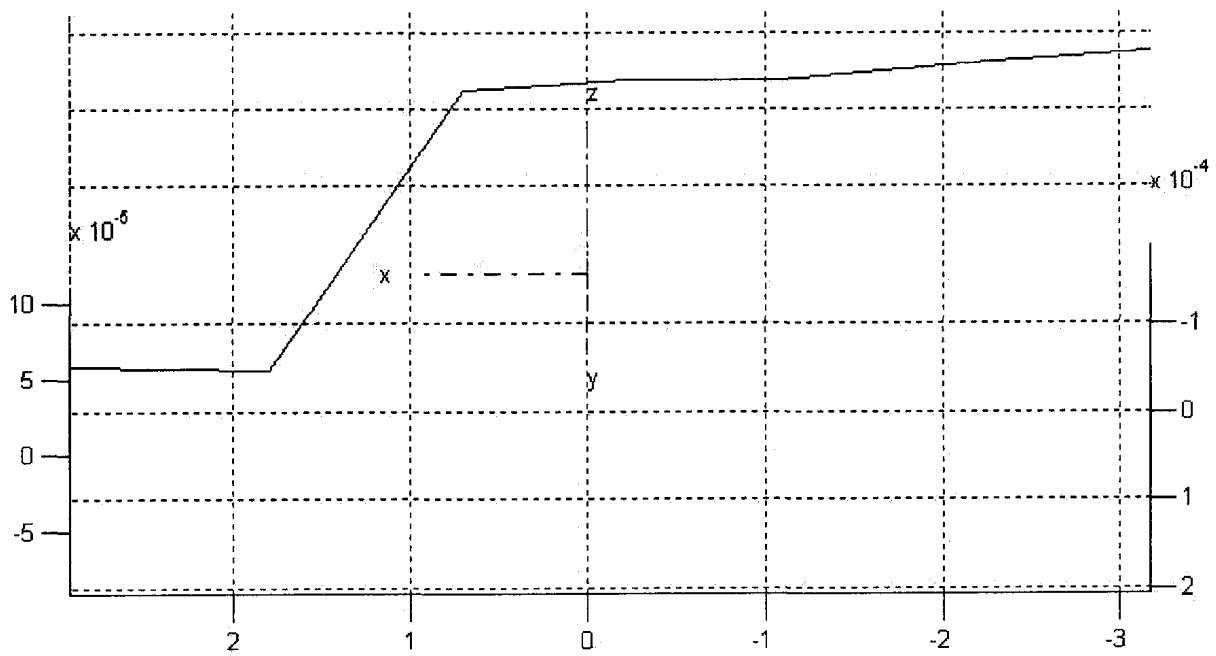


Figure A.4 Second mode from PPM for 9 mm long beam

## Appendix B

### Supplementary Stabilization Diagrams and ANPSD

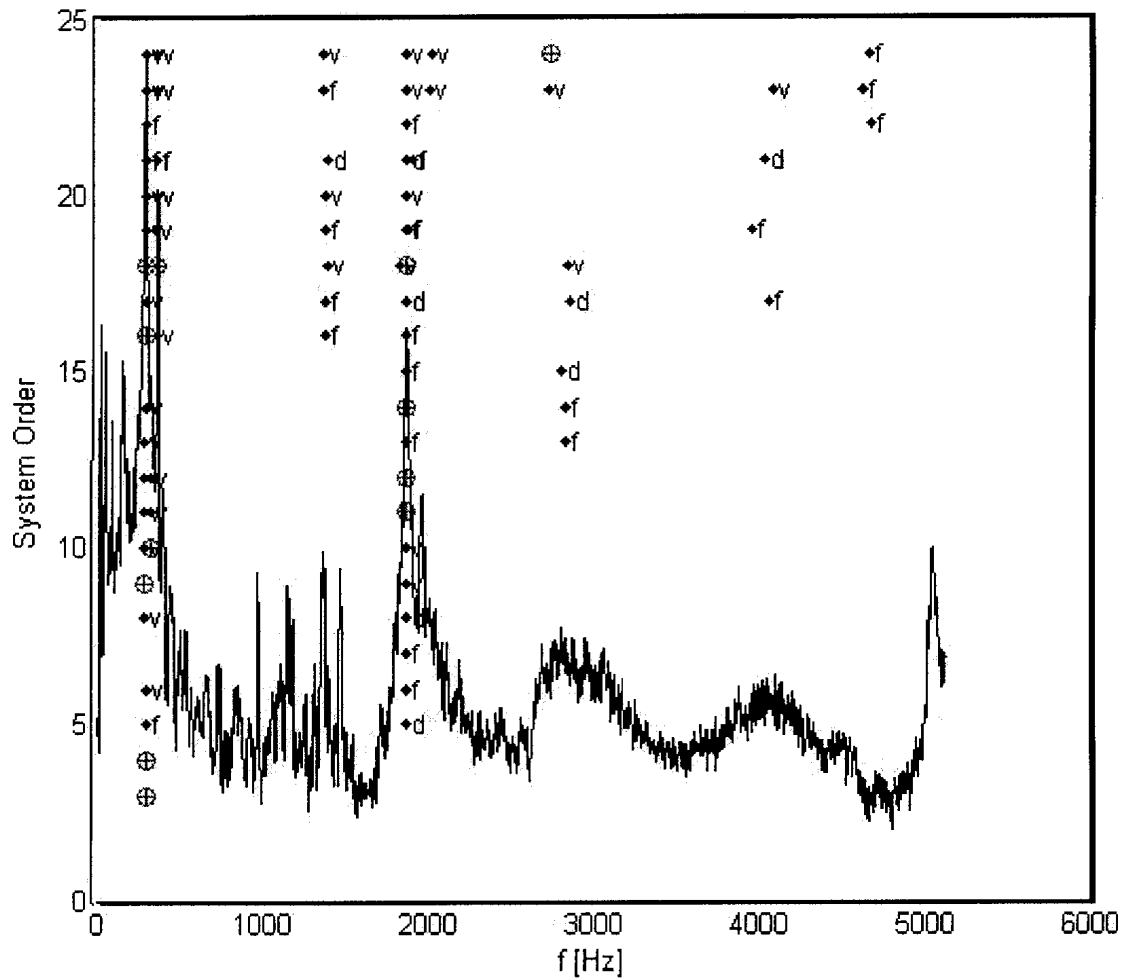


Figure B.1 Stabilization diagram for 7.5 mm long beam  $\oplus$  stable poles,  $v$  stable vector,  $f$  stable frequency,  $d$  stable damping and  $o$  pole.

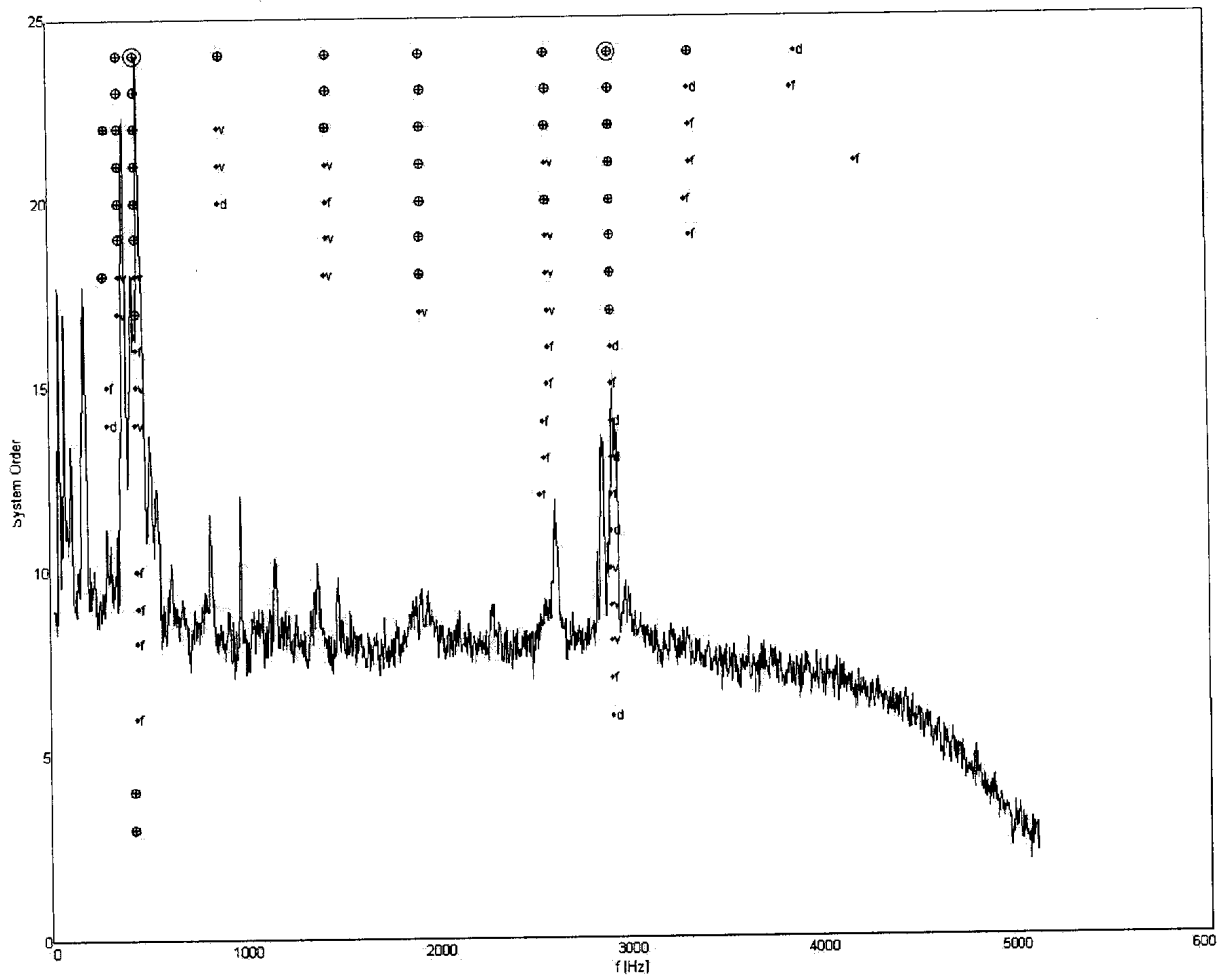


Figure B.2 Stabilization diagram for the 6.4 mm long beam  $\oplus$  stable poles,  $\nu$  stable vector,  $f$  stable frequency,  $d$  stable damping and  $o$  pole.

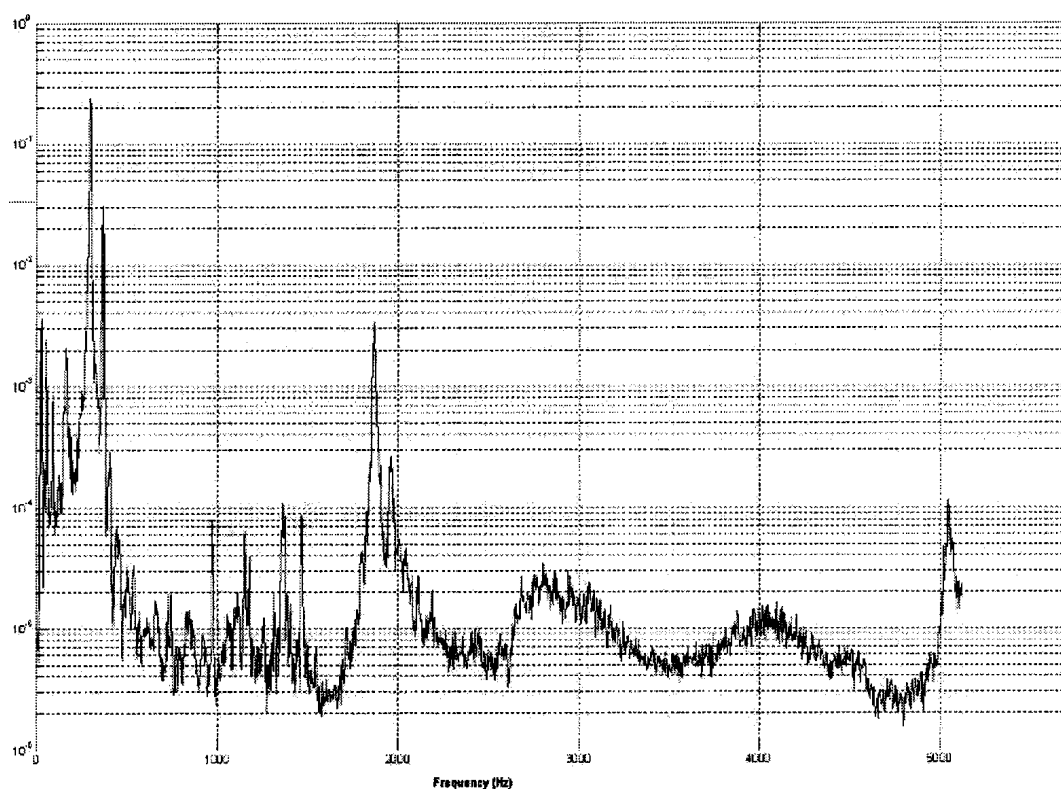


Figure B.3 ANPSD for 7.5 mm (MACEC presents this plot without units For the y-axis and the values are normalized for easier peak identification)

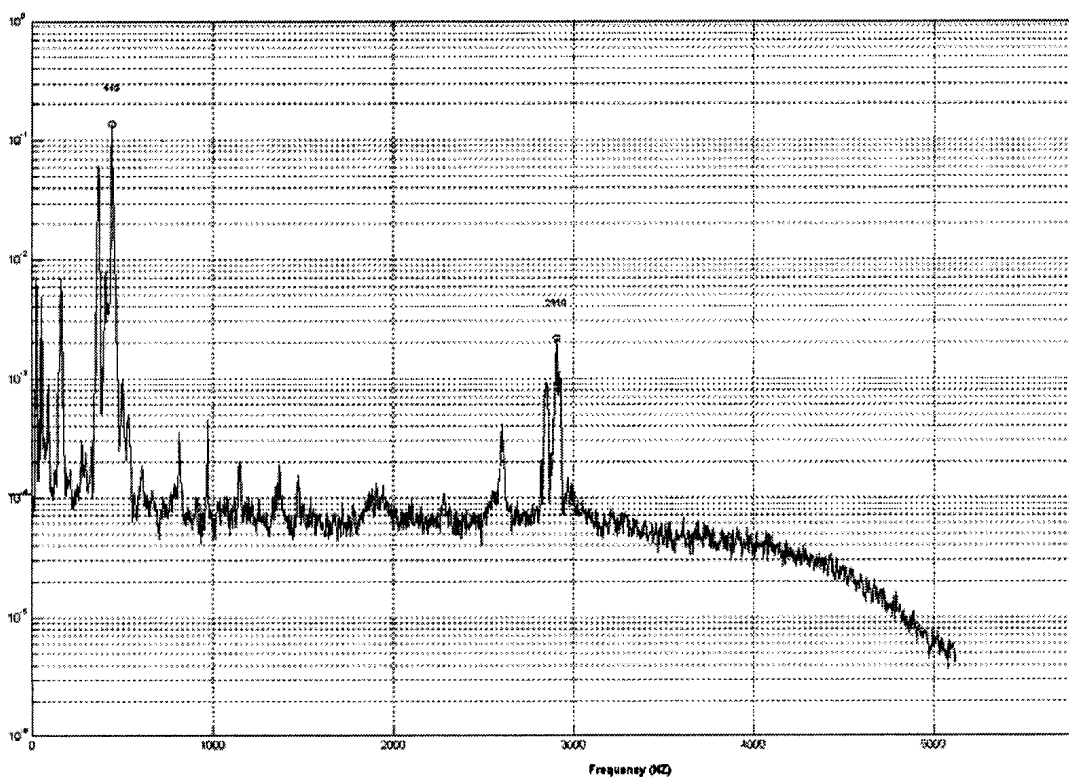


Figure B.4 ANPSD for 6.4mm long beam. ANPSD for 9mm long beam (MACEC presents this plot without units for the y-axis and the values are normalized for easier peak identification)

## Appendix C

### Supplementary FRFs from Polytec

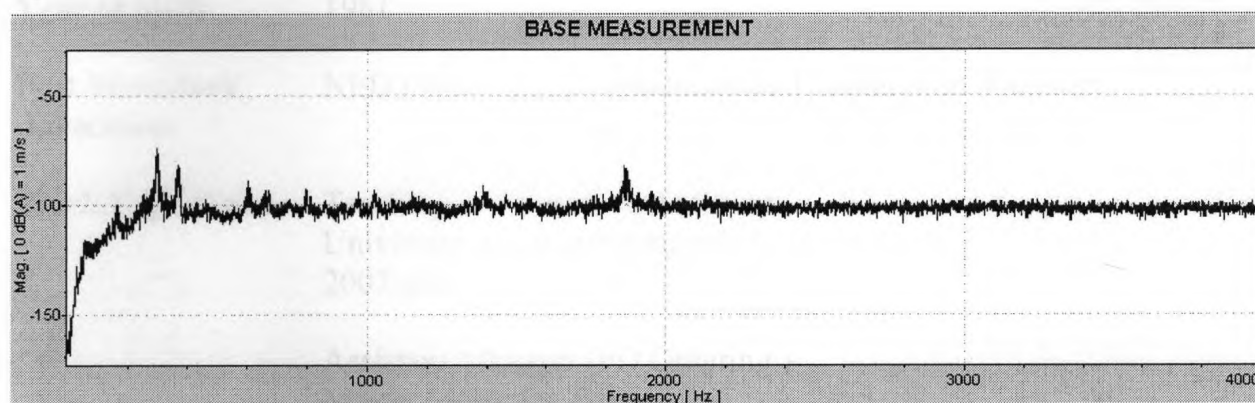


Figure C.1 Average spectrum of frequency measurements from MSV for 7.5 mm long wire

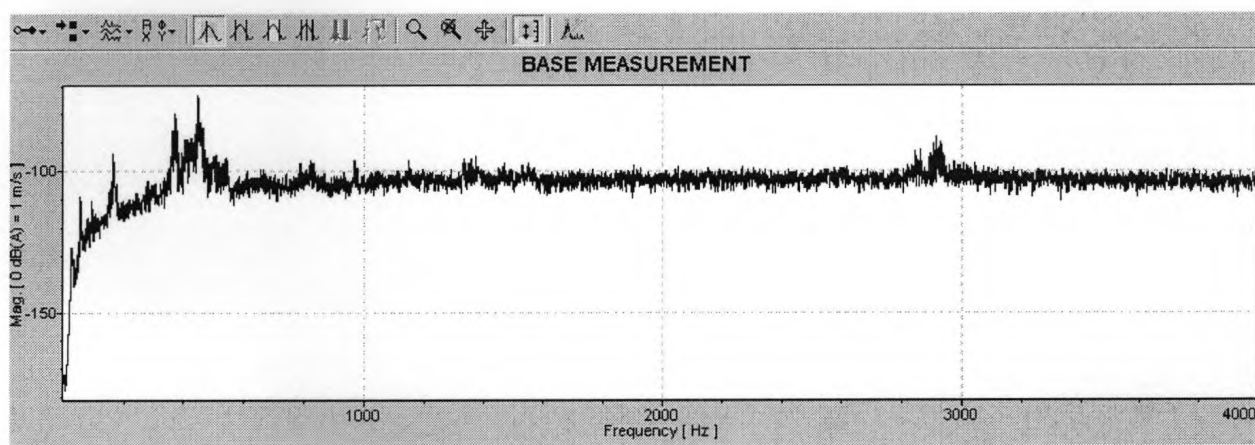


Figure C.2 Average spectrum of frequency measurements from MSV for 6.4 mm long wire